Spark Ignition Measurements in Jet A: part II

Julian J. Lee and Joseph E. Shepherd

Graduate Aeronautical Laboratories
California Institute of Technology
Pasadena, CA 91125

January 22, 2000

Explosion Dynamics Laboratory Report FM 99-7

Prepared for and supported by the National Transportation Safety Board
Under Order NTSB12-98-CB-0415

Abstract

An improved system for measuring the ignition energy of liquid fuel was built to perform experiments on aviation kerosene (Jet A). Compared to a previously used system (Shepherd et al. 1998), the present vessel has a more uniform temperature which can be held constant for long periods of time. This ensures thermal equilibrium of the liquid fuel and the vapor inside the vessel. A capacitive spark discharge circuit was used to generate damped sparks and an arrangement of resistors and measurement probes recorded the voltage and current histories during the discharge. This permitted measurement of the energy dissipated in the spark, providing a more reliable, quantitative measure of the ignition spark strength. With this improved system, the ignition energy of Jet A was measured at temperatures from 35°C to 50°C, pressures from 0.300 bar (ambient pressure at 30 kft) to 0.986 bar (ambient pressure near sea level), mass-volume ratios down to 3 kg/m^3, with sparks ranging from 10 mJ to 0.3 J. Special fuel blends with flash points (T_{fp}) from 29°C to 73.5°C were also tested. The statistical properties of the ignition threshold energy were investigated using techniques developed for high-explosive testing.

Ignition energy measurements at 0.585 bar with high mass-volume ratios (also referred to as mass loadings) showed that the trend of the dependence of ignition energy on temperature was similar for tests using the stored capacitive energy and the measured spark energy. The ignition energy was generally lower with the measured spark energy than with the stored spark energy. The present ignition energy system was capable of clearly resolving the difference in ignition energy between low and high mass-volume ratios. The ignition energy vs. temperature curve for 3 kg/m^3 was shifted approximately 5°C higher than the curve for high mass-volume ratios of 35 kg/m^3 or 200 kg/m^3. The ignition energy was subsequently found to depend primarily on the fuel-air mass ratio of the mixture, although systematic effects of the vapor composition are also evident. As expected, the ignition energy increased when the initial pressure was raised from 0.585 bar to 0.986 bar, and decreased when the pressure was decreased to 0.3 bar. Finally, tests on special fuels having flash points different from that of commercial Jet A showed that the minimum ignition temperature at a spark energy of about 0.3 J and a pressure of 0.986 bar depends linearly on the flash point of the fuel.

Contents

List of Figures

List of Tables

1 Introduction

The present report describes the continuing investigation of the basic flame ignition properties of Jet A vapor in air. In particular, this study addresses specific issues raised in the previous report on Jet A ignition properties (Shepherd et al. 1998).

In the previous work, one of the main findings was that high temperatures play an important role in increasing the relative hazard of a Jet A fuel vapor explosion in an airplane fuel tank. The ignition energy for mixtures of Jet A vapor in air was measured and found to decrease sharply as the temperature was increased from 35°C to 55°C, thereby increasing the risk of accidental ignition by electrical sparks (Shepherd et al. 1998). Several issues were subsequently raised concerning the details of the spark ignition method, properties of the fuel, and other factors influencing the ignition process. Among the outstanding questions raised were: what is the actual energy deposited by the spark discharge, what is the effect of airplane altitude on the ignition energy, what is the effect of changing the flash point of the fuel on the ignition energy, and what is the effect of fuel weathering on the ignition energy.

The present document reports the results of our investigation into these issues. The main objectives of the present study were to repeat the previous ignition energy experiments using an improved spark system and well equilibrated apparatus, investigate the statistical properties of ignition energy data, and further investigate the issues of pressure dependence, mass-volume ratio dependence, and flash point dependence.

This report describes the development and construction of an improved spark discharge system in which the electrical energy dissipated in the spark can be measured. Since the ignition process in the gaseous section above a layer of heated fuel can be extremely sensitive to experimental conditions such as temperature non-uniformities in the vessel and spark gap location, care was taken to eliminate these effects with the present apparatus. Using this improved system, ignition energy tests were done on Jet A fuel provided by ARCO and formulated to have a wide range of flashpoints.

With these more accurate spark energy measurements, it was found that reducing the mass-volume ratio from 35 kg/m^3 or 200 kg/m^3 to 3 kg/m^3 causes a shift in the ignition energy curve of about 5°C towards higher temperatures. It was also found that with direct measurements of the spark energy, the ignition energy was lower than previous measurements using the stored capacitive energy, although the trend of the dependence of ignition energy on temperature was similar. As expected, the ignition energy increased when the initial pressure was raised from 0.585 bar to 0.986 bar, and decreased when the pressure was decreased to 0.3 bar. Finally, tests on special fuels having flash points different from that of commercial Jet A showed that the minimum ignition temperature at a spark energy of about 0.3 J and a pressure of 0.986 bar depends linearly on the flash point of the fuel.

2 Description of the heated ignition energy apparatus

The apparatus used for the present tests is essentially the 1.84 liter vessel described in the previous report (Shepherd et al. 1998) with several improvements made to the design. The main improvements were in the spark discharge circuit (see Section 3), the heating system, which was modified to provide more uniform and controllable temperature control, and the gas feed system.

2.1 Vessel description

The vessel is made of aluminum and has a volume of a 1.84 liter. The interior is cubic with a dimension of 14 cm (Fig. 1). The front and back walls of the vessel have 5.8 cm circular windows for visualization of the event inside and up to 460 ml of liquid fuel can be introduced into the vessel before the liquid level rises above the bottom of the window. The temperature of the vessel can be increased from room temperature to about 80°C.

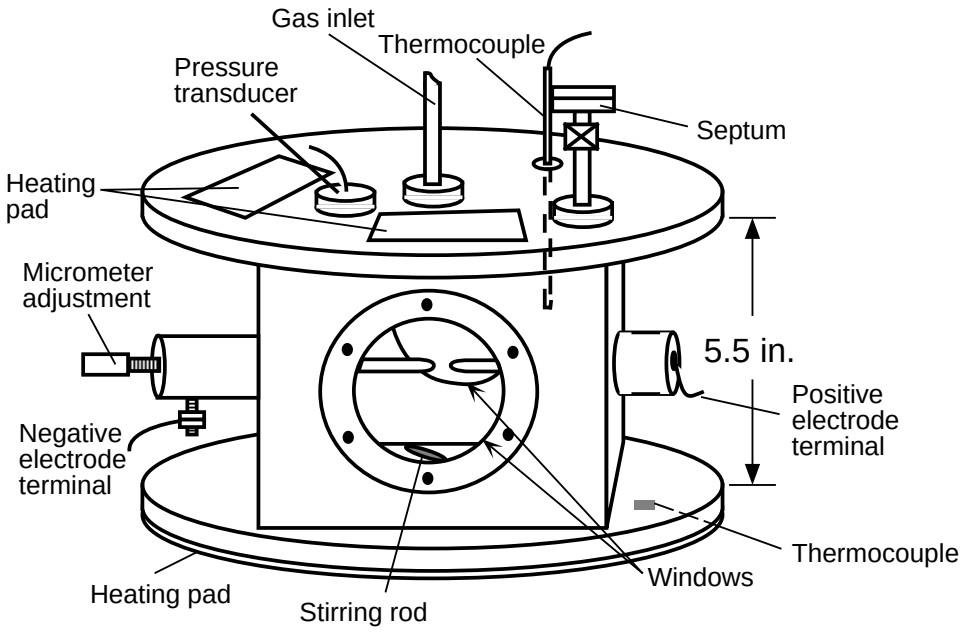

Figure 1: Schematic diagram of the ignition vessel used for ignition energy measurements of liquid fuels.

The entire vessel is placed inside an insulated box in which the air can be heated and circulated by a fan (Fig. 2, number 11). The box is made of wood and is lined with aluminum-backed fiberglass insulation 1 inch thick. The inner dimensions of the box are 38.5 cm x 54 cm x 31 cm. Several 5 W/in^2 heating pads are placed directly on the vessel and inside a circulation duct made of a 93 mm diameter PVC pipe. These heaters are controlled by solid-state heater-control relays connected to a CN77544 Omega temperature controller. The thermocouple used to provide temperature feedback to the controller measured the air temperature in the box and

is located in the far right hand side of the box, far from the heating pads (Fig. 2, number 10). Using this arrangement, the vessel and the air surrounding the vessel can be heated to the target temperature with an absolute accuracy of ± 1°C and a variation of temperature within the insulated box of no more than 1°C.

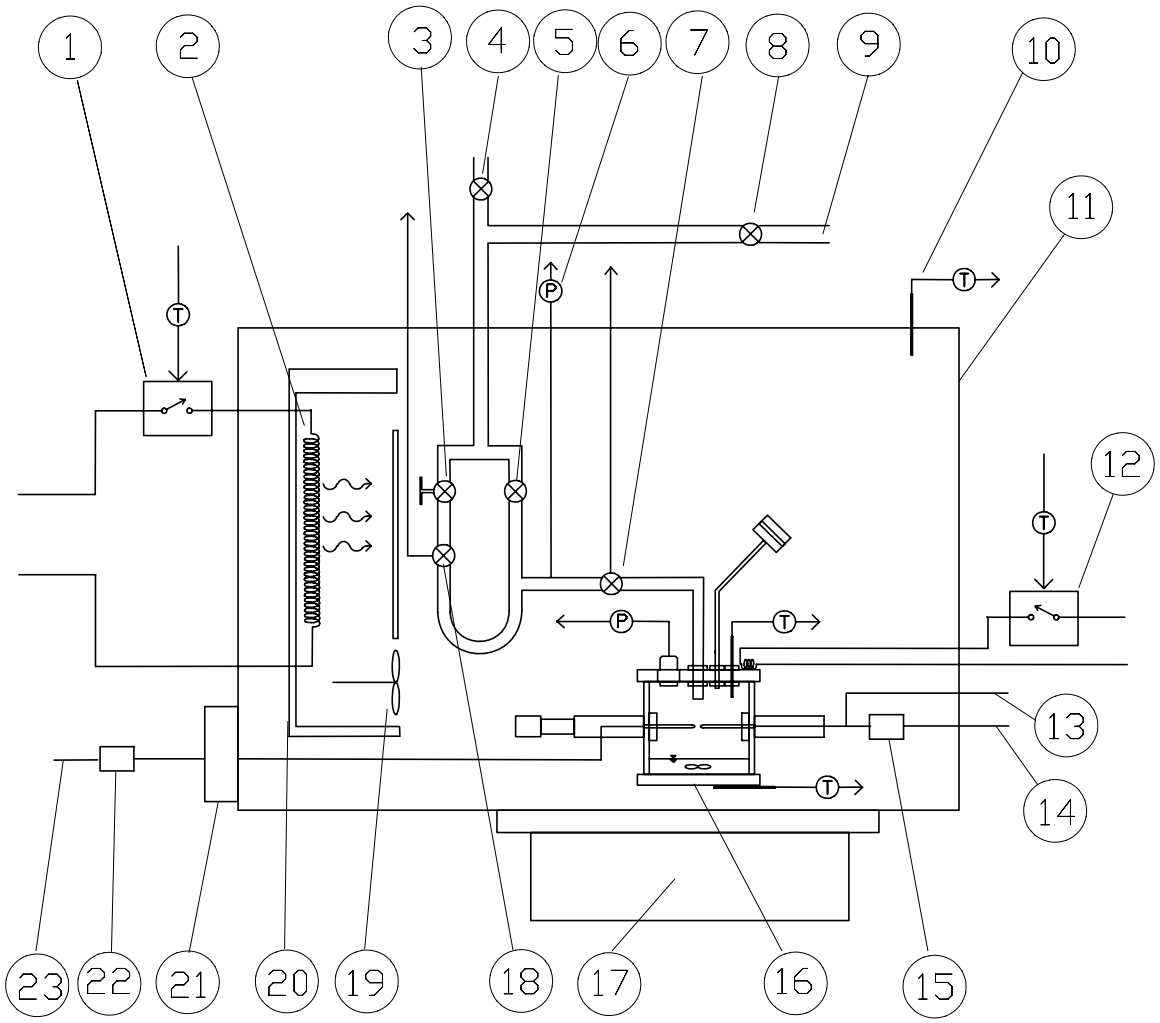

Figure 2: Schematic diagram of the entire heated ignition energy vessel system. The elements in the schematic are: 1) and 12) heater-control relays, 2) heating pads, 3) needle valve, 4) bleed valve, 5) rapid venting valve, 6) MKS pressure gage, 7) electro-pneumatic valve, 8) vacuum valve, 9) vacuum line, 10) box air thermocouple, 11) insulated box, 13) high-voltage probe terminal, 14) positive terminal from discharge circuit, 15) and 22) damping resistors, 16) ignition vessel, 17) magnetic mixer, 18) solenoid valve, 19) circulation fan, 20) circulation duct, 21) current transformer, 23) ground terminal from discharge circuit.

The gas feed in and out of the vessel is controlled by an arrangement of electrically-activated and manual valves (Fig. 2, numbers 3, 4, 5, 7, 8, and 18). With this system, gas can be introduced or removed from the vessel remotely while the pressure in the gas manifold

is monitored by a precision MKS model# 121AA-01000A pressure transducer (Fig. 2, number 6).

Two electrodes protrude into the vessel to provide a spark gap approximately at the center of the chamber. The electrodes consist of stainless steel rods 1/8 inch in diameter. The positive electrode was stationary and the grounded or negative electrode was adjustable in order to vary the spark gap size. The gap size used in the present experiments was 5.4 mm, larger than the 3.3 mm used in the previous experiments. Gap size and geometry do have an effect on the ignition energy threshold as discussed in Section 3.4.4 of Shepherd et al. (1998). However, if flanges are not used on the electrodes and the gap is sufficiently greater than the quenching distance, then the ignition energy threshold is only weakly dependent on the electrode spacing. This is the situation in the present experiments.

The electrode arrangement is shown in Fig. 3. The electrode tips were conically tapered then rounded as shown in Fig. 4.

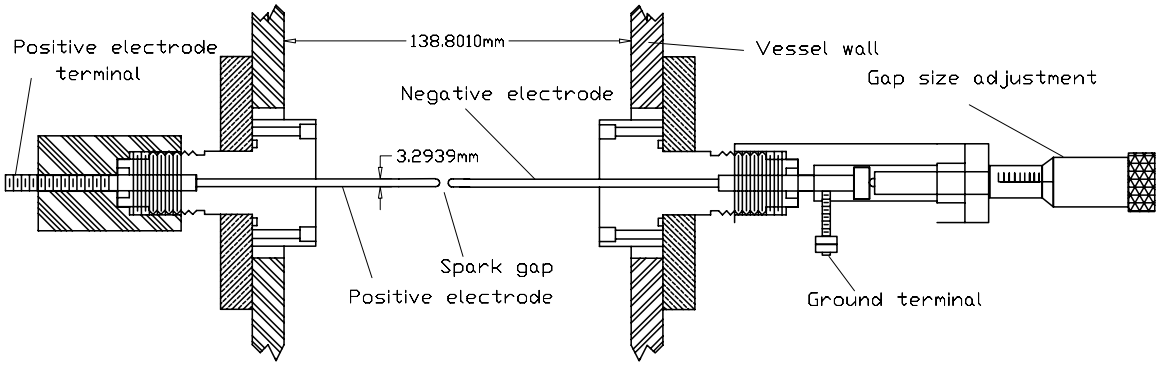

Figure 3: Schematic diagram of adjustable-gap-width electrodes of the ignition energy vessel.

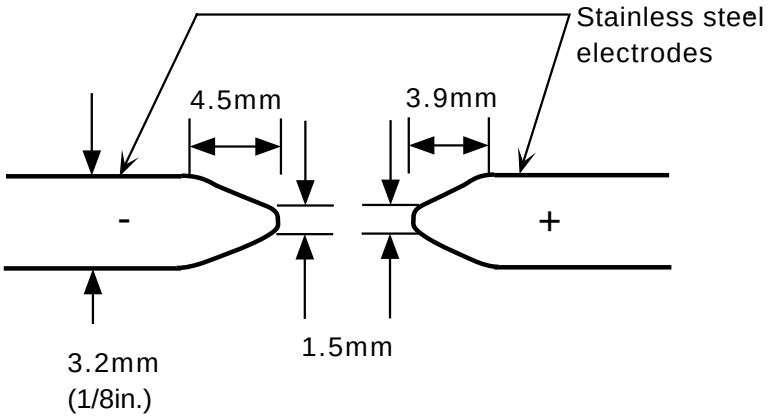

Figure 4: Schematic diagram of electrode tip geometry.

The typical test procedure for an ignition energy measurement basically consists of injecting the fuel sample into the vessel at low pressure to avoid evacuating any fuel vapor, bleeding in air until the desired test pressure is reached, then triggering sparks at a certain energy while

raising the temperature in plateaus until ignition occurs. The standard operating procedure of the ignition energy vessel is given in Appendix A.

2.2 Diagnostic measurements

The explosion event was monitored by various diagnostic gages in the vessel (Fig. 1). The pressure history inside the chamber was measured using a Kulite XT-190 static pressure transducer located at the top of the vessel. The temperature history was measured using a K-type thermocouple with 0.005 inch diameter wire for fast response. The pressure and temperature signals were amplified and recorded on a computer through a National Instruments AT-MIO-64E-3 digital acquisition board. The board was controlled by a LabView^{TM} program which processed and stored the pressure and temperature data (Appendix G).

The explosion was also filmed through the circular windows on the front and back walls of the vessel. Using a color-Schlieren arrangement as shown in Fig. 5, an image of the density gradients in the gas in the vessel can be seen, enabling the flame front to be recorded. A light source using a 250 W quartz-tungsten-halogen bulb was used to illuminate the event in the vessel, and lenses were used to provide the required parallel light beam. The image was captured by a CCD video camera and fed to a video recorder. Thus the progression of the explosion event was recorded using high-quality S-VHS video.

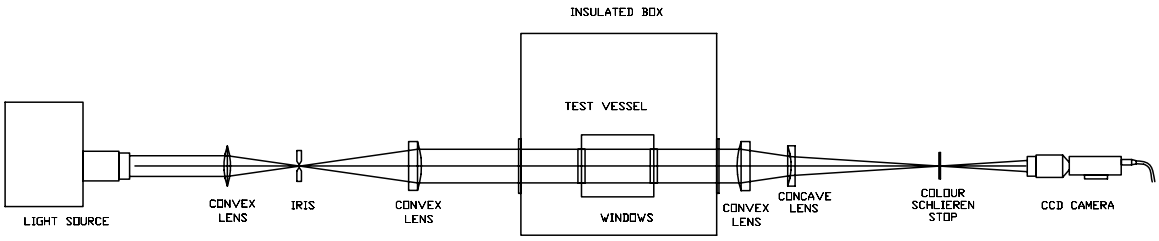

Figure 5: Schematic diagram of the color-Schlieren arrangement used to record the explosion event in the vessel.

2.3 Observation of ignition or failure

As in Shepherd et al. (1998), the ignition or failure to ignite following a spark discharge was observed through the pressure history and video recordings of the flame bubble inside the vessel. Successful ignition of a flame was accompanied with a rapid pressure increase within 0.5 sec to about 3 bar inside the vessel (Fig. 6a), while failure to ignite resulted in no measurable pressure rise after the spark. The temperature in the vapor space of the vessel was also observed to increase (Fig. 6b); however, the response of the thermocouple was not fast enough to follow the temperature rise of the flame, hence, the temperature history does not indicate true temperatures and only provides a confirmation of successful ignition.

The two columns of three video images in Fig. 7 show the processes of ignition or failure in the chamber. The left column frames (Fig. 7a) show the successive steps in an ignition failure process. The toroidal bubble of hot gas generated by the spark can be seen in the top frame.

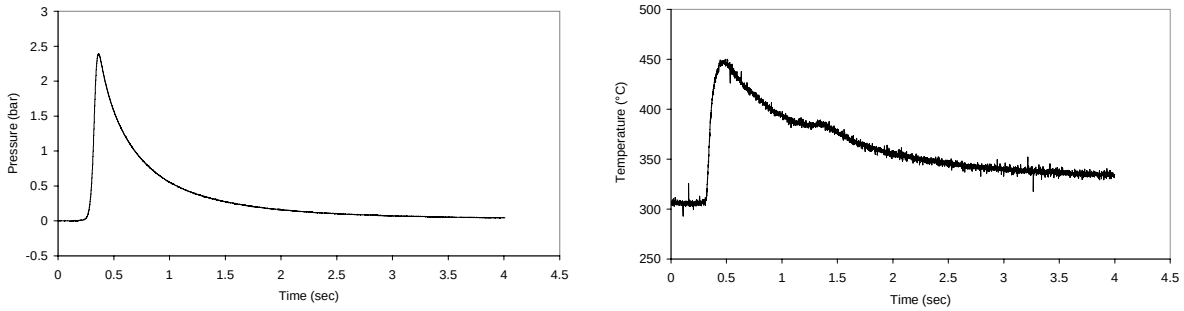

(a) (b)

Figure 6: The (a) pressure and (b) temperature histories of the successful ignition of the fuel-air vapor at 0.585 bar for mass-volume 35 kg/m^3 (80 ml) at 35.5°C (test# 197).

As time advances, the initial bubble loses definition (middle frame) and dissipates completely (bottom frame). The ignition process does not seem to be highly sensitive to the shape of the initial hot gas bubble, as failure also occurs for irregular bubble shapes with the same spark energy. The right column frames (Fig. 7b) show the successive steps in a successful ignition process. The irregularly-shaped bubble in the top frame grows and remains clearly defined in the middle frame and develops into a spherical flame bubble in the last frame. Only the edge of the flame bubble is visible in the last frame because the spark gap is not centered in the window view.

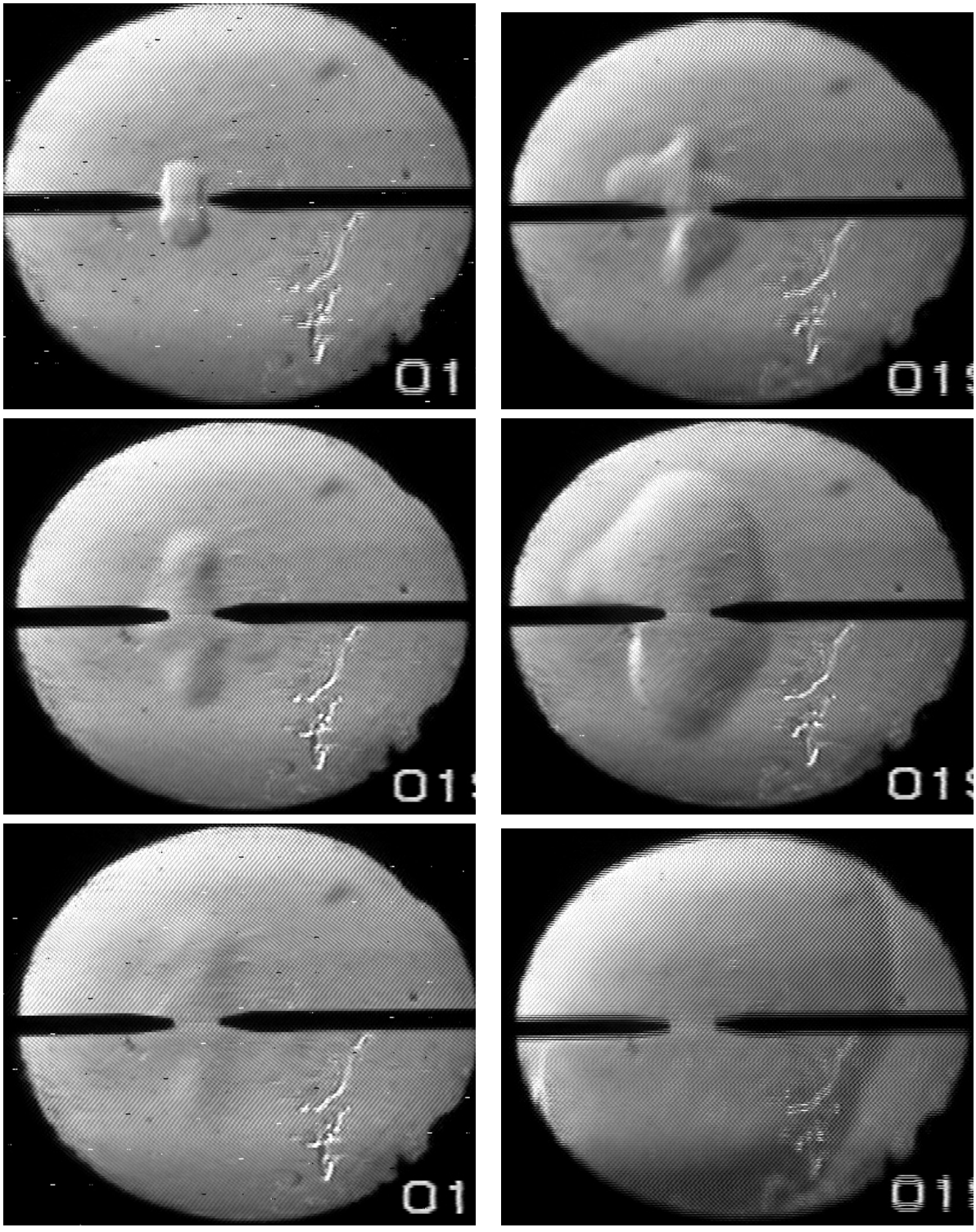

(a) (b)

Figure 7: Video frames showing (a) the failure of ignition (test# 193), and (b) successful ignition (test# 194). The two columns of three frames progress in time from top to bottom and time between frames is 2 ms

3 Development of an improved spark discharge system

In a flammable mixture of proper concentration and sufficient volume to support a self-propagating flame, ignition will occur if a source is capable of imparting sufficient energy to the mixture. The main theories of ignition propose that the critical energy for ignition is related to the energy required to form a flame kernel of a critical size. These theories have been reviewed and discussed in Shepherd et al. (1998). The most convenient way to deposit energy into a combustible system in a manner approaching an ideal point source configuration is to use an electrical spark discharge.

In the case of capacitive spark ignition, the main ignition mechanism involves a conversion of the stored electrical energy into heat which generates the flame kernel. This process of thermalization is very complex and is not fully understood though it has been the subject of many experimental and numerical studies (Kono et al. 1988; Borghese et al. 1988; Reinmann and Akram 1997). As discussed in these works, the process of ignition by a spark-generated kernel is highly complex involving many stages of development, and is therefore very sensitive to the manner in which the electrical energy is delivered to the spark gap.

Because the spark properties depend strongly on the electrical characteristics of the discharge circuit, the ignition energy also depends on the circuit parameters. A general review of the dependence of ignition energy on spark properties is found in Magison (1978). More recent studies by Kono et al. (1976) and Parker (1985) use modern electronic components such as transmission line elements to store the electrical energy and thyratrons for accurate high-speed switching to control the spark properties and provide a more meaningful quantitative measure of the spark energy. These studies indeed show that the ignition energy of propane-air mixtures depends on the duration of the spark, the size of the gap, the geometry of the electrodes, and the current and voltage histories of the spark.

In the present study, the circuit parameters such as capacitance, inductance, resistance, and switching were carefully controlled to obtain relatively smooth and repeatable voltage and current histories for the sparks. By so doing, the spark duration could be controlled and the spark voltage and current could be directly measured using a 500 MHz bandwidth oscilloscope. Thus, a quantitative measure of the energy dissipated in the spark could be calculated, eliminating the uncertainties associated with relying on the stored energy ($1/2CV^2$) as an estimate of the spark energy (Shepherd et al. 1998).

3.1 Description of spark circuit

3.1.1 Circuit operation

The spark circuit of the present system is the capacitive discharge circuit shown in Fig. 8. The electrical energy is stored in C1 which is charged to the desired voltage through the 4.7 MΩ resistor R1. In the present tests, either a 0.602 μF or a 0.0842 μF were used for C1. When the voltage across the electrodes rises to the charging voltage, the spark does not occur because the gap between the electrodes is large enough to prevent spontaneous breakdown across the gap. The breakdown voltage for the present electrodes is given for various gap sizes and different ambient pressures in Appendix B. In order to initiate the spark, a 30 kV pulse is generated by

the TM-11A. This pulse momentarily increases the voltage across the gap above the breakdown voltage and initiates the spark discharge. The diodes D1 and D2 each consist of thirty 1N4007 rectifier diodes. D1 prevents the spark discharge current from flowing back through the TM-11A, and D2 prevents the trigger pulse from flowing back into the capacitor and power supply. The resistors R2 and R3 provided damping for the capacitive discharge and varied the pulse duration. The negative electrode has a FB-43-5621 Amidon ferrite bead attached to its terminal. This ferrite bead provides a small amount of high frequency noise reduction.

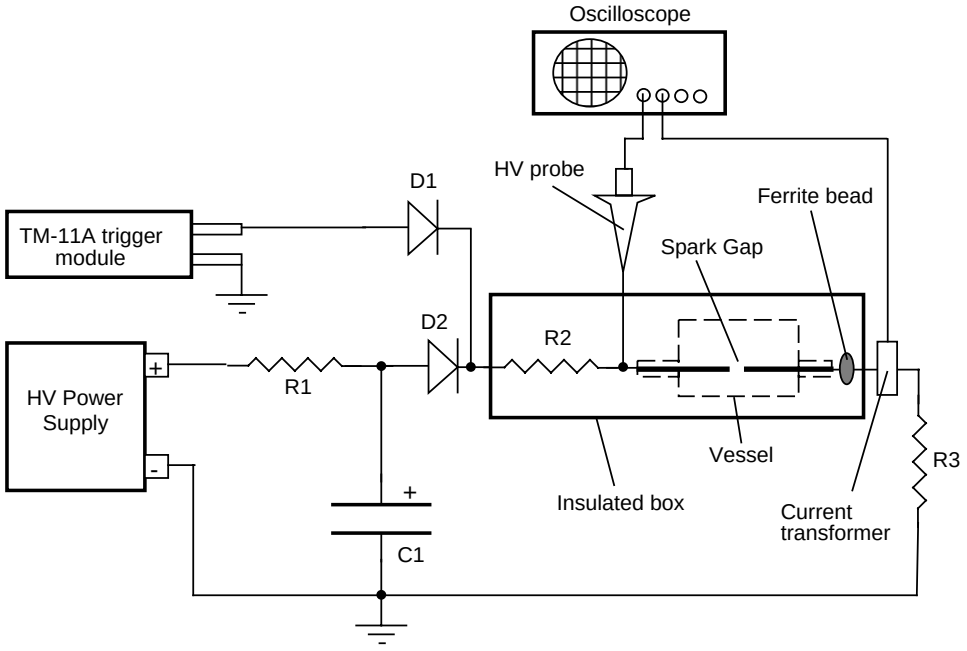

Figure 8: Circuit diagram of the discharge circuit used in the present work.

To obtain repeatable and reliable sparks, it was necessary to clean the electrode tips at least every 3 to 4 discharges. The tips were cleaned after every successful ignition of the fuel vapor. This was done by wiping the tips with acetone and then using ultra-fine sand paper to remove any remaining grit. This procedure was necessary because small amounts of deposits such as dirt or oxidation on the surface of the electrode tips could change their electrical properties. The biggest problem was the formation of a film of fuel on the tip by condensation or splashing. The fuel film acted as an insulator, changing the breakdown characteristics of the electrodes and ultimately the spark energy. Cleaning the tips before each test and making sure that the fuel in the vessel was heated more slowly than the air surrounding the vessel, minimized the effects of foreign substances coating the tips and changing the spark properties.

3.1.2 Voltage and current measurement

The voltage and current were directly measured in order to compute the discharge characteristics. The spark voltage is measured at the positive electrode terminal as shown in Fig. 9 using a high-voltage probe. Because of the damping resistor R3, the voltage drop across the spark

could not be measured between points B and C since the spark current would discharge into the ground return of the probe, causing a large shift in the offset of the oscilloscope. Instead, the voltage drop between B and E is measured, which is the drop across the spark and R3 in series. When this voltage is later used to calculate the spark energy, the energy dissipated by R3 is accounted for and subtracted from the total dissipated energy across both elements.

The voltage probe used was a Tektronics 6015A x1000 high voltage probe with an input resistance of 100 MΩ, an input capacitance of 3 pF, and a bandwidth of DC to 75 MHz (at the -3 dB point). The probe compensation was adjusted over a wide range of frequencies using a square wave generator (Appendix C).

The spark current was measured between points C and D (Fig. 9) using an Ion Physics CM-1-L current monitor. This transformer has a bandwidth of 0.2 Hz to 6 MHz and a nominal sensitivity of 0.01 Amp/Volt.

In verification tests of the energy dissipated by R3, an additional high voltage probe was used to measure the voltage drop across R3 alone by measuring the voltage between points D and E.

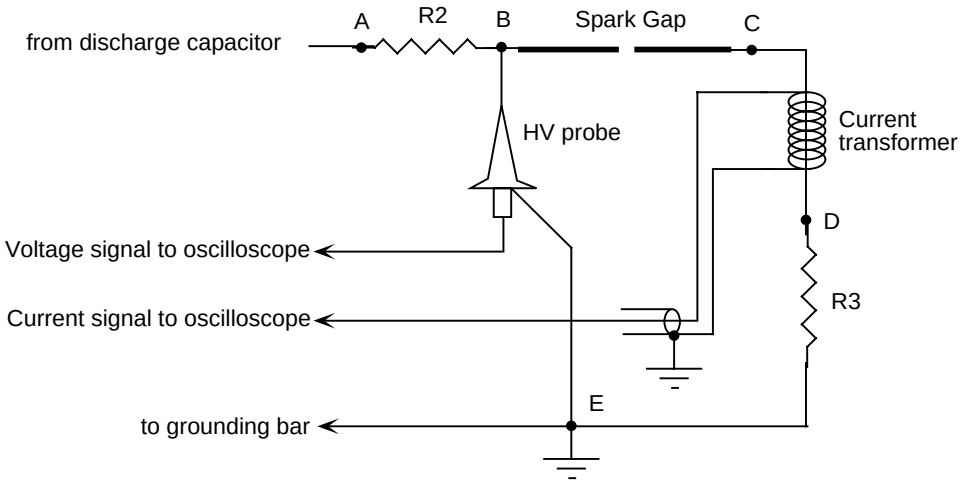

Figure 9: Circuit diagram showing the measurement arrangement of the voltage and current used in the spark energy calculation.

3.1.3 Signal recording

The signals from the voltage and current probes were recorded on a Tektronics TDS 640A digital storage oscilloscope with a bandwidth of 500MHz. The digitized signals were then transferred to a computer through the GPIB bus using a National Instruments AT-GPIB/TNT card for subsequent processing and analysis.

3.1.4 Damping resistors

As shown in Fig. 8, damping resistors were placed on the positive and negative electrodes. The resistors were placed as close as possible to the vessel in order to minimize the stray circuit

reactance seen by the spark gap. The resistors used in the present tests varied from 7.15Ω to 95.6Ω (Appendix D). The resistor values were chosen to damp the voltage and current histories and produce the desired pulse duration. Only carbon composition resistors having a solid carbon core (e.g. Allen-Bradley carbon composition type) or high power ceramic core resistors (e.g. Dale NH-series) were found adequate for this purpose. Due to the high voltages involved, wire-wound or resistive film resistors were found to arc internally and could not be used.

The damping resistors play several important roles in the discharge circuit. The main purpose of these resistors is to reduce high frequency oscillations in the spark current by providing damping during the spark discharge. In the absence of these resistors, the circuit is underdamped, resulting in relatively high frequency oscillations in the voltage and current flowing through the spark (Fig. 10). The voltage history in Fig. 10a shows the 0.602μF capacitor was charged to about 9 kV. The voltage suddenly drops as the capacitor spontaneously discharges and subsequently oscillates at a frequency of about 1 MHz. The current history in Fig. 10b shows that the current increases as current begins to flow through the spark and then oscillates at 1 MHz. For the smaller 0.0842μF, the frequency is higher. Although the 1 MHz oscillations shown in Fig. 10 are within the operating bandwidths of the voltage and current probes, they are close to the upper limit, particularly for the current transformer which has an upper limit of 6 MHz, and the resulting small phase shifts in the current and voltage can cause large errors in the amplitude of the power, rendering the spark energy calculation very inaccurate. For example, the ringing voltage and current of Fig. 10 resulted in a measured spark energy twice the stored energy which is clearly unrealistic.

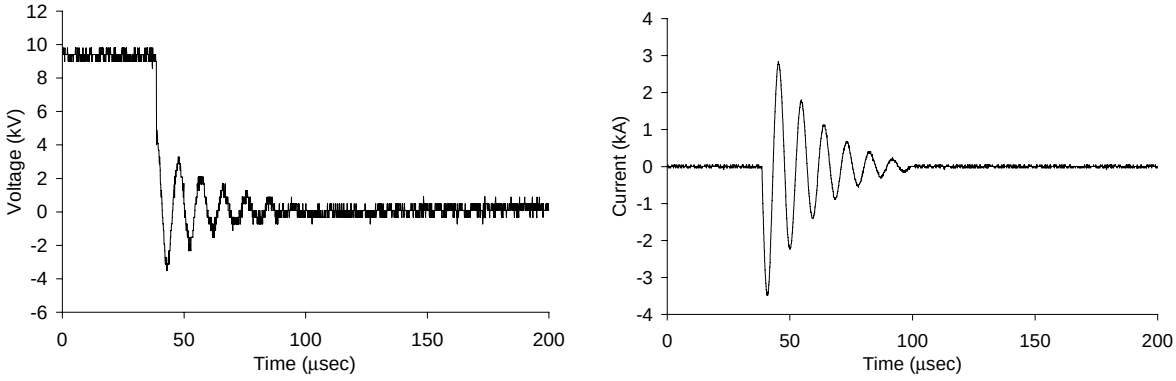

(a) (b)

Figure 10: The (a) voltage history and (b) current history of an underdamped spark resulting from the discharge of a 0.602μF capacitor.

With damping resistors, the damped spark discharge no longer contains high frequency components (Fig. 11). The voltage history in Fig. 11a starts at the charging voltage of 5.5 kV, then increases sharply due to the trigger pulse from the TM-11A. When the spark discharge occurs, the voltage drops sharply at first, then gradually as the capacitor discharges slowly through the damping resistors. The current history in Fig. 11b shows that the current increases sharply as the spark discharge begins, then decreases gradually. Since the voltage and current

histories are smooth and uniform, lacking high frequency components, they can be measured more accurately and more reliably.

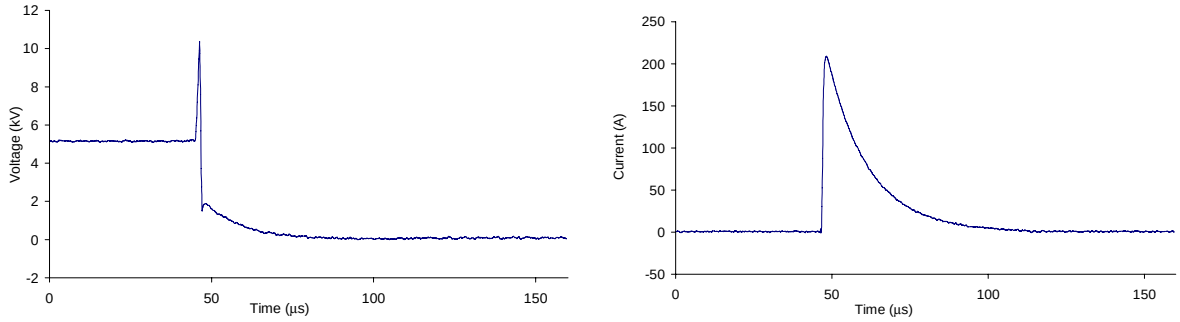

(a) (b)

Figure 11: The (a) voltage history and (b) current history of a damped spark resulting from the discharge of a 0.602μF capacitor with a 14.3Ω resistor on the positive electrode and a 7.15Ω resistor on the negative electrode providing the damping (test# 197).

Together with the discharge capacitor, the damping resistors form an RC discharge circuit that controls the duration of the spark discharge. The spark duration throughout the ignition energy tests (Appendix D) was between 20 μsec and 30 μsec.

Stray reactance (capacitance and inductance) in the circuit can also cause undesirable noise and high frequency oscillations, especially when the connecting wires are long. The presence of the damping resistors can alleviate this problem if properly positioned. By placing the resistors as close as possible to the electrode terminals located outside the vessel, they effectively dominate the circuit impedance seen by the spark. The only sources of stray reactance seen by the spark are the reactance of the electrodes from the tip to the terminal, and the reactance of the voltage and current probes, which are minimal. Hence, the positioning of the damping resistors as close as possible to the spark gap resistively decouples the spark from the stray circuit reactance and reduces spurious noise and oscillations in the voltage and current histories.

Finally, the damping resistors reduce the spark energy by dissipating part of the stored energy. Since the spark gap is in series with the damping resistors, the fraction of the stored energy dissipated by the gap depends on the ratio of the spark resistance (between points B and C in Fig. 9) to the total resistance (between points A and E in Fig. 9). The stored energy (E_{stored}) in the capacitor is given by:

$$E_{stored} = 1/2CV^2, \tag{1}$$

where C is the capacitance of the discharge capacitor C1 (Fig. 8) and V is the charging voltage across C1. If we assume that all the stored energy is dissipated in the resistive elements from point A to point E (Fig. 9), then the total energy dissipated (E_{total}) by definition is:

$$E_{total} = E = \int_0^\infty v(t)i(t)dt \approx E_{stored}, \tag{2}$$

where $v(t)$ is the voltage at point A during the discharge and $i(t)$ is the current through the circuit. Since the spark energy (E_{spark}) is:

$$E_{spark} = E = \int_0^\infty v_{spark}(t) i(t) dt, \tag{3}$$

where $v_{spark}(t)$ is the voltage across the spark which is given by:

$$v_{spark}(t) = \frac{v(t) R_{spark}}{R2 + R3 + R_{spark}}. \tag{4}$$

Equations 2 to 4 can be combined such that:

$$\frac{E_{spark}}{E_{stored}} = \frac{R_{spark}}{R2 + R3 + R_{spark}}. \tag{5}$$

However, since the spark resistance varies with time and with the current, simple circuit analysis above cannot be used to determine the fraction of stored energy dissipated in the spark. Only direct measurement of the current and voltage histories of the spark are adequate to estimate the spark energy.

3.2 Spark energy measurement

3.2.1 Signal processing and calibration

Once the voltage and current histories are transferred to a computer (cf. 3.1.3), they are processed by a program written in LabView^{TM} (Appendix H) for conversion into the proper units and calculation of the spark power and energy. Several steps of signal processing are required before the signals can be analyzed.

To convert the raw voltage signal from the oscilloscope into actual volts, the signal is multiplied by 996, the attenuation factor measured during the probe calibration test (Appendix C). The raw current signal is converted into amperes by dividing it by .01016 V/A, the current transformer sensitivity at 50 kHz given by the frequency curve supplied by the manufacturer. This frequency was chosen by considering a typical spark pulse duration of approximately 20 μs as the period of a wave.

Before each actual spark test, it was found necessary to perform a calibration test by replacing the spark gap with a mechanical switch outside the vessel. The switch provided an alternate discharge path to the spark gap to allow testing of the spark energy measurement system without producing a spark in the vessel. The high voltage probe was moved from point B to point D (Fig. 9) to measure the voltage across R3 during the discharge. In this way the system was calibrated by measuring the energy dissipated across R3 only. The value of the relatively small DC offset (typically zero to 20 V compared to the spark voltages above 1 kV) generated by the mutually-induced electrostatic potential difference in the cables could be measured during this calibration test (Appendix F) and later subtracted from the measured voltage signal during an actual spark measurement.

During an actual spark energy measurement with the voltage probe at point B (Fig. 9), the energy calculation program (Appendix H) would calculate the energy dissipated by the spark gap and R3 together, then subtract the energy dissipated by R3 alone. During the calibration test, the voltage probe is only measuring the voltage across R3, hence the spark gap is bypassed and the program should calculate zero energy after subtracting the R3 energy. In practice the program does not calculate a value of zero due to small frequency response errors in the voltage and current measurements. To solve this problem, the value of R3 entered in the spark measurement program (Appendix H) was adjusted until the energy difference was zero. This preliminary calibration procedure before each test increased the accuracy of the voltage measurement and reduced the error in the spark energy calculation.

A final step of signal processing is performed on the voltage and current histories before they are used for the spark energy calculation. A ten-point moving average is applied to the voltage and current waveforms in order to reduce high-frequency random noise in the signals.

3.2.2 Spark energy calculation

The energy dissipated by the spark is calculated by integrating the power over time. The spark power $P(t)$ was obtained by multiplying the voltage history $v(t)$ and the current history $i(t)$:

$$P(t) = v(t)i(t), \tag{6}$$

then the power is integrated over time:

$$E = \int_0^\infty v(t)i(t)dt. \tag{7}$$

A typical spark energy determination from the voltage and current histories of Fig. 11 is shown in Figs. 12 and 13. The power consumed by the spark and the negative terminal resistor R3 in series is calculated by multiplying the voltage ($v_{SR3}(t)$) measured between point B and the ground at point E (Fig. 9) with the current ($i(t)$) through the spark loop. This power is:

$$P_{SR3}(t) = v_{SR3}(t)i(t), \tag{8}$$

and is represented by the gray line in Fig. 12. The thin solid line represents the power consumed by the resistor R3 and was obtained using:

$$P_{R3}(t) = i(t)^2(R3). \tag{9}$$

The energy dissipated by the resistor R3 and spark together (E_{SR3}) can be obtained by integrating the power P_{SR3} over time:

$$E_{SR3} = \int_0^\infty P_{SR3}(t)dt, \tag{10}$$

and is represented by the gray line in Fig. 13. The initial part of the energy curve from zero to about 45 μs increases slightly in a linear fashion. This occurs in the power calculation because

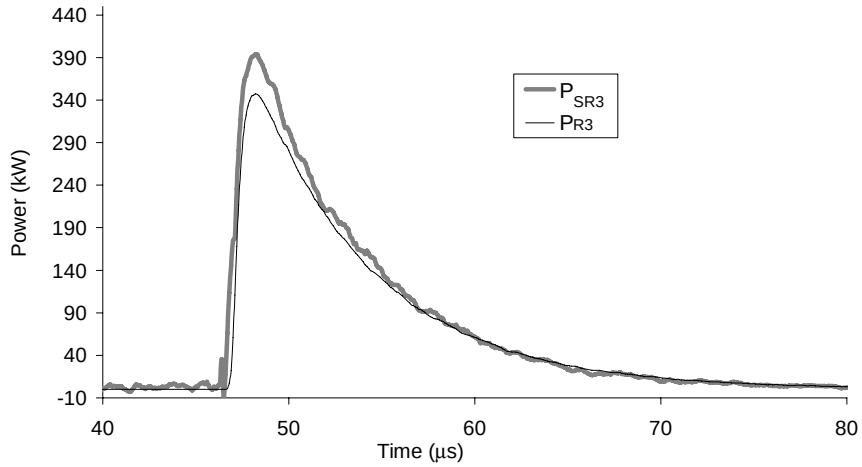

Figure 12: The power consumed by the spark and the resistor (R3) together (P_{SR3}), and the power consumed by R3 alone (P_{R3}). The power histories shown are for test# 197, the discharge of a 0.602 μF capacitor charged to 5.5 kV with a 14.3 Ω resistor on the positive electrode and a 7.15 Ω resistor on the negative electrode.

a small positive bias in the current (Fig. 11b) is strongly amplified when multiplied by the large DC component (5.5 kV) in the voltage (Fig. 11a). The energy dissipated by R3 alone (E_{R3}) is:

$$E_{R3} = \int_0^\infty P_{R3}(t)dt, \tag{11}$$

and is represented by the solid thin line in Fig. 13. The energy dissipated by the spark (E_{spark})

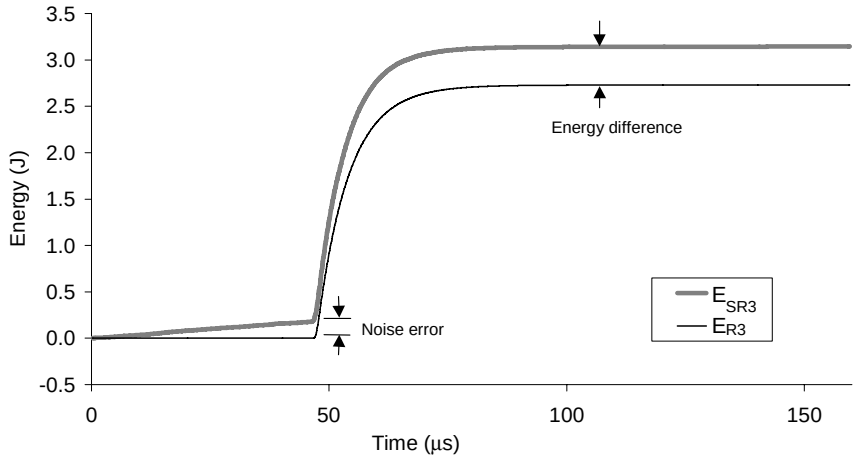

Figure 13: The energy dissipated by the spark and the resistor (R3) together (E_{SR3}), and the energy dissipated by R3 alone (E_{R3}). The dissipated energies shown are for test# 197, the discharge of a 0.602 μF capacitor charged to 5.5 kV with a 14.3 Ω resistor on the positive electrode and a 7.15 Ω resistor on the negative electrode.

is thus the energy difference between E_{SR3} and E_{R3} correcting for the noise error (N_{err}):

$$E_{spark} = E_{SR3} - E_{R3} - N_{err}. \tag{12}$$

The spark energy (E_{spark}) for test# 197 shown in Figs. 11, 12, and 13 is 0.023 J.

In order to verify the previously described method of computing the spark energy, the energy dissipated by R3 (E_{R3}) was calculated by an alternate method. A second compensated high voltage probe was placed directly on the negative electrode, directly measuring the voltage across R3 (between points D and E of Fig. 9). Hence the power (P'_{R3}) across R3 is given by:

$$P'_{R3}(t) = v_{R3}(t)i(t), \tag{13}$$

where v_{R3} is the voltage across R3. The energy dissipated by R3 (E'_{R3}) is:

$$E'_{R3} = \int_0^\infty P'_{R3}(t)dt. \tag{14}$$

As before, the spark energy is determined using Eq. 12 but substituting E'_{R3} for E_{R3}. For all cases using this alternate method, the spark energy was no more than 3% from the spark energy computed by the previous method, hence providing some confidence in the validity of the energy determination method.

4 Statistical variation of ignition energy measurements

The present ignition energy experiment constitutes a type of sensitivity test. In sensitivity experiments, the critical level of stimulus that produces a certain response in a test sample is measured. For example, typical sensitivity experiments include the measurement of the critical height from which a weight is dropped onto an explosive that will cause ignition, or the critical dose of insecticide necessary to kill a certain type of insect.

In the present testing, the stimulus level is the measured spark discharge energy. The critical value of energy required for ignition is the desired result of the testing. The result of any one test is either a “go” (ignition) or “nogo” (no ignition). Due the statistical nature of the near-limit ignition process, energy levels for “go” and “nogo” results will overlap in repeat trials at nominally identical initial conditions. This gives the appearance of scatter in the data and makes the critical energy for ignition ambiguous.

Because the critical level of stimulus is not clear-cut, it is necessary to find the statistical properties of the response of the test sample to different levels of stimulus. These statistical methods are particularly useful in hazard assessments. In the common drop-weight sensitivity test for explosives, many statistical methods have been developed to estimate the mean value of the critical height where the explosive has a 50% probability of igniting, as well as the standard deviation of the mean value (Dixon and Massey Jr. 1983).

Previous studies on gaseous ignition usually do not report [1] statistical data related to measurements of the critical energy level. In order to place the determination of ignition energy on a firmer statistical basis, we have investigated several methods of analyzing our ignition energy data. The statistical methods examined include the Bruceton Test, the One-Shot method, and the “Method of Minimum Contradictoriness” (Zukas and Walters 1998). Although the first two techniques were unsuccessful, the last was used to find the median value (with a 50% probability of “go” or “no go”) of the logarithm of the spark energy. As a practical matter, too few data are available in most cases for the statistical methods to provide meaningful results. For that reason, we have resorted to a graphical method based on using the highest “nogo” and lowest “go” results in order to simply characterize the data.

4.1 Bruceton Test

The most widely used method to calculate the statistical properties of explosive testing is the “Bruceton Staircase Technique” (Zukas and Walters 1998) also called the “Up and Down” method (Dixon and Massey Jr. 1983). This method applies to sensitivity tests where the result is “go” or “no go”, where “go” corresponds to a successful ignition after a certain stimulus and “no go” corresponds to a failure to ignite after a certain stimulus. In Bruceton testing, the conditions of the next test depend on the result of the previous test. First the size of the interval between the stimulus levels must be chosen so that the stimulus level can be increased or decreased incrementally. If a ”go” is obtained when testing a sample with a certain stimulus level, the stimulus level is decreased by one interval for the next test. If a “no go” is obtained,

[1] One notable exception is the study of Plummer (1992) which examined the statistical fluctuations in a large data set associated with minimum ignition energy testing in mixtures of JP-8 and air.

the stimulus is increased by one interval. The test proceeds until a sufficient number of tests has been performed to obtain meaningful statistics. The required number of tests is typically large (50-100 as in Sandia National Laboratories 1990), but it has been suggested that reliable results can be obtained for explosive tests with only 20 tests (Zukas and Walters 1998). Special techniques have been developed to obtain statistical properties with as little as 10 to 15 tests (Dixon and Massey Jr. 1983), but they usually require prior knowledge of the approximate values of the statistical properties. Once an adequate number of tests has been performed, the results can be analyzed to obtain the median value of the stimulus level, i.e., the stimulus level with a 50% probability of producing a "go" or a "no go", and the standard deviation. For the case where the distribution of the stimulus levels is normal, the mean is equal to the median.

For the Bruceton technique to be applicable, the data must meet certain conditions (Dixon and Massey Jr. 1983; Zukas and Walters 1998):

- the test variable or stimulus level should be normally distributed,
- the interval between test variable values must be fixed and smaller than twice the standard deviation,
- each test should be carried out on a new sample to eliminate "explosive memory effect",
- a statistically significant number of tests needs to be conducted,
- the criteria of judgement between "go" and "no go" should be consistent.

4.2 "One-Shot" Method

The "One-Shot" or "Langlie" method (Langlie 1962) has also been used successfully for explosive tests (Sandia National Laboratories 1990). The stimulus level of the next test is determined by the results of previous tests using a more sophisticated rule than the Bruceton test. This method has the advantage that the interval between the stimulus levels need not be chosen a priori. The test data must otherwise meet the same conditions as in the Bruceton test, in particular, that the test variable must be normally distributed. The One-Shot test can also provide reliable statistics for a relatively small number of tests (10 to 15).

The "One-Shot method" (Langlie 1962) was chosen to analyze the statistical properties of the ignition energy experiment. This method requires a minimal number of a priori assumptions to be made regarding the statistical properties of the experiment. The minimum and maximum stimulus defining the limiting values within which the test stimuli are distributed must be chosen. The stimulus levels are determined by the test method. The stimulus level for a test is found by counting backwards through the previous tests until an equal number of "go" and "no go" results are found, then the average between the level of this test and the last test performed is used as the level for the next test. If an equal number of "go" and "no go" results cannot be found, then the average between the level of the last test and the limiting level (the lower limit if the last test is a "go", and the upper limit if the last test is a "no go") is used. The One-Shot method can provide meaningful statistics after 10 to 15 tests have been performed.

To use the One-Shot method, a test variable that is normally distributed in the experiment should be chosen. In the drop-weight explosive test, the logarithm of the drop height has been found to have a normal distribution (Sandia National Laboratories 1990). It is assumed in the present experiments that the ignition energy is analogous to the drop height and that the logarithm of the spark energy has a normal distribution in this experiment.

4.2.1 The ignition energy test series

Tests following the One-Shot method were performed on ARCO Jet A with a flash point of 46.4°C (Shepherd et al. 1999) at a pressure of 0.585 bar, the atmospheric pressure at an altitude of 14 kft (Shepherd et al. 1997), and a mass-volume ratio of 200 kg/m^3. This mass-volume ratio corresponds to a quarter-full vessel (about 460 ml) where the level of the fuel is just below the vessel window. The spark energy was varied between 8 mJ and 150 mJ and the spark gap was 5.4 mm. Two successive series of tests were performed with two fresh batches of fuel: tests# 134 to 146, and tests# 147 to 164 (Appendix D). The two series were combined to form a single One-Shot test series totaling 25 tests as shown in Fig. 14. The "go" points represent a successful flame ignition by the spark, and the "no go" points represent a failure to ignite by the spark. The results of 25 tests are shown for various spark energies following the One-Shot procedure.

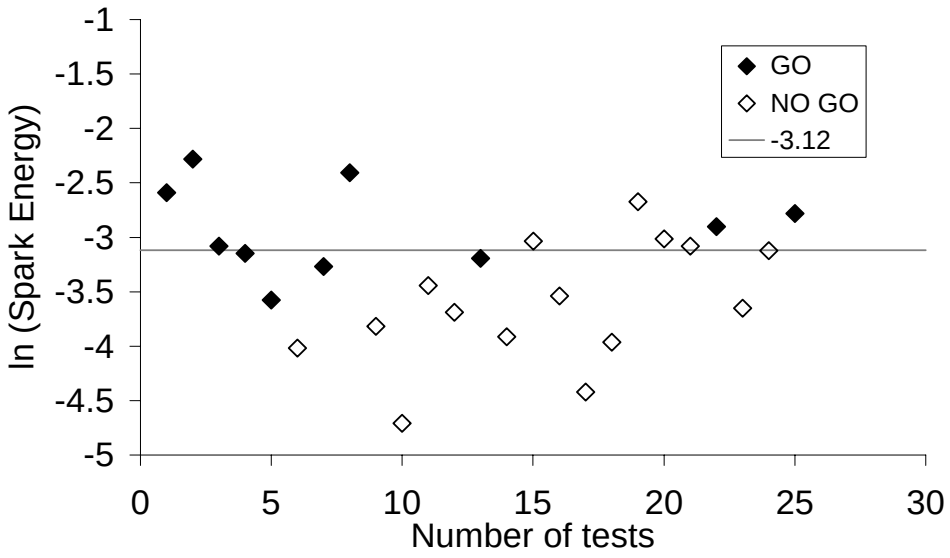

Figure 14: The series of ignition energy tests performed for a One-Shot series at 38°C or 39°C 0.585 bar, for a quarter-full vessel (200 kg/m^3). The median value of -3.12 is also shown.

4.2.2 Estimate of median value of the ignition energy

The median value of the ignition energy was calculated using the "Method of Minimum Contradictoriness" described in Zukas and Walters (1998). If we assume a certain median value

for the spark energy, a “no go” result for a test at a spark energy above the median is contradictory, and a “go” result at a spark energy below the median is also contradictory. The method searches for a median value by minimizing the number of contradictory results. This is achieved by seeking the minimum of the function F_x:

$$F_x = \sum (x_c - x)^2, \tag{15}$$

where x is the value of the assumed median and x_c is the value of a contradictory result. The function F_x reaches a minimum at the median value where the number of contradictory results is minimized.

The function F_x is shown for the logarithm of the spark energies (Fig. 14) in Fig. 15. The median value is -3.12 at the minimum, corresponding to an energy of 44 mJ. Hence, the median ignition energy for the Jet A at a pressure of 0.585 bar, 200 kg/m^3, and a temperature between 38°C and 39°C is about 44 mJ. The median value of -3.12 is also shown in Fig. 14.

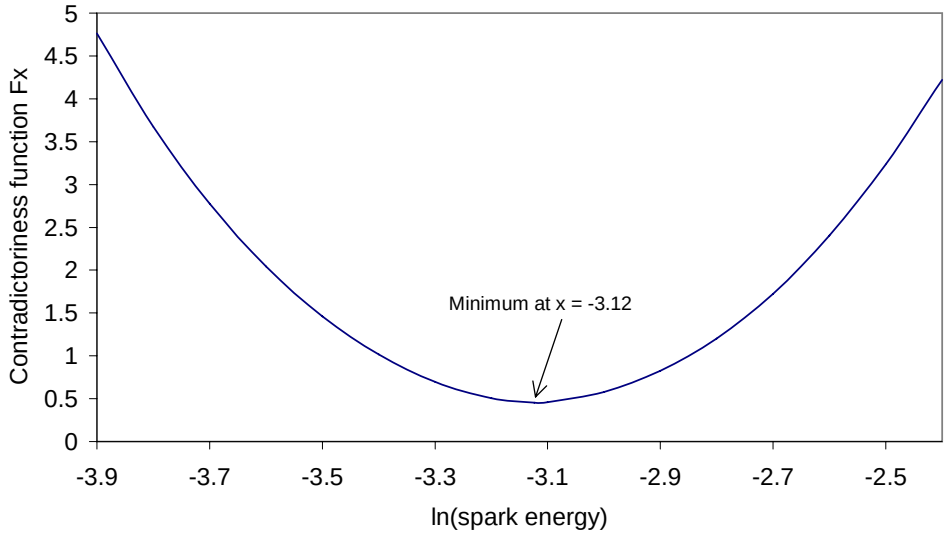

Figure 15: The “contradictoriness” function F_x for the logarithm on the spark energy (Fig. 14).

4.2.3 One-Shot analysis methodology

The One-Shot analysis (Langlie 1962) method did not converge when applied to the test data shown in Fig. 14. Apparently, our ignition energy data does not satisfy the criteria for the analysis, but the reasons for this are not yet clear. Possible reasons are that: the chosen test variable, the logarithm of the spark energy, may not have a normal distribution; there was too much scatter and bias in the spark energies to adequately represent the statistical properties of the experiment; the amount of data may have been insufficient. Corrections were made for systematic errors in the test data such as temperature discrepancies between different tests, fuel weathering in the vessel, and the unequal number of “go and “no go” results, as described in detail in Appendix I, but convergence was not obtained. Further investigation of the statistical

properties of the ignition energy would likely require a larger number of data points (e.g. 50 to 100) as in the Sandia National Laboratories (1990) study. This was not feasible for the present study.

5 Ignition energy tests

In previous ignition energy tests reported in Shepherd et al. (1998), the fuel used was commercial Jet A purchased from Los Angeles International Airport (LAX). In this study, the ignition tests were performed on Jet A fuel supplied directly from ARCO (DeJovine 1998). The commercial Jet A from ARCO was called “base fuel” and had an average measured flash point of 46.4°C (Shepherd et al. 1999). A 55 gallon drum of base fuel was manufactured and delivered to Caltech by ARCO in the Fall of 1998. This fuel was also used in a series of tests in the quarter-scale test facility in Denver, CO (Shepherd et al. 1998; Brown et al. 1999). The fuel vapor composition was analyzed by Woodrow and Seiber (1999), and its thermodynamic properties and composition are discussed in Shepherd et al. (1999). Fuel from this same drum was used throughout the present ignition energy tests.

5.1 Ignition energy dependence on temperature

The ignition energy was measured for high mass-volume ratios of 35 kg/m^3 (80 ml) and 200 kg/m^3 (460 ml) at a pressure of 0.585 bar between about 33°C and 40°C. For this range of temperatures, the ignition energy was found to decrease sharply from 300 mJ at about 35°C to 10 mJ at about 40°C, as shown in Fig. 16. The raw data of the ignition energy measurement is shown with the spark energies where ignition occurred (”go”) and where failure of ignition occurred (”no go”). Note that the 40°C upper limit of the temperature range is due to the lower limit of about 10 mJ that can be measured with the ignition circuit used in the present experiments. Higher temperatures, up to 60°C in some locations within the center wing tank of a 747, are of interest but these could not be examined with present apparatus. Simple linear extrapolation of the trend shown in Fig. 16 indicates that the ignition energy is about 1 mJ at 43°C. The U-shaped dependence of ignition energy on composition (see Section 4 of Shepherd et al. 1998), implies that that the ignition energy will be less than 1 mJ for temperatures higher than 43°C up to some maximum temperature associated with creating a too rich mixture.

Tests were performed at a mass-volume ratio of 35 kg/m^3 in order to shorten the fuel filling procedure. At this ratio, there was 80 ml of fuel forming a layer about 8 mm thick which is sufficient to submerge the magnetic mixing rod. Figure 16 shows that there is no apparent difference in the ignition energy between 35 kg/m^3 and 200 kg/m^3. This is consistent with Jet A ignition energy experiments by Lee (1999) which show that the ignition energy is only affected by the mass-volume ratio below about 5 kg/m^3 where the ignition temperature at a fixed spark energy increases as the mass-volume ratio decreases. Tests at 35 kg/m^3 are thus assumed to adequately represent the combustion properties of Jet A at high mass-volume ratios where the effects of depletion of lighter components is minimal (Shepherd et al. 1997). Experiments were henceforth conducted with this smaller, more convenient, quantity of fuel, and results at mass-volume ratios of 35 kg/m^3 or 200 kg/m^3 are grouped together and referred to as “high mass-volume ratio” or “high M/V”.

The raw ignition energy results (Fig. 16) can be represented more clearly by showing only the data points representing the highest “no go” results and the lowest “go” results as well as limit lines, as shown in Fig. 17. The limit lines are exponential fits to the highest ”no go”

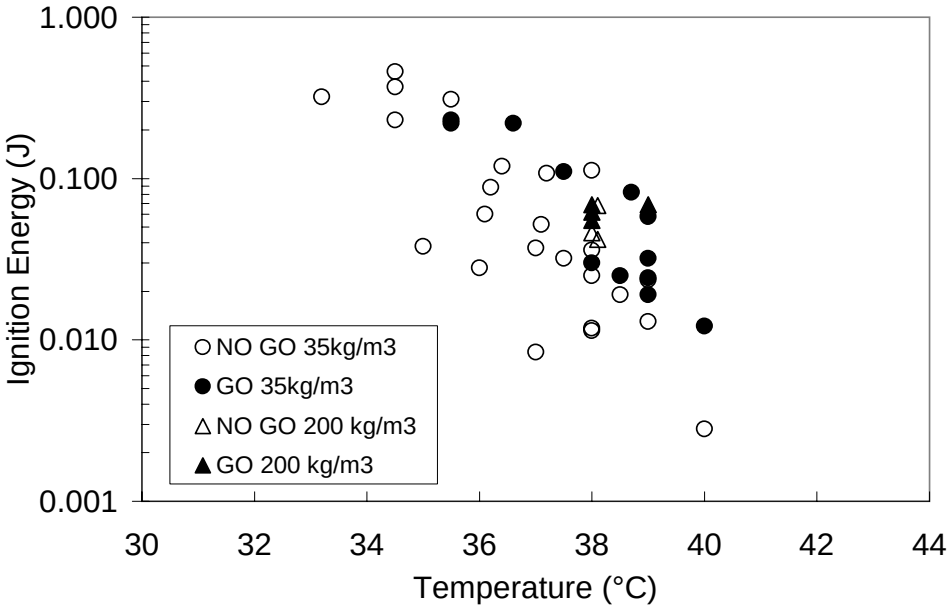

Figure 16: The dependence of ignition energy on temperature for ARCO Jet A (flash point temperature T_{fp} =46.4°C) at 0.585 bar for mass-volume ratios (M/V) of 35 kg/m^3 and 200 kg/m^3.

results and the lowest "go" results. The equations describing these fits are:

$$y_{nogo} = 10^{11} e^{-0.757T}, \tag{16}$$

where y_{nogo} is the spark energy (J) for the "no go" results and T is the temperature (°C), and

$$y_{go} = 5 \cdot 10^{8} e^{-0.602T}, \tag{17}$$

where y_{go} is the spark energy (J) for the "go" results and T is the temperature (°C). The shaded region between these two lines can be interpreted as a band of uncertainty separating the regions of a non-flammable mixture and a flammable mixture (Fig. 18), i.e., the region to the left of the band represents non-flammable mixtures, the region to the right of the band represents flammable mixtures, and the region within the band represents mixtures that may or may not ignite at the corresponding spark energies.

The present ignition energy results are shown together with previous measurements with LAX Jet A at 200 kg/m^3 (Shepherd et al. 1998) in Fig. 19. The band of uncertainty for the present measurements with measured spark energies is shown with the ignition energy results previously obtained using the stored capacitor energy. The trend of rapidly decreasing ignition energy with increasing temperature is similar in both sets of experiments. It is apparent that the measured spark energies are lower than the stored capacitor energies, which is in agreement with spark discharge studies suggesting that only a fraction of the stored capacitor energy is dissipated in short-duration sparks (Grenich and Tolle 1983). Some reasons for the observed differences are: 1) there may be residual charge left on the capacitor; 2) a very short (ns) duration discharge is much less effective than a longer (20-50 μs) one; 3) the differences in

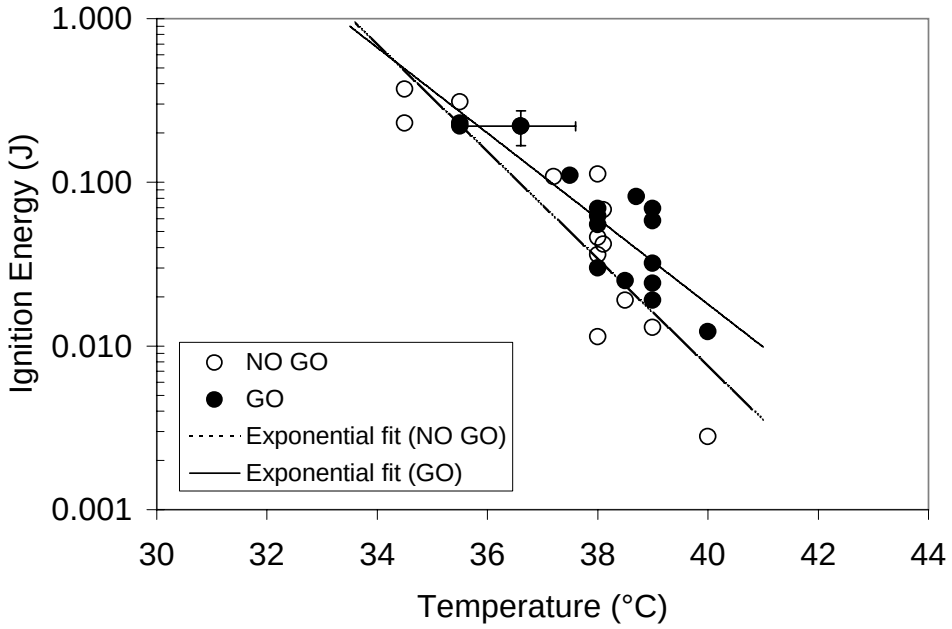

Figure 17: The dependence of ignition energy on temperature for ARCO Jet A (flash point temperature T_{fp} =46.4°C) at 0.585 bar for high M/V showing limit lines obtained from exponential fits to the highest "no go" results and the lowest "go" results. The error bars shown on one of the points indicate the maximum range of uncertainty as discussed in Section 5.1.1.

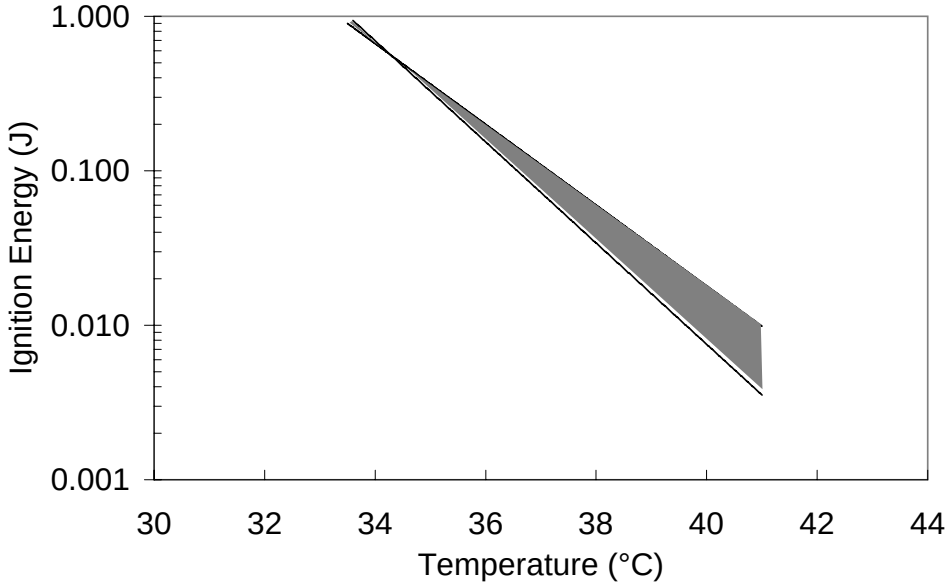

Figure 18: The dependence of ignition energy on temperature for ARCO Jet A (flash point temperature T_{fp} =46.4°C) at 0.585 bar for high M/V showing the band of uncertainty between the limit lines.

efficiency of overdamped vs underdamped discharge circuits. Although the trends are similar in the two data sets, only the present results with measured energy are quantitatively useful.

The results from the two experiments cannot be compared further because of the insufficient amount of data in previous measurements, and the important differences between the two apparatus and the spark generating circuits. The present experimental set up differs from the previous one in that the gap size is 5.4 mm rather than 3.3 mm, the electrode tip geometry is partially conical rather than rounded, damping resistors were used, completely changing the electrical characteristics of the spark, and a TM-11A trigger system was used instead of a mechanical switch. The most important difference in the present system is that the energy dissipated in the spark is measured directly, providing a more quantitative measure of the strength of the ignition source.

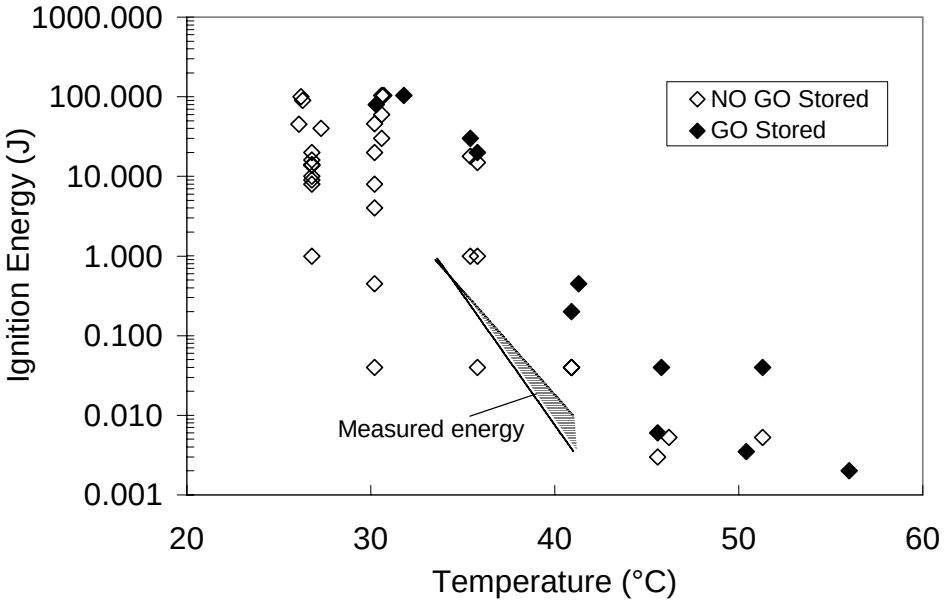

Figure 19: The band of uncertainty between the limit lines showing the present ignition energy measurements at 0.585 bar for high M/V shown with previous ignition energy results from Shepherd et al. (1998).

5.1.1 Uncertainty of the ignition energy measurements

The absolute error in the ignition energy cannot be determined because independent measurements of the spark energy cannot be made. Miniature calorimeter measurements have been attempted (Reinmann and Akram 1997), but the error in the accuracy of the instrument was large. Furthermore, the relationship between the measured ignition energy and the theoretical ignition energy developed in ignition models (Litchfield 1960; Lewis and von Elbe 1961) has not yet been determined. Nevertheless, the dissipated spark energy measured in this study provides a quantitative measure of the energy deposited into the system by a spark. The present method is an improvement over the stored electrical energy estimate (e.g. $1/2CV^2$) since it

eliminates uncertainty in the results caused by random discharge effects such as shot-to-shot variations due to changes in the electrode tip surface, bad connections, and changes in the breakdown properties of the test mixture. The error in the spark energy measurements is due mainly to uncertainty associated with various components in the spark measurement system.

The main sources of error in the ignition energy measurements come from: the accuracy of the thermocouples, the accuracy of the pressure gauge used to measure the initial pressure, the accuracy of the scale used to measure the quantity of fuel, the accuracy of the voltage and current probes, the quantization error in the oscilloscope, the quantization error in the processing of the signals, and the statistical scatter in measurements of the offsets used in the data processing programs.

There are two sources of uncertainty and error in the temperature measurements. First, the temperature within the vessel may be nonuniform. Second, the thermocouples and read-out systems are imperfect. Substantial efforts were made to insure temperature uniformity in and around the test vessel. The entire apparatus was enclosed in an insulated box through which was circulated hot air. The test vessel was heated by electrical heaters connected to a control system. The liquid in the interior of the vessel was stirred constantly during the test. We measured the temperatures of the liquid and the vapor space in the vessel, and they were the same (within the meter accuracy of 0.1°C). There are three thermocouples: on the vessel surface (outside, on the bottom plate), in the vessel (in the vapor space), and in the insulated box air space (far right hand corner). We never observed a temperature difference of more than 0.5°C between the three. The output of the thermocouple in the box fluctuated constantly by about $\pm$0.3°C. These fluctuations were very rapid (the reading changed 3 or 4 times a second), so we suspect that it was caused by noise pickup on the thermocouple line rather than actual temperature variations.

The thermocouples used in the present system have an accuracy of about $\pm$1°C. This value represents the variation between different thermocouples of this type relative to an absolute temperature measurement. The absolute uncertainty in the temperature measurements is therefore $\pm$1°C. For a single thermocouple, there can therefore be a systematic error of up to $\pm$1°C relative to the absolute temperature. However, the measurement uncertainty associated with a single thermocouple is much smaller, at approximately $\pm$0.1°C which is the meter accuracy. The value of $\pm$1°C thus represents a conservative estimate of the uncertainty in the temperature measurement. Errors associated to the test mixture are due to the MKS pressure gauge which has an accuracy of $\pm$0.1 Torr, and the electronic scale used to measure the fuel which has an accuracy of $\pm$0.01 g. A more realistic evaluation of the error in the fuel quantity would be $\pm$0.1 g, since small quantities of fuel can be lost during the syringe handling procedure.

Evaluating the uncertainty in the ignition energy is more involved due to the complexity of the voltage and current signals and the finite bandwidth of the measurement probes, but a rough estimate can be made by considering each source of uncertainty. Accuracy errors from the voltage and current probes cause a relatively small error in the spark energy. The voltage probe has an accuracy of:

- 25% p-p for the first 200 ns
- $<$10% p-p after 200 ns

- $\pm$5% after the first 400 ns

- DC attenuation: 0.018%/kV

Since only about 3% of the spark energy is dissipated during the first 400 ns of the discharge (Fig. 13), the uncertainty in the spark energy due to the probes is mostly due to error in the voltage measurement after 400 ns, i.e., about $\pm$5%. This value is an upper bound since the voltage pulse changes slowly after the first 5 μs (Fig. 11a) so the error is probably closer to the DC attenuation error for the later part of the signal (less 0.1%). The single-frequency accuracy of the current transformer is 0.5%, and does not contribute much error to the spark energy. An upper bound for the uncertainty in the spark energy resulting from the measurement probes can therefore be estimated at $\pm$5%.

The DC offset used in the spark calculation (Appendix H) was measured in over 80 calibration tests at different circuit conditions and was found to have a standard deviation of about $\pm$150%. This corresponds to an error in the spark energy of less than 2%. The value of R3 used in the energy calculation program (R3 is called R_{neg} in the program: Appendix H) has also been determined through over 80 calibration tests and was found to have a standard deviation of $\pm$0.6%. This corresponds to an error in the spark energy of less than 3%.

Finally, the largest source of error in the spark energy measurement comes from quantization errors. Since the voltage and current is recorded digitally by an oscilloscope, there is an uncertainty of $\pm\frac{1}{2}$ LSB (Least Significant Bit). The LSB error is about $\pm$7% for both E_{SR3} and E_{R3} (Fig. 13), resulting in a total uncertainty of $\pm$14% for the spark energy.

In summary, the above estimate for an upper bound for the total uncertainty of the ignition energy due to measurement errors is approximately $\pm$24%. The maximum uncertainty in the temperature is approximately $\pm$1°C. These maximum uncertainty values are shown as error bars on one of the ignition energy data points in Fig. 17.

The instrument errors discussed above describe the uncertainty in the values of the measured properties of the data, however the uncertainty in the ignition limit also depends on the inherent randomness of the ignition phenomenon. Since the ignition energy is a limit phenomenon, it is sensitive to very small experimental variations such as the spark kernel geometry or even small movements of the mixture gas and is therefore unstable. There is an uncertainty in the ignition energy due to the intrinsic statistical fluctuations of the ignition threshold due to the unstable nature of the phenomenon. Analysis of these statistical fluctuations is discussed in Section 4.2.3.

The limit lines (Fig. 17) and corresponding band of uncertainty (Fig. 18) were chosen as a method of representing the intrinsic statistical properties of the ignition energy data. However, this representation cannot be interpreted quantitatively, since there is insufficient data to accurately determine the statistical properties (see Section 4.2.3). For example, if the statistical properties were known, limit lines representing a 10% probability of "go" and a 10% probability of "no go" could be used to define the band of uncertainty. At present, the band of uncertainty shown in Fig. 18 represents a semi-quantitative guideline to describe the trend of the ignition energy curve, i.e., the spark ignition limit.

5.2 Ignition energy dependence on mass-volume ratio

Previous data on the ignition energy at different mass-volume ratios (Shepherd et al. 1998) was insufficient to determine an influence of the mass-volume ratio on the ignition energy. Due to the small number of data points and the wide scatter of the data, a mass-volume effect could not be distinguished.

Since the base fuel at a low mass-volume ratio was found to have a different composition and vapor pressure than high mass-volume ratios (Shepherd et al. 1998; Shepherd et al. 1999), the ignition energy was expected to be different. Tests were performed at a low mass-volume ratio of 3 kg/m^3 which corresponds to a nearly empty Boeing 747 center wing tank. In the present ignition vessel, 3 kg/m^3 corresponds to about 7 ml of fuel, forming a layer about 3 mm thick on the vessel floor. The ignition energy was measured for 3 kg/m^3, and high M/V (35 kg/m^3 and 200 kg/m^3) at a pressure of 0.585 bar and the raw data is shown in Fig. 20. The spark energies representing the highest "no go" results and the lowest "go" results are shown in Fig. 21 with the limit lines obtained from exponential fits to the data. The exponential fits

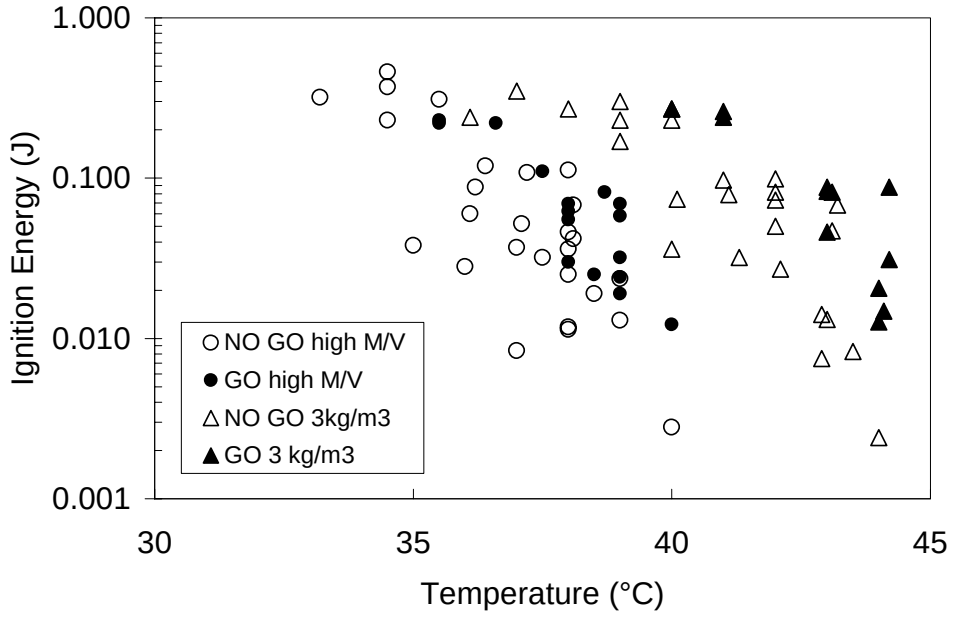

Figure 20: The dependence of ignition energy on temperature for ARCO Jet A (flash point temperature T_{fp} =46.4°C) at 0.585 bar for a low mass-volume ratio of 3 kg/m^3 and high M/V.

for the high M/V case are given by Eqs. 16 and 17, and the fits for the 3 kg/m^3 case are given by:

$$y_{nogo} = 5 \cdot 10^{13} e^{-0.821T}, \tag{18}$$

where y_{nogo} is the spark energy (J) for the "no go" results and T is the temperature (°C), and

$$y_{go} = 4 \cdot 10^{10} e^{-0.636T}, \tag{19}$$

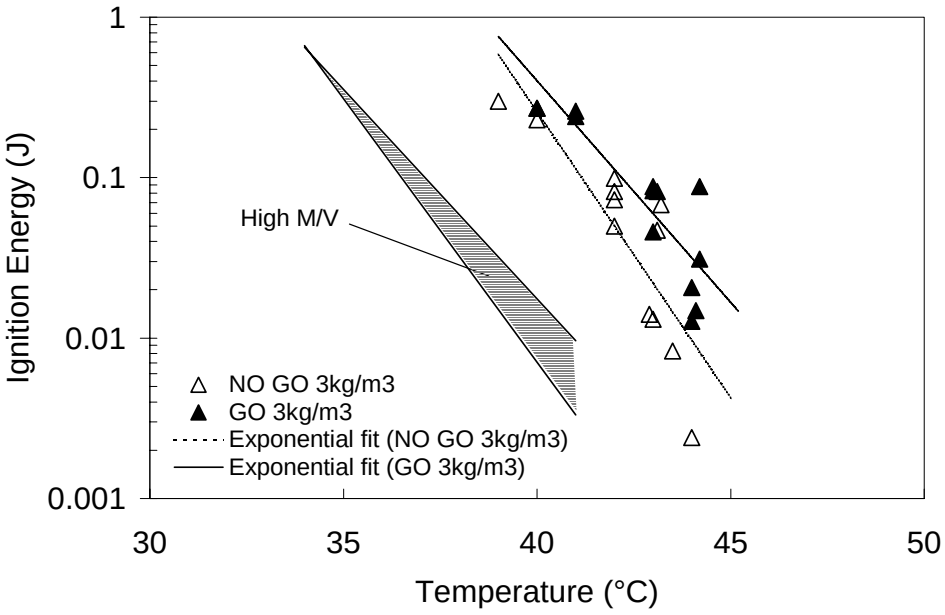

Figure 21: The dependence of ignition energy on temperature for ARCO Jet A (flash point temperature T_{fp} =46.4°C) at 0.585 bar for a low mass-volume ratio of 3 kg/m^3 and high M/V showing limit lines obtained from exponential fits to the highest "no go" results and the lowest "go" results.

where y_{go} is the spark energy (J) for the "go" results and T is the temperature (°C). The corresponding bands of uncertainty separating the regions of a non-flammable mixture and flammable mixtures are shown in Fig. 22.

In the present tests, the difference in ignition energy between high and low mass-volume ratios is clear. The rate of change of ignition energy with temperature appears to be identical for both cases but the curve for 3 kg/m^3 is distinctly shifted along the temperature axis by about 5°C towards higher temperatures. The shift of the ignition energy towards higher temperatures at low M/V may be caused by the relative decrease in the concentration of lighter fuel components in the Jet A or the overall reduction in the fuel concentration, or both. Although the ignition energy at a given temperature is higher for the lower mass loading, the magnitude of the ignition energy at a loading of 3 kg/m^3 is extrapolated to be less than 1 mJ at a temperatures of 48°Cor higher.

At low M/V, the depletion of the more volatile fuel components causes a reduction in vapor pressure of the fuel and consequently a reduction in the concentration of fuel in the vapor space above the liquid, as discussed in Shepherd et al. (1999). Using gas chromatography measurements of the ARCO Jet A (base fuel) (Woodrow and Seiber 1999), the vapor pressure was calculated for mass-volume ratios of 3 kg/m^3 and 400 kg/m^3 and the dependence on temperature was fit using a correlation based on the Clausius-Clapeyron model (Shepherd et al.

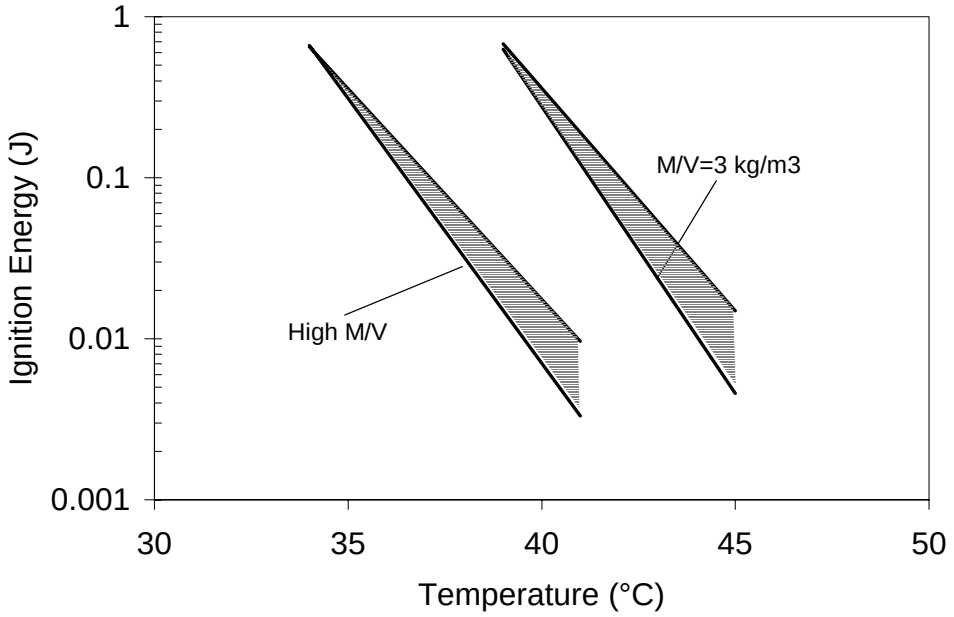

Figure 22: The dependence of ignition energy on temperature for ARCO Jet A (flash point temperature T_{fp} =46.4°C) at 0.585 bar for a low mass-volume ratio of 3 kg/m^3 and high M/V shown by the bands of uncertainty delimited by the limit lines.

1999). The fuel-air mass ratio (f) was then calculated using:

$$f = \frac{P_\sigma(T) W_f(T)}{P_a W_a} \tag{20}$$

where $P_\sigma(T)$ is Clausius-Clapeyron fit of the vapor pressure as a function of temperature, $W_f(T)$ is the functional fit of the average molecular weight as a function of temperature, P_a is the partial pressure of the air in the combustible mixture, and W_a is the molecular weight of air.

For the ARCO Jet A (base fuel) used in the present study, the Clausius-Clapeyron fits for the vapor pressure and the dependence of average molecular weight on temperature are taken from Shepherd et al. (1999). The Clausius-Clapeyron fit for the vapor pressure at a mass loading of 400 kg/m^3 is:

$$P_{\sigma 400}(T) = 6.465 \cdot 10^6 e^{-4243.3/T} \tag{21}$$

where $P_{\sigma 400}(T)$ is the vapor pressure (mbar) and T is the temperature (K). This fit is close to that determined from direct vapor pressure measurements of LAX Jet A in Shepherd et al. (1997). The discrepancy between the values of the coefficients are likely due to inaccuracies caused by the small number of points used for the fit in Eq. 21. The variation of the average molecular weight of the fuel with temperature at a mass loading of 400 kg/m^3 is fit to a linear function given by:

$$W_{f400}(T) = 0.170T + 57.33 \tag{22}$$

where $W_{f400}(T)$ is the molecular weight (g/mol) and T is the temperature (K). The Clausius-Clapeyron fit for the vapor pressure at a mass loading of 3 kg/m^3 is:

$$P_{\sigma 3}(T) = 1.738 \cdot 10^6 e^{-3952.3/T} \tag{23}$$

where $P_{\sigma 3}(T)$ is the vapor pressure (mbar) and T is the temperature (K). The linear fit of the average molecular weight of the fuel to the temperature at a mass loading of 3 kg/m^3 is:

$$W_{f3}(T) = 0.185T + 59.95 \tag{24}$$

where $W_{f3}(T)$ is the molecular weight (g/mol) and T is the temperature (K). Using these relations, the dependence of fuel-air mass ratio (or simply mass ratio) on temperature (Eq. 20) is plotted for the ARCO base fuel at 14 kft (a total mixture pressure of 0.585 bar) for mass-loadings of 3 kg/m^3 and 400 kg/m^3 in Fig. 23.

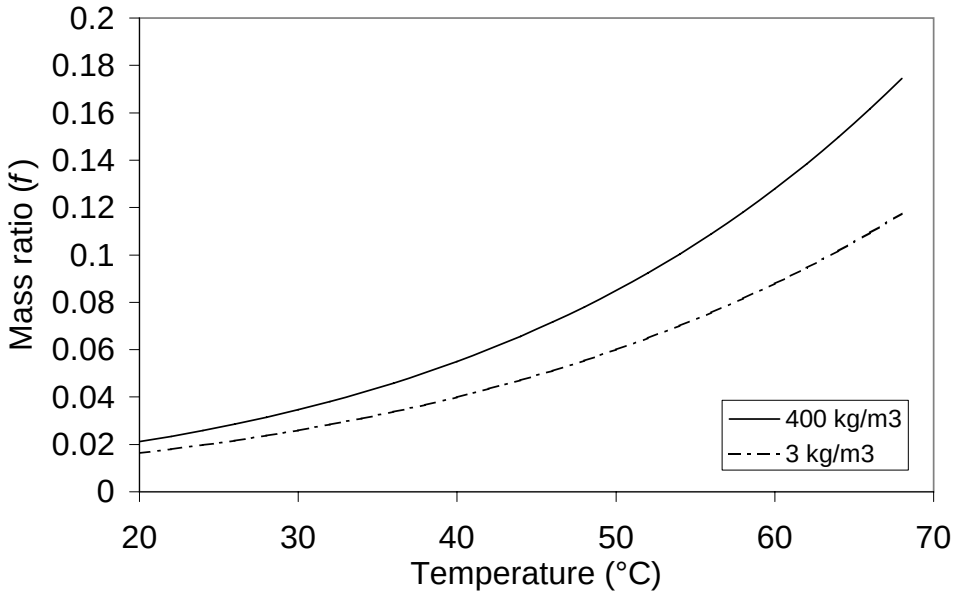

Figure 23: The dependence of fuel-air mass ratio (f) on temperature for ARCO Jet A (flash point temperature of 46.4°C) at mass-volume ratios of 3 kg/m^3 and 400 kg/m^3 at 0.585 bar.

The relations given by Eqs. 21-24 can be used to represent the ignition energy results at different mass-volume ratios (Fig. 20) in terms of the fuel-air mass ratio (f) instead of temperature. By assuming that the vapor composition of the fuel vapor at 400 kg/m^3 is representative of the vapor for high mass-volume ratios of 200 kg/m^3 and 35 kg/m^3, we can use Eq. 20 to obtain the fuel-air mass ratio for the mixtures for which ignition energy measurements were made. The ignition energy dependence on fuel-air mass ratio (or simply mass ratio) is shown in Fig. 24, and the corresponding bands of uncertainty are shown in Fig. 25. The ignition energy results at different mass-volume ratios appear to have similar trends but are displaced along the f axis by about 0.01.

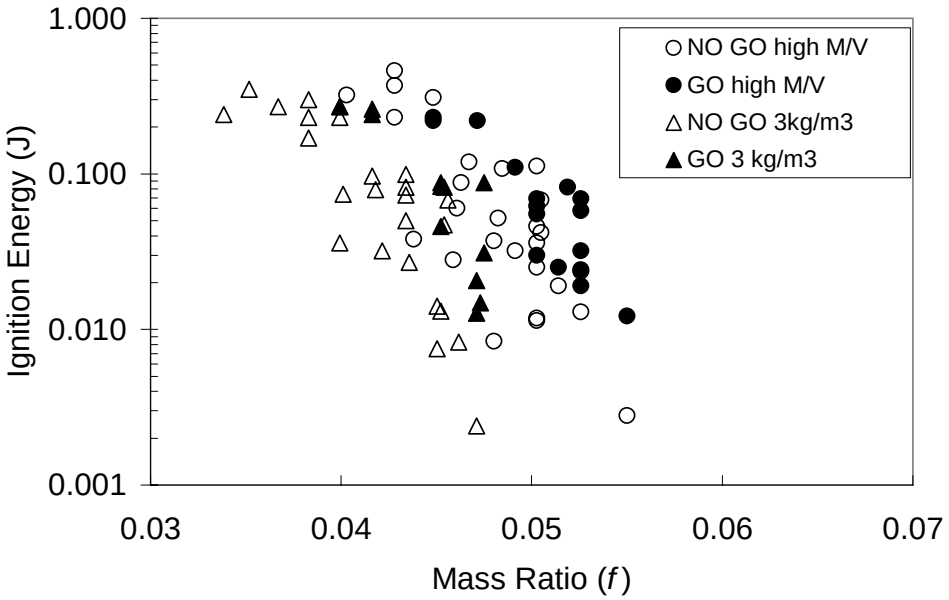

Figure 24: The dependence of ignition energy on fuel-air mass ratio (f) for ARCO Jet A (flash point temperature T_{fp} =46.4°C) at 0.585 bar for 3 kg/m^3 and high M/V.

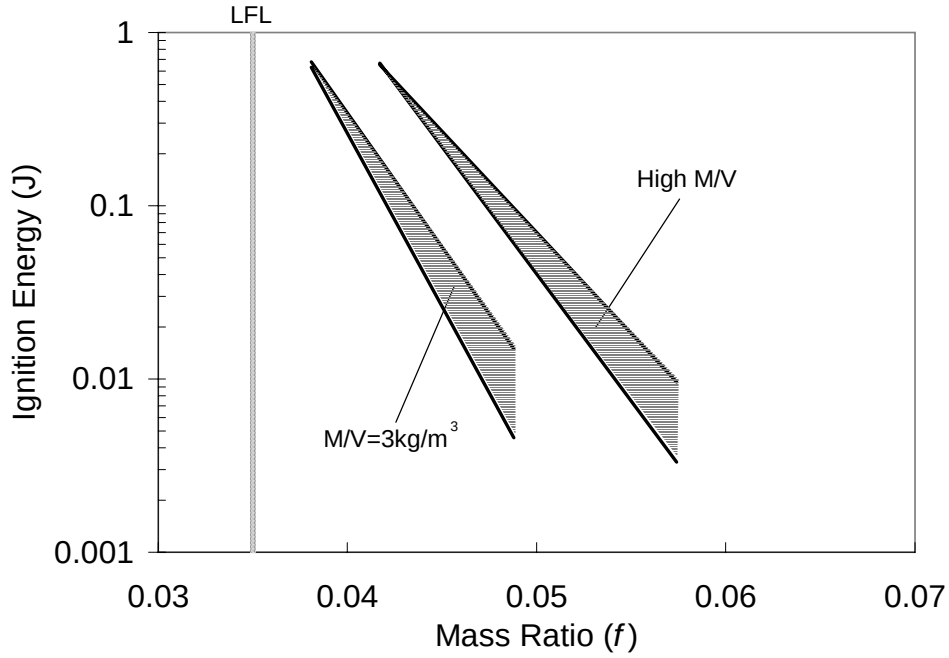

Figure 25: The dependence of ignition energy on fuel-air mass ratio (f) for ARCO Jet A (flash point temperature T_{fp} =46.4°C) at 0.585 bar for 3 kg/m^3 and high M/V represented by bands of uncertainty.

The most plausible explanation for the displacement between the curves in Fig. 25 is that there is a shift in the vapor composition, which has been observed in headspace gas chromatography measurements of Woodrow and Seiber (1999). This composition shift is due to the depletion of low-molecular-mass components for the 3 kg/m^3 case as compared to the high mass-volume ratio case (400 kg/m^3). Consequently, the average molar mass of the 3 kg/m^3 vapor is about 5 to 7 g/mol higher than the high mass-volume ratio cases (Fig. 38 of Shepherd et al. 1998). Previous work on ignition energy indicates a systematic effect of molar mass on minimum ignition energy for pure hydrocarbons (Figs. 1 and 2 of Shepherd et al. 1998) implying that a shift in ignition energy with mass loading is possible.

We also observe that ignition energy results of Fig. 25 occur at higher fuel-air mass ratios than the typical rule-of-thumb lower flammability limit (LFL) given by a fuel-air mass ratio of 0.035. However, since experiments have only been performed with ignition energies less than 0.5 J, we cannot confirm that the LFL of 0.035 applies to the present ignition energy tests or not. Figure 19 and previous results (Shepherd et al. 1998) suggests that at higher spark energies, the Jet A vapor is flammable below 34°C; however, tests must be performed with the present system at higher spark energies (above 0.3 J) to verify this.

5.3 Ignition energy dependence on pressure

In the previous ignition energy report (Shepherd et al. 1998), the influence of increasing altitude on the fuel-air mixture in an airplane fuel tank was discussed. Because the tank is open to the atmosphere, the amount of air in the tank decreases as the altitude increases since the ambient pressure decreases. The amount of fuel vapor in the tank depends mainly on the vapor pressure of the liquid fuel at a given temperature, i.e., in equilibrium, the partial pressure of the fuel vapor is equal to the vapor pressure. If the temperature of the liquid fuel is constant as the altitude increases, the partial pressure of the air decreases while the partial pressure of the fuel vapor remains constant, hence the composition of the mixture in the tank becomes richer. This change in composition with increasing altitude causes a shift in the ignition energy curve towards lower temperatures as discussed in Shepherd et al. (1998).

An additional effect of increasing the altitude is that the total pressure of the fuel-air mixture in the tank is decreased since it is equal to the ambient pressure. At a constant fuel-air mass ratio, the ignition energy has been found to vary with the total mixture pressure for pure hydrocarbon fuels (Lewis and von Elbe 1961). However, this dependence of ignition energy on total pressure is strongest for rich mixtures (Magison 1978) and mixtures near the MIE (Lewis and von Elbe 1961). For lean mixtures, the ignition energy has been found to be independent of pressure for methane-air mixtures (Ronney 1985). For lean Jet A-air mixtures, Nestor (1967) showed that the limiting value (lean flammability limit) of the fuel-air mass ratio at a fixed ignition energy of 20 J was a weak function of initial pressure. Nestor foung a limiting value of f=0.03 at 1 bar, which increased with decreasing pressure to f=0.04 at 0.2 bar. We infer that as the altitude increases, the variation of ignition energy with temperature of Jet A vapors in an airplane fuel tank is dominated by the change in composition due to the decreasing partial pressure of the air in the mixture (Shepherd et al. 1998).

Tests were performed with the ARCO base fuel at ambient laboratory pressure (0.986 bar)

and at 30 kft pressure (0.300 bar) and the results are shown with the tests performed at 14 kft pressure (0.585 bar) in Fig. 26. The corresponding limit lines using exponential fits to the highest "no go" results and the lowest "go" results are shown in Fig. 27. The exponential fits for 0.585 bar were previously given by Eqs. 16 and 17 and the fits for 0.986 bar are given by:

$$y_{nogo} = 6 \cdot 10^{11} e^{-0.625T}, \tag{25}$$

where y_{nogo} is the spark energy (J) for the "no go" results and T is the temperature (°C), and

$$y_{go} = 7 \cdot 10^{12} e^{-0.663T}, \tag{26}$$

where y_{go} is the spark energy (J) for the "go" results and T is the temperature (°C). Since there was insufficient data at 0.300 bar to fit a curve, a small bar was drawn by hand to indicate the ignition energy. A plot of the bands of uncertainty is shown in Fig. 28. The flash points of the Jet A fuel at the different pressures are also shown. The flash points at 0.300 bar and 0.585 bar were estimated by extrapolating the average measured flash point of 46.4°C at sea level (Shepherd et al. 1999) to lower ambient pressures with the rule of thumb that the flash point decreases linearly by 1°F for every 800 ft increase in altitude (Nestor 1967), i.e.,

$$T_{FPextr.} = T_{FPmeas.} - \frac{h}{800}$$

where $T_{FPextr.}$ is the extrapolated flash point in °F, $T_{FPmeas.}$ is the measured flash point at sea level in °F, and h is the altitude in feet.

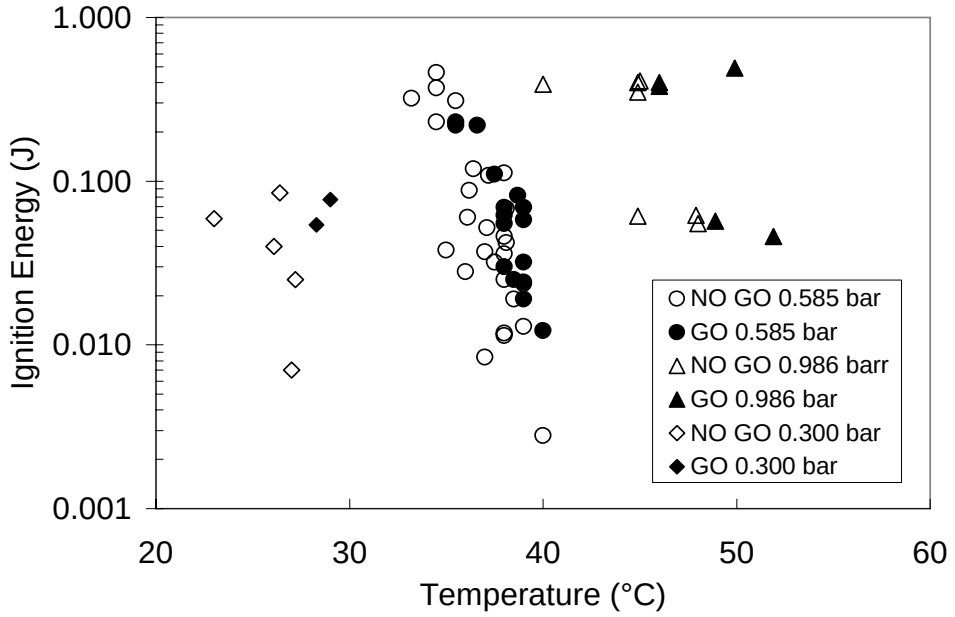

Figure 26: The dependence of ignition energy on temperature for ARCO Jet A (flash point temperature T_{fp} =46.4°C) at 0.300, 0.585 bar and 0.986 bar for high M/V.

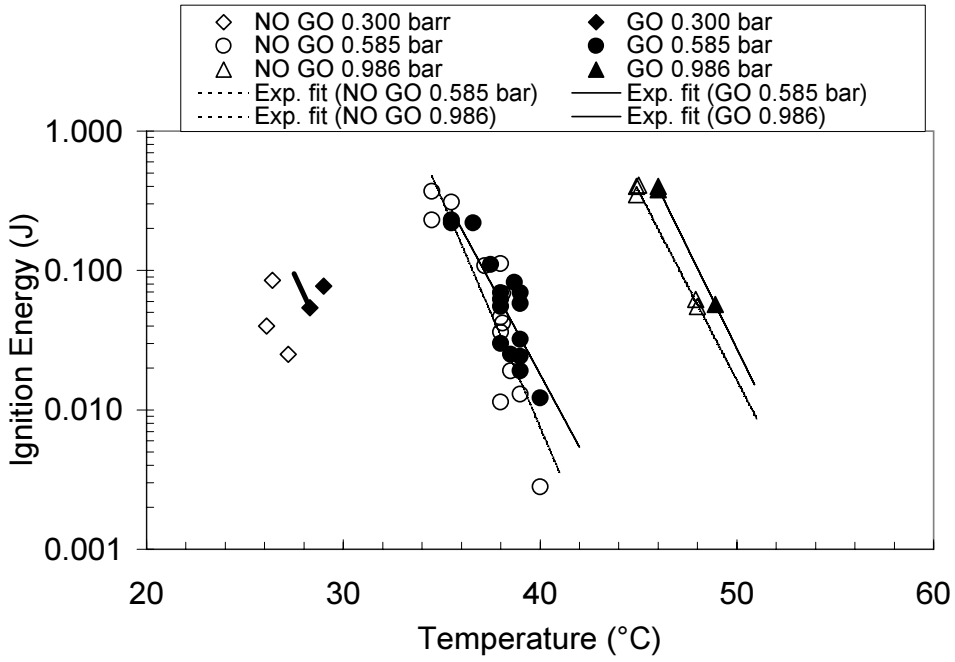

Figure 27: The dependence of ignition energy on temperature for ARCO Jet A (flash point temperature T_{fp} =46.4°C) at 0.300, 0.585 bar and 0.986 bar for high M/V showing limit lines obtained from exponential fits to the highest "no go" results and the lowest "go" results.

The results in Fig. 28 show that the ignition energy curves at 0.585 bar and 0.986 bar have similar trends, but that the latter is displaced about 10°C higher along the temperature axis. At 0.300 bar, the ignition energy appears shifted about 10°C lower along the temperature axis.

Figure 28 shows that the flash point temperature at sea level (46.4°C) coincides with the temperature at which the Jet A vapor can be ignited with a 0.1 J to 0.3 J spark. For lower pressures of 0.585 bar and 0.300 bar, the extrapolated flash point is also observed to occur at an ignition energy of 0.1 J to 0.3 J. Hence the rule of thumb for predicting the flash point at different pressures provides a good indication of the flammability of the fuel vapor at different altitudes. However, Fig. 28 also confirms that the fuel vapor can be ignited at temperatures below the flash point if the ignition energy is high enough, i.e., above 0.3 J.

By using previous fuel vapor composition analyses (Woodrow and Seiber 1999), the ignition energy results at different pressures (Fig. 26) can be shown as a function of the fuel-air mass ratio (f) instead of temperature. As in section 5.2, we assume that the fuel vapor properties at high mass loadings (35 kg/m^3 and 200 kg/m^3) can be approximated by fuel vapor at a mass loading of 400 kg/m^3. Equations 21 and 22 can be used to estimate the vapor pressure and molecular weight of the fuel respectively. The relation for the fuel-air mass ratio (Eq. 20) provides f at various altitudes by using the appropriate partial pressure of air at total mixture pressures of 0.300 bar (30 kft) and 0.986 bar (sea level). The dependence of f on temperature at different altitudes is shown in Fig. 29.

Using the dependence of f on temperature (Fig. 29), the ignition energy results at different

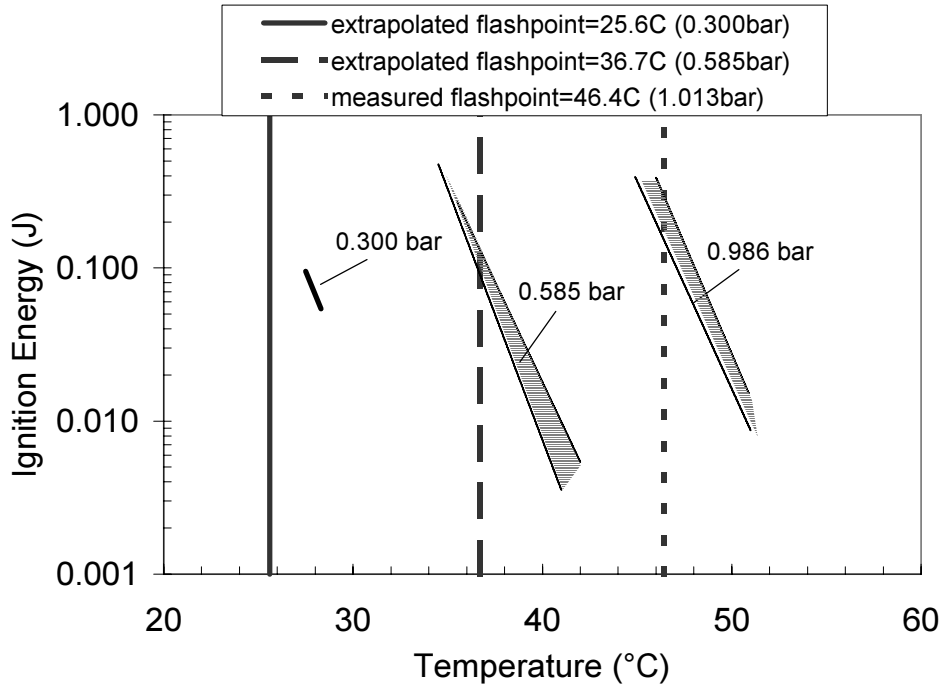

Figure 28: The dependence of ignition energy on temperature for ARCO Jet A (flash point temperature T_{fp} =46.4°C) at 0.300, 0.585 bar and 0.986 bar for high M/V shown by the bands of uncertainty delimited by the limit lines. Also shown is the measured flash point of the fuel at sea level and the extrapolated flash points at 0.300 bar and 0.585 bar.

pressures (Fig. 26) can be shown as a function of f (Fig. 30). The bands of uncertainty corresponding to the results of Fig. 30 are shown in Fig. 31. The ignition energy curves for 0.585 bar and 0.986 bar have similar trends, but are displaced from one another along the f axis by less than 0.005. This difference is significantly smaller than a difference of approximately 0.02 to 0.06 (Fig. 29) which corresponds to a 10°C difference between the curves as shown in Fig. 28. This indicates that at these two pressures, the ignition energy depends primarily on the fuel-air mass ratio (f). Interpreting the observed displacement of the ignition threholds will require a more in-depth evaluation of the fuel vapor composition analysis (Woodrow and Seiber 1999).

The ignition energy at 0.300 bar is shifted about 0.01 higher along the f axis than the other curves, indicating that at this pressure, the fuel-air mixture is more difficult to ignite. This suggests that although the ignition energy is still strongly dependent on f, additional effects must come into play at low pressures. Some of these effects have been reported by Nestor (1967) who was not able to ignite fuel vapors below some critical pressure.

The present results can also be compared to predictions of the shift in the ignition energy in Shepherd et al. (1998). By assuming that the ignition energy at a fixed value of f is pressure independent, the shift in the ignition energy curve at different altitudes was estimated in Shepherd et al. (1998). In that report, an average molecular mass for the fuel was assumed and the measured vapor pressure of Jet A at different temperatures was used to find the partial

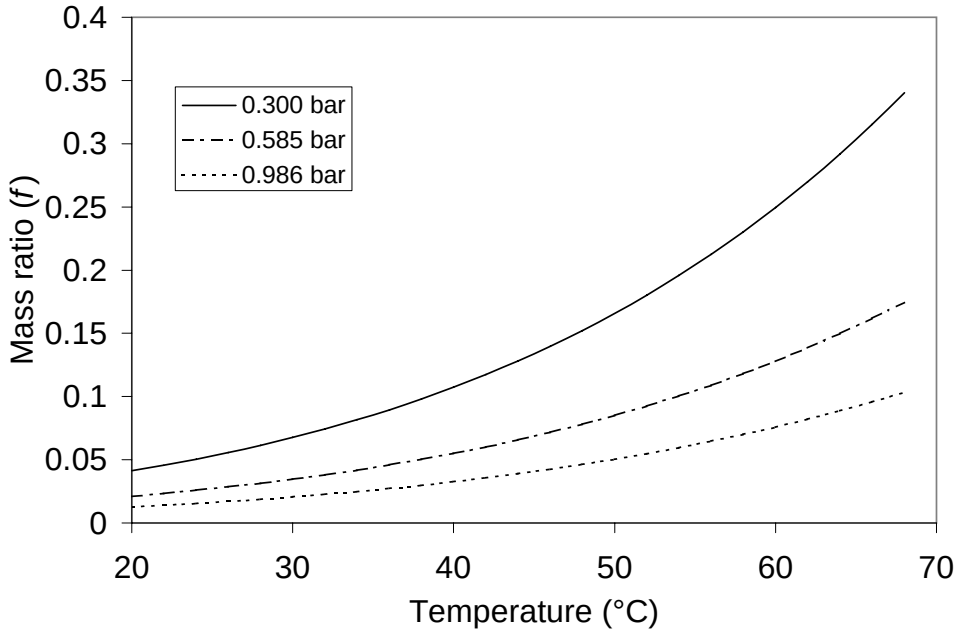

Figure 29: The dependence of fuel-air mass ratio (f) on temperature for mixture pressures of 0.300 bar (30 kft), 0.585 bar (14 kft), and 0.986 bar (sea level) for ARCO base fuel (T_{fp} =46.4°C) at 400 kg/m^3.

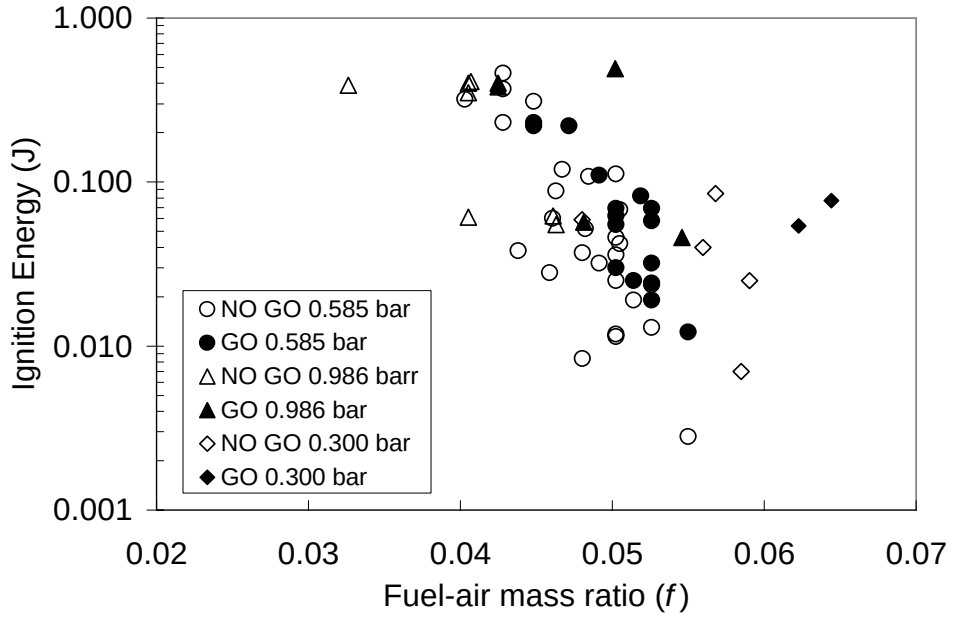

Figure 30: The dependence of ignition energy on fuel-air mass ratio (f) for ARCO Jet A (flash point temperature T_{fp} =46.4°C) for mixture pressures of 0.300 bar (30 kft), 0.585 bar (14 kft), and 0.986 bar (sea level) for ARCO base fuel (T_{fp} =46.4°C) at 400 kg/m^3.

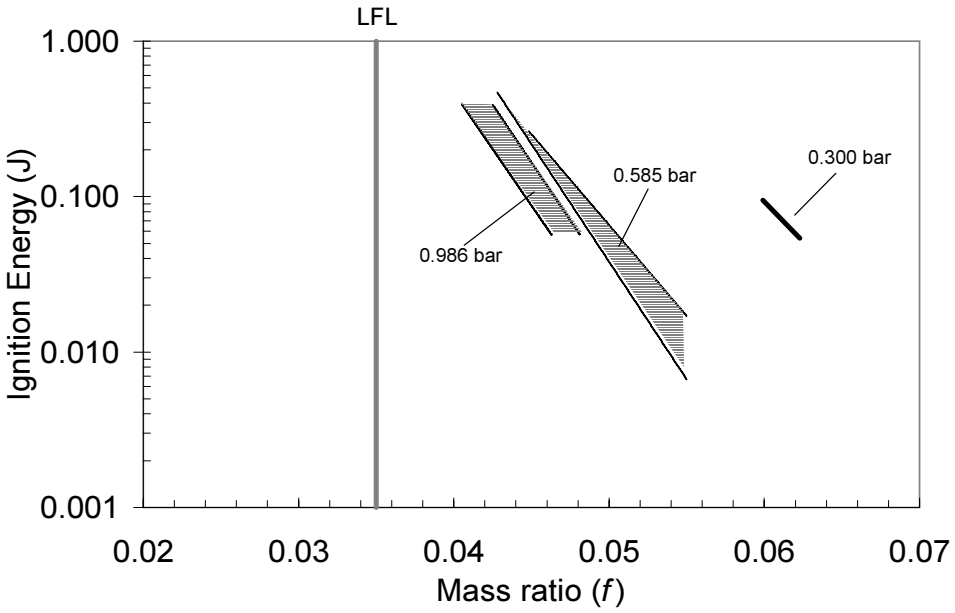

Figure 31: The dependence of ignition energy on f for ARCO Jet A (flash point temperature T_{fp} =46.4°C) at 0.300, 0.585 bar and 0.986 bar for high M/V shown by the bands of uncertainty delimited by the limit lines. Also shown is the rule-of-thumb LFL of 0.035

pressure of the fuel in the fuel-air vapor mixture. The mixture composition at different altitudes was estimated by adding the appropriate partial pressure of air. By thus obtaining the dependence of ignition energy on fuel-air mass ratio at different altitudes, it was then possible to estimate the dependence of ignition energy on temperature at different altitudes by using the vapor pressure dependence on temperature of the fuel. Hence the effect of altitude on ignition energy was predicted for altitudes of 30 kft (ambient pressure of 0.3 bar) and sea level (ambient pressure of 1 bar) by shifting the experimentally measured ignition energy curve at 14 kft (ambient pressure of 0.585 bar) in Shepherd et al. (1998). The predictions indicated that when the ambient pressure was increased to 1 bar, the ignition energy was found to shift by about 10°C towards higher temperatures, and when the ambient pressure was decreased to 0.3 bar, the ignition energy was found to shift about 10°C towards lower temperatures (Fig. 43 in Shepherd et al. (1998)). These shifts of the ignition energy curve are in agreement with the present experimental results in Fig. 28, lending further support to the proposition that the ignition energy is primarily a function of the fuel-air mass ratio.

5.4 Ignition energy dependence on flash point

In the previous section, it was found that the flash point temperature (T_{fp}) is close to the temperature at which the fuel vapors ignite at 0.986 bar with a 0.3 J spark (Fig. 28). This suggests a correlation between spark ignition energy thresholds and fuel flash point that may be useful in assessing fuel flammability hazards. This correlation was tested by conducting tests on special fuels with different flash points (Fig. 32) that were processed for Caltech at the

ARCO refinery (DeJovine 1998).

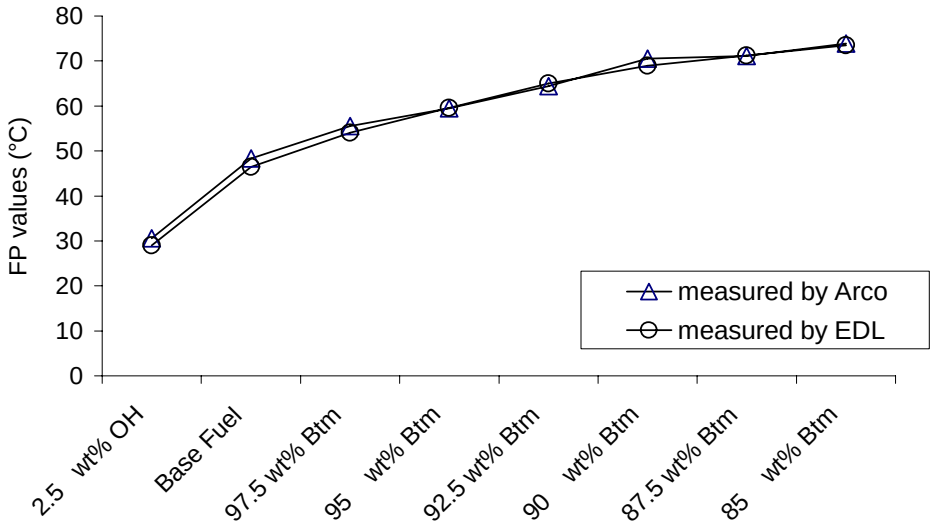

Figure 32: The flash points of special fuel mixtures processed by ARCO reproduced from Shepherd et al. (1999). Both the flash points measured by ARCO and the Explosion Dynamics Laboratory (EDL) at Caltech (ASTM D56 1988) are shown.

By maintaining the pressure at 0.986 bar and spark energy at about 0.3 J, the ignition temperature of the fuel vapor was measured by raising the temperature of the fuel until a critical minimum temperature was reached and the fuel vapors ignited (Fig. 33). For ARCO base fuel, this temperature coincides with the flash point temperature of 46.4°C. Further tests were performed on three other fuels: 2.5 wt% OH (a T_{fp} of 29.0°C), 97.5 wt% Btm (a T_{fp} of 54.0°C), and 85 wt% Btm (a T_{fp} of 73.5°C). These tests supported the correlation between the flash point and the 0.3 J ignition temperature.

By plotting the results in terms of the ignition temperature ($T_{ignition}$) as a function of the flash point temperature (Fig. 34), a linear relationship becomes apparent. Hence, an increase in the flash point of the fuel results in a corresponding linear increase in the minimum temperature for spark ignition at 0.986 bar with a 0.3 J spark. It is possible that this linear dependence is also valid for other spark energies and pressures but further tests are required to confirm this.

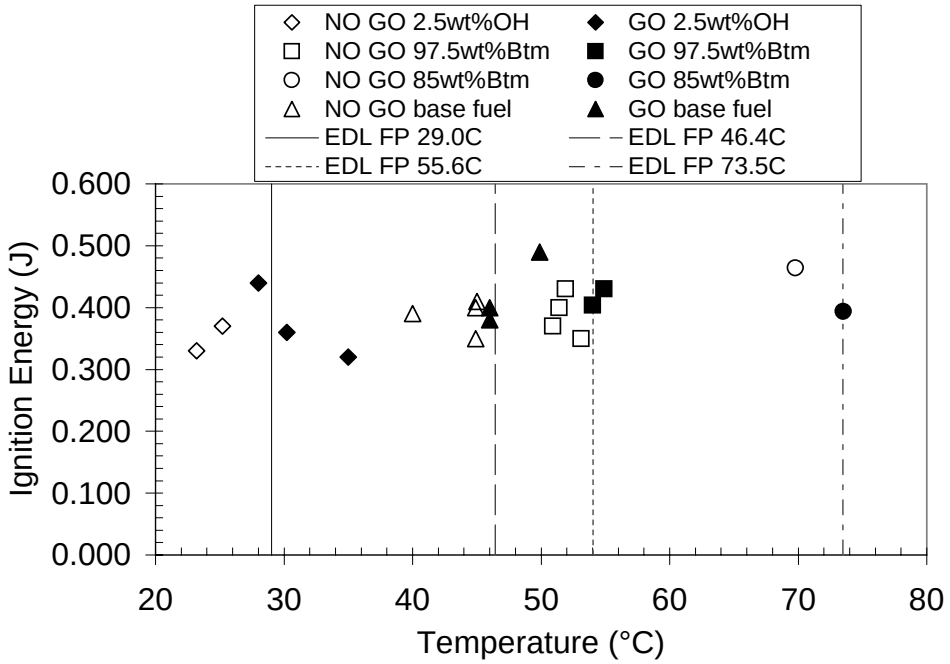

Figure 33: The dependence of ignition energy on temperature at 0.986 bar, high mass-volume ratio, and spark energy of about 0.3 J for ARCO fuels with four different flash points.

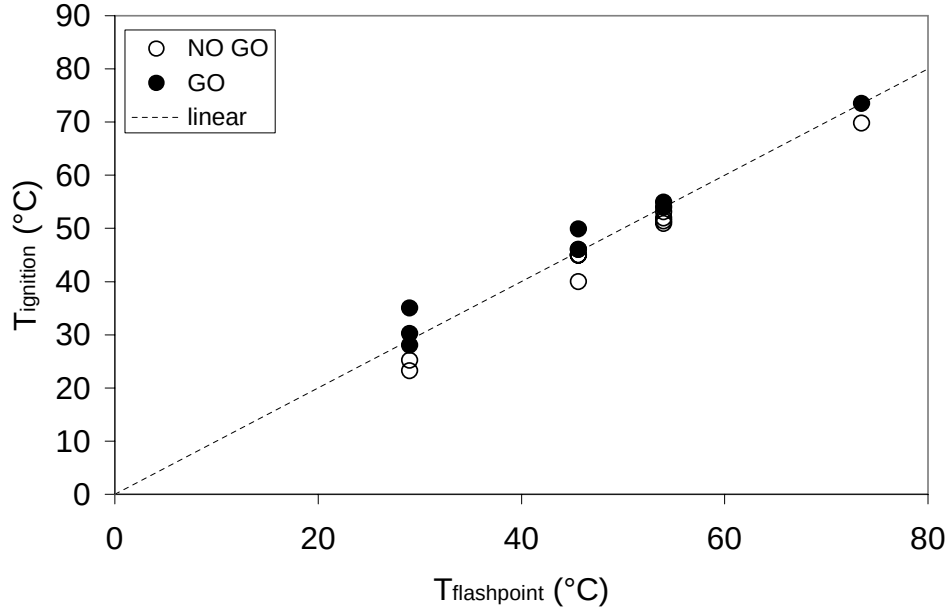

Figure 34: The dependence of minimum ignition temperature ($T_{ignition}$) for a 0.3 J spark on the flash point temperature ($T_{flashpoint}$). The flash point was measured with the standard ASTM D56 test (ASTM D56 1988).

6 Conclusion

6.1 Summary of results

A thermally-controlled vessel for performing ignition energy measurements of liquid fuel vapors was constructed. Along with a newly–designed spark energy measurement circuit, the experimental arrangement was successfully tested for damped sparks 20 μs in duration with energies from 10 mJ to 300 mJ. Several methods of statistical analysis of ignition energy data were applied to the data. A simple method of analysis succeeded while more sophisticated methods did not converge.

The ignition energy was measured for ARCO Jet A fuels at pressures of 0.300 bar, 0.585 bar, and 0.986 bar, at two high mass-volume ratios (35 kg/m^3 and 200 kg/m^3) and one low mass-volume ratio (3 kg/m^3), at temperatures from 26°C to 74°C, with spark energies between 10 mJ and 0.3 J. The following results were obtained:

1. The ignition energy decreased from about 0.3 J at 35°C to about 10 mJ at 40°C for ARCO base fuel (with a flash point of 46.4°C) at 0.585 bar and high mass-volume ratios (35 kg/m^3 and 200 kg/m^3).

2. The ignition energy dependence on temperature was measured for ARCO base fuel at 0.585 bar and high mass-volume ratios (35 kg/m^3 or 200 kg/m^3) with measured spark energies as opposed to stored spark energies. The trend of the ignition energy curve for measured spark energies is similar to that for LAX Jet A with stored spark energies. The measured spark energies were a factor of 10-50 lower than the stored spark energies for temperatures between 35°C and 40°C for LAX Jet A.

3. For ARCO base fuel at a pressure of 0.585 bar, the ignition energy dependence on temperature for a low mass-volume ratio of 3 kg/m^3 is shifted about 5°C higher than the ignition energy dependence on temperature for high mass-volume ratios (35 kg/m^3 and 200 kg/m^3).

4. For ARCO base fuel at 0.585 bar, the ignition energy at low (3 kg/m^3) and high (35 kg/m^3 and 200 kg/m^3) mass-volume ratios depends strongly on the fuel-air mass ratio. However, additional effects such as the change in the relative amounts of individual fuel components in the vapor may influence the ignition energy.

5. For ARCO base fuel at high mass-volume ratios (35 kg/m^3 and 200 kg/m^3), the ignition energy dependence on temperature at 0.585 bar is shifted about 10°C higher when the mixture pressure is increased to 0.986 bar and about 10°C lower when the pressure is decreased to 0.300 bar.

6. The shift of the ignition energy at different pressures agrees with Nestor's rule-of-thumb for estimating the flash point change with increasing altitude (1°F decrease in the flash point for every increase in altitude of 800 ft).

7. For ARCO base fuel at high mass volume ratios (35 kg/m^3 and 200 kg/m^3), the ignition energy at mixture pressures of 0.300 bar, 0.585 bar, and 0.986 bar depends strongly on the fuel-air mass ratio. At 0.300 bar, low pressure effects can begin to influence the ignition energy.

8. The flash point of ARCO base fuel (46.4°C) corresponds roughly to the temperature at which the fuel vapor ignites with a 0.3 J spark at 0.986 bar for high mass-volume ratios.

9. The temperature at which the fuel vapor ignites with a 0.3 J spark at 0.986 bar is approximately equal to the flash point temperature for special fuels with flash points of 29°C, 46.4°C (base fuel), 55.6°C, and 73.5°C.

6.2 Relationship to Previous Tests

There is a substantial literature on spark ignition for hydrocarbon fuels that was reviewed in Shepherd et al. (1998). There are some important points of comparisons and distinction between those works and the present study. The most cited previous studies are those that are reproduced in Lewis and von Elbe (1961), which relied on stored energy and examined near-stoichiometric mixtures. It is from those studies that a characteristic minimum ignition energy of 0.2 mJ has been proposed for spark ignition for hydrocarbon fuel (including Jet A) mixtures with air. The history of ignition energy estimates for Jet A is discussed in Section 2 of Shepherd et al. 1998.

The present tests all involve significantly higher ignition energies, 10 to 300 mJ vs the .2 to 5 mJ used in the Lewis and von Elbe data. This is due to the much leaner mixtures that we are considering and the difficulty in measuring very low energies with the present experimental setup. Due to the stray capacitance in the cicuit and the effect of the measuring probes, we were unable to reliably measure ignition energies less than 10 mJ. This is what limited the maximum temperatures that were used in the ignition energy testing. The present data therefore only provides an upper bound on the measured minimum spark ignition energy for Jet A-air mixtures.

Our data on the variation of ignition energy with fuel concentration (temperature) is reasonable and consistent with previous studies (Ronney 1985, Shepherd et al. 1998) on hydrocarbon fuels. The increase of ignition energy with deceasing fuel concentration in lean mixtures is well known and ignition energies up to 3 J near the lean limit of methane-air mixtures were measured by Ronney (1985). Ignition energies of up to 100 J for near-limit mixtures of hexane and propane with air were measured by Shepherd et al. (1998).

The minimum value of the spark ignition energy (MIE) has not been quantified in our study. However, extrapolations of our data are consistent with a MIE lower than 1 mJ. The minimum ignition energy measured by Ronney for methane-air was about 0.5 mJ, while Lewis and von Elbe found a stored value of about 0.2 mJ. In our previous study (Shepherd et al. 1998), ignition in Jet A-air mixtures was obtained at stored energies as low as 1 mJ at temperatures above 50°C, a pressure of 0.585 bar and mass loadings of both 3 and 200 kg/m^3. The minimum ignition energy for JP-8 vapor in air was examined by Plummer (1992) using the stored energy technique and values between 0.4 and 0.9 mJ were obtained.

We conclude that the results are consistent with the known data on simple hydrocarbon fuels and aviation kerosene. Although the minimum ignition energy was not quantified in this study, a value between 0.2 and 1 mJ is consistent with all of the available data.

6.3 Implications for Airplane Safety

One of the main findings from this study is that the ignition energy of a mixture of Jet A vapor and air can be correlated primarily with the overall fuel-air mass ratio even though the fuel is composed of many components. This conclusion has several implications regarding the risk of accidental ignition of the fuel vapor in an airplane fuel tank.

- This study confirms the earlier findings on the strong dependence of ignition energy on fuel temperature for both high and low mass-volume ratios (Fig. 22). This is a simple consequence of the strong dependence of fuel vapor pressure on temperature.

- The magnitude of the ignition energy of the fuel vapor for the conditions appropriate to the TWA 800 incident (a mass loading of 3 kg/m^3 and pressure of 0.585 bar) is estimated to vary from 0.5 J at 40°C to less than 0.5 mJ at 50°C.

- The present results demonstrate that there are competing effects when considering the role of the mass-volume ratio (mass loading) of the fuel in airplane safety. Increasing the mass-volume ratio in center wing tanks that are subject to external heating, as in the TWA 800 incident, can decrease the fuel temperature at the time of take off. This decrease in fuel temperature is simply due to the greater heat capacity of a larger mass of fuel. A tank containing a larger amount of fuel will heat up more slowly and therefore reach a lower temperature in a given amount of time. However, at a given temperature, the fuel vapor pressure is higher for a highly loaded tank (greater than 35 kg/m^3) than for an almost empty one (less than 3 kg/m^3). Using ignition energy thresholds as a measure of flammability, we find that a decrease in fuel temperature of more than 5°C is required to offset the increase in fuel vapor pressure at higher mass-volume ratios at 14 kft. Note that a 10°C decrease in fuel temperature is associated with a three-order-of-magnitude increase in ignition energy.

- Since the fraction of air in the fuel tank ullage decreases with increasing altitude, the fuel vapor-air mixture becomes richer and the ignition energy decreases for lean mixtures. Consequently, the benefits of decreasing fuel temperature are reduced by the effect of altitude on flammability (Fig. 28). Ultimately, low-pressure effects on spark discharges and cooling of the fuel by the airstream limit the decrease in ignition energy with increasing altitude.

- Preliminary experiments with different flash point fuels show that the flash point appears to correlate directly with the ignition temperature at a fixed energy level of 0.3 J. This implies that raising the flash point of the fuel in an airplane tank can raise the critical temperature at which spark ignition of the ullage vapor can occur for a given spark energy (Fig. 34).

Acknowledgments

Julian Lee was partially supported by a fellowship from FCAR of Quebec, Canada.

George Chung and Carrie Garner provided conscientious and indispensable technical assistance by performing a large part of the experiments.

Douglas Shepherd provide valuable assistance in developing the computer data analysis programs and Pavel Svitek assisted in the construction and design of the experimental setup.

The ARCO refinery in Carson, CA, provided the fuel samples that were used in this study. We thank Jim DeJovine, David Tong, Aaron Nagayama, Thinh Pham, David Smith, James McGetrick, and Eugene Zaluzec for their assistance in providing these samples.

Suzy Dake assisted in the proofreading and final preparation of this document.

References

ASTM D56 (1988). *Standard Test Method for Flash Point by Tag Closed Tester*. American Society for Testing and Materials.

Borghese, A., A. D'Alessio, M. Diana, and C. Venitozzi (1988). Development of hot nitrogen kernel, produced by a very fast spark discharge. In *Proc. 22nd Symp. (Intl) on Comb.*, pp. 1651–1659.

Brown, L. L., R. T. Lynch, and T. M. Samaras (1999, July). TWA Flight 800 1/4-Scale Fuel Tank Explosions Phase II, Fall 1998 & Spring 1999 Test Series, Final Report. Technical Report ARA Projects 4810 and 5057, Applied Research Associates, Inc.

DeJovine, J. M. (1998, September 15). Private communication. ARCO Products Company-Los Angeles Refinery, Carson, California 90745.

Dixon, W. J. and F. J. Massey Jr. (1983). *Introduction to Statistical Analysis*. McGraw-Hill.

Grenich, A. F. and F. F. Tolle (1983). Electrostatic safety with explosion suppresant foams. Technical Report AFWAL-TR-83-2015, Air Force Aero Propulsion Laboratories, Wright-Patterson Air Force Base, Ohio.

Kono, M., S. Kumagai, and T. Sakai (1976). The optimum condition for ignition of gases by composite sparks. In *Proc. 16nd Symp. (Intl) on Comb.*, pp. 757–766.

Kono, M., K. Niu, T. Tsukamoto, and Y. Ujiie (1988). Mechanism of flame kernel formation produced by short duration sparks. In *Proc. 22nd Symp. (Intl) on Comb.*, pp. 1643–1649.

Langlie, H. J. (1962). A test-to-failure program for thermal batteries. In *Sixteenth Annual Power Sources Conference*, pp. 117–120. PSC Publications Committee.

Lee, T. (1999, March). Private communication. Arizona State University.

Lewis, B. and G. von Elbe (1961). *Combustion, Flames and Explosions of Gases*. Academic Press.

Litchfield, E. L. (1960). Minimum ignition energy concept and its application to safety engineering. Report of Investigations 5671, Bureau of Mines.

Magison, E. (1978). *Electrical Instruments in Hazardous Locations* (Third ed.)., pp. 57–116. The Instrument society of America.

Nestor, L. (1967). Investigation of turbine fuel flammability within aircraft fuel tanks. Final Report DS-67-7, Naval Air Propulsion Test Center, Naval Base, Philadelphia.

Parker, S. J. (1985). *Electrical Spark Ignition of Gases and Dusts*. Ph. D. thesis, City University, London.

Plummer, J. A. (1992). Technical Report LT-92-764, Lightning Technologies, Inc.

Reinmann, R. and M. Akram (1997). Temporal investigation of a fast spark discharge in chemically inert gases. *J. Phys. D: Appl. Phys. 30*, 1125–1134.

Ronney, P. (1985). Effect of gravity on laminar premixed gas combustion ii: Ignition and extinction phenomena. *Combust. Flame 62*, 121–133.

Sandia National Laboratories (1990). ”Sandia National Laboratories” Review of the USS IOWA Incident for the General Accounting Office. Technical Report SAND90-1158/450/6-90, Sandia National Laboratories Report.

Shepherd, J. E., J. C. Krok, and J. J. Lee (1997, June). Jet A explosion experiments: Laboratory testing. Explosion Dynamics Laboratory Report FM97-5, California Institute of Technology.

Shepherd, J. E., J. C. Krok, J. J. Lee, L. L. Brown, R. T. Lynch, T. M. Samaras, and M. M. Birky (1998, July). Results of 1/4-scale experiments, vapor simulant and liquid Jet A tests. Explosion Dynamics Laboratory Report FM98-6, California Institute of Technology.

Shepherd, J. E., J. J. Lee, and J. C. Krok (1998, June). Spark ignition measurements in Jet A. Explosion Dynamics Laboratory Report FM97-9, California Institute of Technology.

Shepherd, J. E., C. D. Nuyt, and J. J. Lee (1999, December). Flashpoint and Chemical Composition of Aviation Kerosene (Jet A). Explosion Dynamics Laboratory Report FM99-4, California Institute of Technology.

Woodrow, J. E. and J. N. Seiber (1999, August). The Laboratory Characterization of ARCO Jet Fuel Vapor under Simulated Flight Conditions. Draft final report for NTSB, Order No. NTSB12-98SP-0360, University of Nevada, Reno, Nevada.

Zukas, J. and W. Walters (Eds.) (1998). *Explosive effects and applications*, Chapter 8: Hazard assessment of explosives and propellants, pp. 267–271. Springer-Verlag NY.

A Standard Operating Procedure

1. Clean chamber and electrodes
2. Put chamber under vacuum
3. Heat chamber to approximately operating temperature
4. Clean electrodes
5. Put chamber under vacuum
6. Heat to operating temperature
7. Raise pressure to 250 torr
8. Inject fuel through septum (Fig. 1) with syringe
9. Increase pressure to 10 torr below the target test pressure
10. Start stirrer (Fig. 2, number 17)
11. Allow chamber to equilibrate at target temperature
12. Bring pressure to target test pressure
13. Record pressure and temperature values
14. Zero Kulite pressure gauge (Fig. 1) by checking digital acquisition system (DAS) (Appendix E)
15. Check video tape position and lens orientation
16. Update acquisition program information (Appendix G)
17. Deactivate stirrer
18. Reattach thermocouple to DAS
19. Activate TM-11 module
20. Charge capacitor
21. Set scope trigger
22. Start video
23. Start sampling program (Appendix G)
24. Check scope ready

25. Fire
26. Deactivate TM-11 and power supply
27. Discharge capacitor (below 1kV)
28. Stop video
29. Set temperature controller to next test temperature
30. Reactivate stirrer
31. Download scope data (Appendix H)
32. Review video
33. Record energy values
34. Print copies of DAS and spark data
35. Return to step 11 for the next shot
36. Repeat until test is a “GO”

B Electrode breakdown voltage

Table 1 shows the breakdown voltage at which a capacitor will discharge across the gap of the electrodes in the ignition energy vessel. The discharges were in air at 0.585 bar. Tests with a 3 mm gap were done by mechanically switching a capacitor charged to a certain voltage onto the electrodes. Tests for 4 mm and 5.4 mm were done by slowly increasing the voltage across the electrodes until the discharge occurred.

Fig. 35 shows the dependence of the breakdown voltage on pressure across the ignition energy vessel electrodes.

Gap size (mm)	Vbd$_{min}$ (kV)	Vbd$_{max}$ (kV)	Comments
3	7	9	Mechanical switching
4	5.9	-	Gradual voltage increase
5.4	7.0	-	Gradual voltage increase

Table 1: The breakdown voltages for different gap sizes in the ignition energy vessel at 0.585 bar.

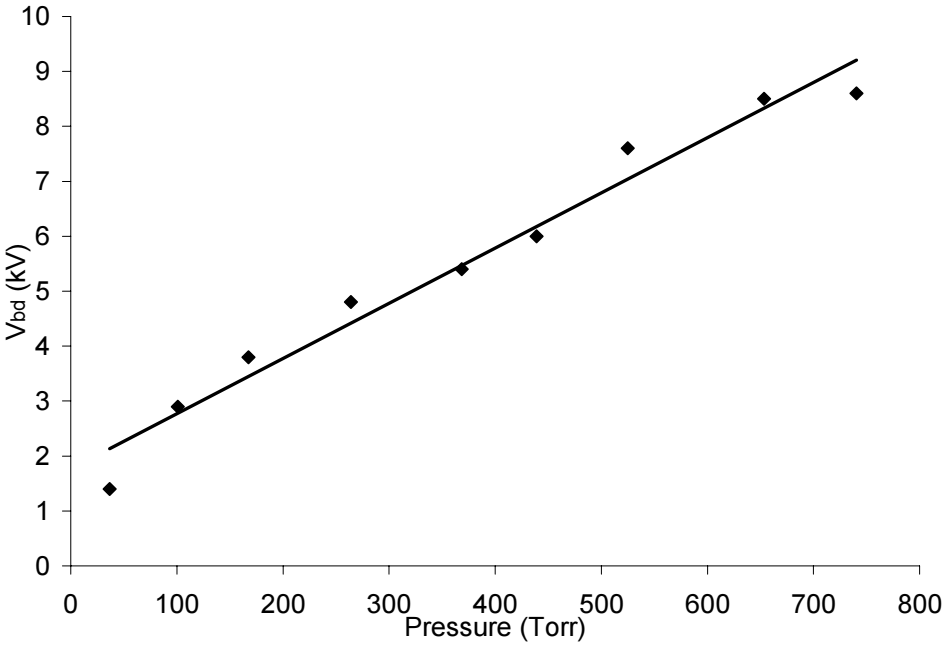

Figure 35: The minimum breakdown voltage across the electrode gap of the ignition vessel at different pressures for a gap size of 5.4 mm.

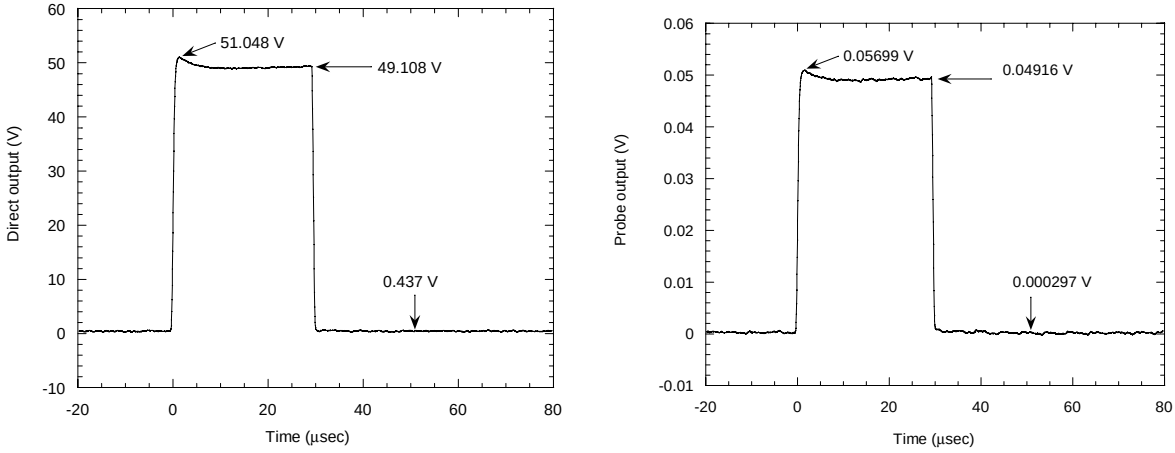

(a) (b)

Figure 36: Calibration of the Tektronics 6015A high voltage probe. A 50 V peak-to-peak square wave (a) is used for the calibration and the high voltage probe output is shown in (b).

C High voltage probe calibration

The attenuation factor of the high voltage probe was calculated by dividing the amplitudes of the square wave measured directly and the attenuated wave through the probe:

$$attn = Ampl_{wave}/Ampl_{probe},$$

where $attn$ is the attenuation factor, $Ampl_{wave}$ is the calibration signal measured directly, and $Ampl_{probe}$ is the attenuated signal measured through the probe:

$$attn = 48.671/0.04886 = 996.$$

Hence, the attenuation factor of the high voltage probe is 996, which is close to the specified attenuation of x1000.

D Table of all tests

Test #	Fuel Type	Fuel Source	Fuel Quant (g)	Fuel Quant (mL)	Mass/Vol (kg/m^3)	V (kV)	C (µF)	R+ (Ω)	R- (Ω)	Gap (mm)	P (torr)	T (°C)	IE w/ spike (J)	IE w/o spike (J)	Peak Pressure (bar)	Ignition	Comments
86	Jet A	Base Fuel															
87	Jet A	Base Fuel	368.2		200	12	0.598	0	7.15	3	439.0	40.2	39.000		2.67	go	
88	Jet A	Base Fuel	368.2		200	14	0.075	40.5	0	3	439.2	39.9	5.850			nogo	
89	Jet A	Base Fuel	368.2		200	8	0.598	0	7.15	3	439.2	39.7	16.340		2.47	go	
90	Jet A	Base Fuel	368.2		200	6.15	0.598	0	7.15	3	438.6	39.9	9.820		2.68	go	
91	Jet A	Base Fuel	368.2		200	13.63	0.075	48	48.3	3	439.0	40.5	3.750			nogo	
92	Jet A	Base Fuel	368.2		200	4.81	0.598	0	7.15	3	439.0	40.0	6.110		2.55	go	
93	Jet A	Base Fuel	368.2		200	4.26	0.598	0	7.15	3	439.0	40.1	4.750			nogo	
94	Jet A	Base Fuel	368.2		200	4.54	0.598	0	7.15	3	439.1	39.9	5.350		2.47	go	
95	Jet A	Base Fuel	368.2		200	4.41	0.598	0	7.15	3	439.0	40.2	5.040		2.52	go	
96	Jet A	Base Fuel	368.2		200	9.18	0.075	48.3	47.4	3	439.0	40.2	1.910			nogo	
97	Jet A	Base Fuel	368		200	12.01	0.075	48.3	47.4	3	439.1	40.5	2.960		3.16	go	
98	Jet A	Base Fuel	368		200	10.78	0.075	48.3	47.4	3	438.9	40.2	2.140		3.08	go	
99	Jet A	Base Fuel	368		200	7.41	0.075	48.3	47.4	3	438.9	39.9	1.130		3.03	go	
100	Jet A	Base Fuel	368		200	6	0.075	96.2	47.4	3	439.0	40.2	481.000		3	go	
101	Jet A	Base Fuel	368		200	5.14	0.075	601	48.3	3	438.9	40.5	132.000		3.06	go	
102	Jet A	Base Fuel	368		200	8.9	0.00515	96.2	48.3	3	438.9	40.0	39.000			nogo	
103	Jet A	Base Fuel	368		200	12.11	0.00515	96.2	48.3	3	439.1	40.4	140.000			nogo	
104	Jet A	Base Fuel	368		200	5.31	0.075	601	48.3	3	439.0	40.3			3.05	go	
105	Jet A	Base Fuel	368		200	5.31	0.075	601	48.3	3	438.9	40.5				go	
106	Jet A	Base Fuel	368		200	5	0.0842	45.1	47.5	3	438.8	39.6	0.095		2.93	go	
107	Jet A	Base Fuel	368		200	5	0.0842	45.1	47.5	3	438.9	37.2					
108	Jet A	Base Fuel	368		200	5	0.0842	45.1	47.5	3	438.7	37.6					
109	Jet A	Base Fuel	368		200	6	0.0842	45.1	47.5	3	438.8	37.4	0.037			nogo	
110	Jet A	Base Fuel	368		200	13	0.0842	45.1	47.5	3	438.8	36.8	0.025			nogo	
111	Jet A	Base Fuel	368		200	1.3	0.0842	45.1	47.5	3	438.8	37.1	0.065			nogo	
112	Jet A	Base Fuel	368		200	7.5	0.0842	45.1	47.5	3	438.8	37.2	0.190		2.64	go	mechanical switch system
113	Jet A	Base Fuel	368		200	4	0.0842	45.1	47.5	3	438.8	37.2	0.056		2.71	go	same fuel as #112,mechanical switch system
114	Jet A	Base Fuel	368		200	4	0.0842	95.6	47.5	3	438.8	37.2	0.062			nogo	same fuel as #112,mechanical switch system
115	Jet A	Base Fuel	368		200	4	0.0842	95.6	47.5	3	438.8	37.2	0.031			nogo	same fuel as #112,mechanical switch system
116	Jet A	Base Fuel	368		200	5	0.0842	45.1	47.5	3	438.8	37.2	0.036			nogo	same fuel as #112,mechanical switch system
117	Jet A	Base Fuel	368		200	5	0.0842	45.1	47.5	3	438.8	37.2					same fuel as #112,TM-11A trigger system
118	Jet A	Base Fuel	368		200	5	0.0842	45.1	47.5	3	438.8	37.3					same fuel as #112,TM-11A trigger system
119	Jet A	Base Fuel	368		200	1	0.0842	45.1	47.5	4	438.8	37.2	0.025			nogo	same fuel as #112,TM-11A trigger system,energy with negative spike
120	Jet A	Base Fuel	368		200	1.64	0.0842	45.1	47.5	4	438.8	37.2	0.037			nogo	same fuel as #112,TM-11A trigger system,energy with negative spike
121	Jet A	Base Fuel	368		200	5	0.0842	45.1	47.5	4	438.8	37.2	0.090			nogo	same fuel as #112,TM-11A trigger system
122	Jet A	Base Fuel	368		200	1	0.0842	45.1	47.5	5.4	438.8	39.0	0.029			nogo	same fuel as #112,TM-11A trigger system
123	Jet A	Base Fuel	368		200	7	0.0842	45.1	47.5	5.4	438.8	39.2	0.150		2.86	go	same fuel as #112,TM-11A trigger system
124	Jet A	Base Fuel	368		200	3.79	0.0842	45.1	47.5	5.4	438.9	38.9	0.104		2.77	go	same fuel as #112,TM-11A trigger system
125	Jet A	Base Fuel	368		200	3.68	0.0842	45.1	47.5	5.4	438.8	39.0	0.046			nogo	same fuel as #112,TM-11A trigger system
126	Jet A	Base Fuel	368		200	3.5	0.0842	45.1	47.5	5.4	438.8	39.1	0.087			nogo	same fuel as #112,TM-11A trigger system
127	Jet A	Base Fuel	368		200	5.34	0.0842	45.1	47.5	5.4	439.0	39.1	0.139		2.8	go	same fuel as #112,TM-11A trigger system,energy with negative spike
128	Jet A	Base Fuel	368		200	4.83	0.0842	45.1	47.5	5.4	439.0	39.0	0.134			nogo	same fuel as #112,TM-11A trigger system
129	Jet A	Base Fuel	368		200	5.71	0.0842	45.1	47.5	5.4	438.8	38.9	0.064			go	same fuel as #112,TM-11A trigger system
130	Jet A	Base Fuel	368		200	5.71	0.0842	45.1	47.5	5.4	439.0	39.2	0.090		2.75	go	same fuel as #112,TM-11A trigger system
131	Jet A	Base Fuel	368		200	4.72	0.0842	45.1	47.5	5.4	438.8	39.0	0.058			nogo	same fuel as #112,TM-11A trigger system
132	Jet A	Base Fuel	368		200	5.16	0.0842	45.1	47.5	5.4	438.9	39.0	0.032			nogo	same fuel as #112,TM-11A trigger system
133	Jet A	Base Fuel	368		200	5.15	0.0842	45.1	47.5	5.4	438.9	39.0	0.037			nogo	same fuel as #112,TM-11A trigger system
134	Jet A	Base Fuel	368		200	4.86	0.0842	45.1	47.5	5.4	438.8	39.0	0.075		2.96	go	TM-11A trigger system
135	Jet A	Base Fuel	368		200	4.62	0.0842	45.1	47.5	5.4	439.0	39.0	0.102		2.95	go	same fuel as #134,TM-11A trigger system
136	Jet A	Base Fuel	368		200	4.33	0.0842	45.1	47.5	5.4	439.1	39.0	0.046	0.059	2.92	go	same fuel as #134,TM-11A trigger system, energy with negative spike
137	Jet A	Base Fuel	368		200	2.22	0.0842	45.1	47.5	5.4	438.8	39.1	0.043	0.022	2.88	go	same fuel as #134,TM-11A trigger system, energy with positive spike
138	Jet A	Base Fuel	368		200	1	0.0842	45.1	47.5	5.4	439.1	39.0	0.028	0.012	2.85	go	same fuel as #134,TM-11A trigger system, energy with positive spike
139	Jet A	Base Fuel	368		200	1	0.0842	95.6	47.5	5.4	438.8	39.0	0.018	0.008		nogo	same fuel as #134,TM-11A trigger system, energy with positive spike
140	Jet A	Base Fuel	368		200	2	0.0842	95.6	47.5	5.4	438.8	39.1	0.038	0.011	2.85	go	same fuel as #134,TM-11A trigger system, energy with positive spike
141	Jet A	Base Fuel	368		200	3.4	0.0842	45.1	47.5	5.4	439.0	36.0	0.079			nogo	same fuel as #134,TM-11A trigger system
142	Jet A	Base Fuel	368		200	3.4	0.0842	45.1	47.5	5.4	439.0	37.2	0.052			nogo	same fuel as #134,TM-11A trigger system
143	Jet A	Base Fuel	368		200	3.4	0.0842	45.1	47.5	5.4	439.0	38.1	0.038			nogo	same fuel as #134,TM-11A trigger system, energy with negative spike
144	Jet A	Base Fuel	368		200	3.4	0.0842	45.1	47.5	5.4	439.0	38.0	0.044			nogo	same fuel as #134,TM-11A trigger system
145	Jet A	Base Fuel	368		200	3.4	0.0842	45.1	47.5	5.4	438.9	36.0	0.054			nogo	same fuel as #134,TM-11A trigger system, energy with negative spike
146	Jet A	Base Fuel	368		200	3.4	0.0842	45.1	47.5	5.4	438.9	37.0	0.070	0.048		nogo	same fuel as #134,TM-11A trigger system
147	Jet A	Base Fuel	368		200	3.41	0.0842	45.1	47.5	5.4	438.9	38.1	0.090	0.05	2.86	go	TM-11A trigger system
148	Jet A	Base Fuel	368		200	2.26	0.0842	45.1	47.5	5.4	438.8	38.0	0.022			nogo	same fuel as #147,TM-11A trigger system
149	Jet A	Base Fuel	368		200	2.93	0.0842	45.1	47.5	5.4	438.8	38.0	0.009	0.01		nogo	same fuel as #147,TM-11A trigger system, energy with negative spike
150	Jet A	Base Fuel	368		200	2.93	0.0842	45.1	47.5	5.4	438.8	38.0	0.032			nogo	same fuel as #147,TM-11A trigger system

Test #	Fuel Type	Fuel Source	Fuel Quant (g)	Fuel Quant (mL)	Mass/Vol (kg/m^3)	V (kV)	C (µF)	R+ (Ω)	R- (Ω)	Gap (mm)	P (torr)	T (°C)	IE w/ spike (J)	IE w/o spike (J)	Peak Pressure (bar)	Ignition	Comments
151	Jet A	Base Fuel	368		200	4.37	0.0842	45.1	47.5	5.4	438.8	38.0	0.025	0.032		nogo	same fuel as #147,TM-11A trigger system, energy with negative spike
152	Jet A	Base Fuel	368		200	4.37	0.0842	45.1	47.5	5.4	438.9	38.0	0.041	0.045	2.85	go	same fuel as #147,TM-11A trigger system, energy with negative spike
153	Jet A	Base Fuel	368		200	3.21	0.0842	45.1	47.5	5.4	438.9	38.0	0.020			nogo	same fuel as #147,TM-11A trigger system
154	Jet A	Base Fuel	368		200	3.21	0.0842	45.1	47.5	5.4	439.0	38.0	0.048	0.024		nogo	same fuel as #147,TM-11A trigger system, energy with positive spike
155	Jet A	Base Fuel	368		200	3.23	0.0842	45.1	47.5	5.4	439.0	38.0	0.029			nogo	same fuel as #147,TM-11A trigger system
156	Jet A	Base Fuel	368		200	3.22	0.0842	45.1	47.5	5.4	439.0	38.0	0.012			nogo	same fuel as #147,TM-11A trigger system, energy with negative spike
157	Jet A	Base Fuel	368		200	3.22	0.0842	45.1	47.5	5.4	439.0	38.0	0.019			nogo	same fuel as #147,TM-11A trigger system, energy with negative spike
158	Jet A	Base Fuel	368		200	4.1	0.0842	45.1	47.5	5.4	439.0	38.0	0.069	0.036		nogo	same fuel as #147,TM-11A trigger system, energy with positive spike
159	Jet A	Base Fuel	368		200	4.23	0.0842	45.1	47.5	5.4	439.0	38.0	0.049	0.053		nogo	same fuel as #147,TM-11A trigger system, energy with negative spike
160	Jet A	Base Fuel	368		200	4.91	0.0842	45.1	47.5	5.4	439.0	38.0	0.046	0.054		nogo	same fuel as #147,TM-11A trigger system, energy with negative spike
161	Jet A	Base Fuel	368		200	4.91	0.0842	45.1	47.5	5.4	438.8	38.0	0.055		2.81	go	same fuel as #147,TM-11A trigger system, energy with negative spike
162	Jet A	Base Fuel	368		200	4.67	0.0842	45.1	47.5	5.4	438.8	38.0	0.026			nogo	same fuel as #147,TM-11A trigger system, energy with negative spike
163	Jet A	Base Fuel	368		200	4.67	0.0842	45.1	47.5	5.4	438.8	38.1	0.068	0.044		nogo	same fuel as #147,TM-11A trigger system, energy with positive spike
164	Jet A	Base Fuel	368		200	6	0.0842	45.1	47.5	5.4	438.8	38.0	0.062		2.75	go	same fuel as #147,TM-11A trigger system
165	Jet A	Base Fuel	368		200	6	0.0842	45.1	47.5	5.4	439.0	38.0	0.069		2.72	go	TM-11A trigger system
166	Jet A	Base Fuel	368		200	6	0.0842	45.1	47.5	5.4	439.0	38.0	0.072			nogo	TM-11A trigger system
167	Jet A	Base Fuel	368		200	7.8	0.0842	45.1	47.5	5.4	439.0	38.0	0.068			nogo	TM-11A trigger system
168	Jet A	Base Fuel	368		200	3.4	0.0842	45.1	47.5	5.4	439.0	38.1	0.042	0.032		nogo	TM-11A trigger system
169	Jet A	Base Fuel	368		200	3.4	0.0842	45.1	47.5	5.4	439.0	39.0	0.069	0.023	2.83	go	TM-11A trigger system
170	Jet A	Base Fuel		80	35	1	0.0842	45.1	47.5	5.4	439.0	38.0	0.004	0.0002	2.91	nogo	TM-11A trigger system, energy with positive spike
171	Jet A	Base Fuel		80	35	1	0.0842	45.1	47.5	5.4	439.0	38.0	0.030	0.008	2.89	go	TM-11A trigger system
172	Jet A	Base Fuel		80	35	3.4	0.0842	45.1	47.5	5.4	438.8	36.0	0.028			nogo	TM-11A trigger system
173	Jet A	Base Fuel		80	35	3.4	0.0842	45.1	47.5	5.4	438.8	37.0	0.037	0.019		nogo	TM-11A trigger system
174	Jet A	Base Fuel		80	35	3.39	0.0842	45.1	47.5	5.4	438.9	37.5	0.032	0.021		nogo	TM-11A trigger system
175	Jet A	Base Fuel		80	35	3.39	0.0842	45.1	47.5	5.4	438.9	38.0	0.025			nogo	TM-11A trigger system, energy with negative spike
176	Jet A	Base Fuel		80	35	3.4	0.0842	45.1	47.5	5.4	439.0	38.5	0.019	0.022		nogo	TM-11A trigger system, energy with negative spike
177	Jet A	Base Fuel		80	35	3.39	0.0842	45.1	47.5	5.4	439.0	39.0	0.032		3	go	TM-11A trigger system
178	Jet A	Base Fuel		80	35	3.4	0.0842	45.1	47.5	5.4	438.8	37.0	?			nogo	TM-11A trigger system
179	Jet A	Base Fuel		80	35	3.4	0.0842	45.1	47.5	5.4	438.8	38.0	?			nogo	TM-11A trigger system
180	Jet A	Base Fuel		80	35	3.4	0.0842	45.1	47.5	5.4	438.9	38.5	?			go	TM-11A trigger system
181	Jet A	Base Fuel		80	35	3.4	0.0842	45.1	47.5	5.4	438.9	37.0	0.031	0.009		nogo	TM-11A trigger system, energy with positive spike
182																	TM-11A trigger system
183																	TM-11A trigger system
184	Jet A	Base Fuel		80	35	3.4	0.0842	45.1	47.5	5.4	439.0	37.4	0.021			nogo	TM-11A trigger system, energy with negative spike
185	Jet A	Base Fuel		80	35	3.4	0.0842	45.1	47.5	5.4	438.9	37.9	0.036			nogo	TM-11A trigger system, energy with negative spike
186	Jet A	Base Fuel		80	35	3.4	0.0842	45.1	47.5	5.4	438.8	38.5	0.025		2.88	go	TM-11A trigger system, energy with negative spike
187	Jet A	Base Fuel	5.75		3	3.4	0.0842	45.1	47.5	5.4	439.0	37.5	0.023			nogo	TM-11A trigger system, energy with negative spike
188	Jet A	Base Fuel	5.75		3	3.39	0.0842	45.1	47.5	5.4	438.9	38.5	0.054	0.029		nogo	TM-11A trigger system
189	Jet A	Base Fuel	5.75		3	3.4	0.0842	45.1	47.5	5.4	439.0	39.3	0.035	0.025		nogo	TM-11A trigger system
190	Jet A	Base Fuel	5.75		3	3.39	0.0842	45.1	47.5	5.4	438.9	40.1	0.065	0.03		nogo	TM-11A trigger system
191	Jet A	Base Fuel	5.75		3	3.4	0.0842	45.1	47.5	5.4	438.8	41.3	0.053	0.032		nogo	TM-11A trigger system
192	Jet A	Base Fuel	5.75		3	3.4	0.0842	45.1	47.5	5.4	439.0	42.3	0.054	0.032		nogo	TM-11A trigger system
193	Jet A	Base Fuel	5.75		3	3.4	0.0842	45.1	47.5	5.4	439.0	43.2	0.068	0.035		nogo	TM-11A trigger system
194	Jet A	Base Fuel	5.75		3	3.4	0.0842	45.1	47.5	5.4	439.0	44.2	0.088	0.034	2.85	go	TM-11A trigger system
195	Jet A	Base Fuel		80	35	5.5	0.602	14.3	7.15	5.4	439.0	33.2	0.320			nogo	TM-11A trigger system
196	Jet A	Base Fuel		80	35	5.5	0.602	14.3	7.15	5.4	439.0	34.5	0.230			nogo	TM-11A trigger system, energy with negative spike
197	Jet A	Base Fuel		80	35	5.5	0.602	14.3	7.15	5.4	439.0	35.5	0.230			go	TM-11A trigger system
198	Jet A	Base Fuel		80	35	5.5	0.602	14.3	7.15	5.4	439.0	34.5	0.370			nogo	TM-11A trigger system
199	Jet A	Base Fuel		80	35	5.51	0.602	14.3	7.15	5.4	439.0	35.5	0.220		2.24	go	TM-11A trigger system, energy with negative spike
200	Jet A	Base Fuel		80	35	5.5	0.602	14.3	7.15	5.4	439.0	34.5	0.460			nogo	TM-11A trigger system
201	Jet A	Base Fuel		80	35	5.5	0.602	14.3	7.15	5.4	439.0	35.5	0.310			nogo	TM-11A trigger system
202	Jet A	Base Fuel		80	35	5.51	0.602	14.3	7.15	5.4	439.0	36.6	0.220		2.55	go	TM-11A trigger system
203	Jet A	Base Fuel	5.56		3	5.5	0.602	14.3	7.15	5.4	439.0	36.1	0.240			nogo	TM-11A trigger system
204	Jet A	Base Fuel	5.56		3	5.5	0.602	14.3	7.15	5.4	439.0	37.0	0.350			nogo	TM-11A trigger system
205	Jet A	Base Fuel	5.56		3	5.5	0.602	14.3	7.15	5.4	439.0	38.0	0.270			nogo	TM-11A trigger system, energy with negative spike
206	Jet A	Base Fuel	5.56		3	5.51	0.602	14.3	7.15	5.4	439.0	39.0	0.300			nogo	TM-11A trigger system
207	Jet A	Base Fuel	5.56		3	5.5	0.602	14.3	7.15	5.4	439.0	40.0	0.270		1.95	go	TM-11A trigger system
208	Jet A	Base Fuel	5.56		3	5.5	0.602	14.3	7.15	5.4	439.1	39.0	0.170			nogo	TM-11A trigger system
209	Jet A	Base Fuel	5.56		3	5.5	0.602	14.3	7.15	5.4	439.0	40.0	0.230			nogo	TM-11A trigger system
210	Jet A	Base Fuel	5.56		3	5.5	0.602	14.3	7.15	5.4	438.8	41.0	0.240		2.29	go	TM-11A trigger system
211	Jet A	Base Fuel	5.55		3	5.5	0.602	14.3	7.15	5.4	439.0	39.0	0.230			nogo	TM-11A trigger system
212	Jet A	Base Fuel	5.55		3	5.5	0.602	14.3	7.15	5.4	439.0	40.0	0.270			nogo	TM-11A trigger system
213	Jet A	Base Fuel	5.55		3	5.5	0.602	14.3	7.15	5.4	439.0	41.0	0.260		2.47	go	TM-11A trigger system
214	Jet A	Base Fuel		80	35	1.001	0.0842	45.1	47.5	5.4	439.0	37.0	0.008			nogo	TM-11A trigger system, energy with negative spike
215	Jet A	Base Fuel		80	35	1.002	0.0842	45.1	47.5	5.4	439.0	38.0	0.012			nogo	TM-11A trigger system, energy with negative spike
216	Jet A	Base Fuel		80	35	1.002	0.0842	45.1	47.5	5.4	439.1	39.0	0.013			nogo	TM-11A trigger system, energy with negative spike
217	Jet A	Base Fuel		80	35	1	0.0842	45.1	47.5	5.4	439.1	40.0	0.012		3.06	go	TM-11A trigger system, energy with negative spike
218	Jet A	Base Fuel		80	35	1.002	0.0842	45.1	47.5	5.4	439.0	39.0	0.024			nogo	TM-11A trigger system, energy with negative spike
219	Jet A	Base Fuel		80	35	1	0.0842	45.1	47.5	5.4	439.0	40.0	0.003			nogo	TM-11A trigger system, energy with negative spike
220	Jet A	Base Fuel		80	35	0.999	0.0842	45.1	47.5	5.4	439.1	39.0	0.024		2.95	go	TM-11A trigger system

Test #	Fuel Type	Fuel Source	Fuel Quant (g)	Fuel Quant (mL)	Mass/Vol (kg/m^3)	V (kV)	C (µF)	R+ (Ω)	R- (Ω)	Gap (mm)	P (torr)	T (°C)	IE w/ spike (J)	IE w/o spike (J)	Peak Pressure (bar)	Ignition	Comments
221	Jet A	Base Fuel		80	35	0.999	0.0842	45.1	47.5	5.4	439.0	38.1	0.011			nogo	TM-11A trigger system, energy with negative spike
222	Jet A	Base Fuel		80	35	0.999	0.0842	45.1	47.5	5.4	438.9	39.0	0.019		2.94	go	TM-11A trigger system, energy with negative spike
223	Jet A	Base Fuel	5.52		3	1.002	0.0842	45.1	47.5	5.4	439.0	42.9	0.014			nogo	TM-11A trigger system, energy with negative spike
224	Jet A	Base Fuel	5.52		3	1.003	0.0842	45.1	47.5	5.4	439.0	44.1	0.015		2.91	go	TM-11A trigger system, energy with negative spike
225	Jet A	Base Fuel	5.53		3	1	0.0842	45.1	47.5	5.4	439.0	43.0	0.013			nogo	TM-11A trigger system, energy with negative spike
226	Jet A	Base Fuel	5.53		3	1.001	0.0842	45.1	47.5	5.4	439.0	44.0	0.021	0.007	2.88	go	TM-11A trigger system
227	Jet A	Base Fuel	5.52		3	1.004	0.0842	45.1	47.5	5.4	439.0	43.0	0.015			nogo	TM-11A trigger system
228	Jet A	Base Fuel	5.52		3	1	0.0842	45.1	47.5	5.4	439.0	44.0	0.002			nogo	TM-11A trigger system, energy with negative spike
229	Jet A	Base Fuel	5.52		3	5.71	0.0842	45.1	47.5	5.4							TM-11A trigger system
230	Jet A	Base Fuel	5.48		3	1.004	0.0842	45.1	47.5	5.4	439.1	42.9	0.008			nogo	TM-11A trigger system, energy with negative spike
231	Jet A	Base Fuel	5.48		3	1.002	0.0842	45.1	47.5	5.4	438.9	43.5	0.008			nogo	TM-11A trigger system, energy with negative spike
232	Jet A	Base Fuel	5.48		3	1	0.0842	45.1	47.5	5.4	439.0	44.0	0.013		2.92	go	TM-11A trigger system, energy with negative spike
233	Jet A	Base Fuel	5.56		3	3.4	0.0842	45.1	47.5	5.4	439.1	40.0	0.036			nogo	TM-11A trigger system
234	Jet A	Base Fuel	5.56		3	3.4	0.0842	45.1	47.5	5.4	439.0	41.3	0.032			nogo	TM-11A trigger system, energy with negative spike
235	Jet A	Base Fuel	5.56		3	3.4	0.0842	45.1	47.5	5.4	439.0	42.0	0.050			nogo	TM-11A trigger system
236	Jet A	Base Fuel	5.56		3	3.4	0.0842	45.1	47.5	5.4	439.0	43.0	0.046		2.79	go	TM-11A trigger system
237	Jet A	Base Fuel	5.58		3	3.4	0.0842	45.1	47.5	5.4	439.0	42.1	0.027			nogo	TM-11A trigger system, energy with negative spike
238	Jet A	Base Fuel	5.58		3	3.4	0.0842	45.1	47.5	5.4	439.0	43.1	0.047			nogo	TM-11A trigger system
239	Jet A	Base Fuel	5.58		3	3.4	0.0842	45.1	47.5	5.4	439.0	44.2	0.031		2.96	go	TM-11A trigger system, energy with negative spike
240	Jet A	Base Fuel		80	35	1.001	0.602	14.3	7.15	5.4	439.0	35.0	0.038			nogo	TM-11A trigger system, energy with negative spike
241	Jet A	Base Fuel		80	35	1.002	0.602	14.3	7.15	5.4	439.1	36.1	0.060			nogo	TM-11A trigger system
242	Jet A	Base Fuel		80	35	2	0.602	14.3	7.15	5.4	439.0	36.2	0.088			nogo	TM-11A trigger system
243	Jet A	Base Fuel		80	35	2.001	0.602	14.3	7.15	5.4	439.0	37.2	0.108			nogo	TM-11A trigger system
244	Jet A	Base Fuel		80	35	2.001	0.602	14.3	7.15	5.4	438.9	38.7	0.082		2.95	go	TM-11A trigger system
245	Jet A	Base Fuel		80	35	2	0.602	14.3	7.15	5.4	439.0	36.4	0.119			nogo	TM-11A trigger system
246	Jet A	Base Fuel		80	35	1.999	0.602	14.3	7.15	5.4	439.1	37.1	0.052			nogo	TM-11A trigger system, energy with negative spike
247	Jet A	Base Fuel		80	35	2.004	0.602	14.3	7.15	5.4	439.0	38.0	0.112			nogo	TM-11A trigger system
248	Jet A	Base Fuel		80	35	1.998	0.602	14.3	7.15	5.4	439.0	39.0	0.058		2.97	go	TM-11A trigger system, energy with negative spike
249	Jet A	Base Fuel		80	35	2	0.602	14.3	7.15	5.4	439.0	37.5	0.110		2.73	go	TM-11A trigger system
250	Jet A	Base Fuel	5.56		3	2.003	0.602	14.3	7.15	5.4	439.0	40.1	0.074			nogo	TM-11A trigger system
251	Jet A	Base Fuel	5.56		3	2.005	0.602	14.3	7.15	5.4	439.0	41.1	0.079			nogo	TM-11A trigger system
252	Jet A	Base Fuel	5.56		3	2.002	0.602	14.3	7.15	5.4	439.0	42.0	0.073			nogo	TM-11A trigger system
253	Jet A	Base Fuel	5.56		3	2.002	0.602	14.3	7.15	5.4	439.0	43.1	0.082		2.8	go	TM-11A trigger system
254	Jet A	Base Fuel	5.49		3	1.998	0.602	14.3	7.15	5.4	439.0	41.0	0.081			nogo	TM-11A trigger system, energy with negative spike
255	Jet A	Base Fuel	5.49		3	1.999	0.602	14.3	7.15	5.4	439.0	42.0	0.099			nogo	TM-11A trigger system
256	Jet A	Base Fuel	5.49		3	1.999	0.602	14.3	7.15	5.4	439.0	43.0	0.065		2.79	go	TM-11A trigger system, energy with negative spike
257	Jet A	Base Fuel	5.52		3	1.997	0.602	14.3	7.15	5.4	439.1	42.0	0.067			nogo	TM-11A trigger system, energy with negative spike
258	Jet A	Base Fuel	5.52		3	2.001	0.602	14.3	7.15	5.4	439.0	43.0	0.083		2.8	go	TM-11A trigger system
259	Jet A	Base Fuel		80	35	5.5	0.602	14.3	7.15	5.4	738.0	40.0	0.390			nogo	TM-11A trigger system
260	Jet A	Base Fuel		80	35	5.5	0.602	14.3	7.15	5.4	739.9	44.9	0.400			nogo	TM-11A trigger system
261	Jet A	Base Fuel		80	35	5.5	0.602	14.3	7.15	5.4	740.0	49.9	0.490		4.99	go	TM-11A trigger system
262	Jet A	Base Fuel		80	35	5.5	0.602	14.3	7.15	5.4	738.2	45.0	0.410			nogo	TM-11A trigger system, energy with negative spike
263	Jet A	Base Fuel		80	35	5.5	0.602	14.3	7.15	5.4	740.0	46.0	0.380		3.93	go	TM-11A trigger system
264	Jet A	Base Fuel		80	35	5.5	0.602	14.3	7.15	5.4	737.3	44.9	0.350			nogo	TM-11A trigger system
265	Jet A	Base Fuel		80	35	5.5	0.602	14.3	7.15	5.4	739.8	46.0	0.000		3.96	go	TM-11A trigger system
266	Jet A	Base Fuel		80	35	3.4	0.0842	45.1	47.5	5.4	738.3	44.9	0.061			nogo	TM-11A trigger system
267	Jet A	Base Fuel		80	35	3.4	0.0842	45.1	47.5	5.4	739.9	48.0	0.055			nogo	TM-11A trigger system
268	Jet A	Base Fuel		80	35	3.4	0.0842	45.1	47.5	5.4	739.9	51.9	0.046		5.39	go	TM-11A trigger system
269	Jet A	Base Fuel		80	35	3.4	0.0842	45.1	47.5	5.4	740.0	47.9	0.062			nogo	TM-11A trigger system
270	Jet A	Base Fuel		80	35	3.41	0.0842	45.1	47.5	5.4	739.9	48.9	0.057		4.74	go	TM-11A trigger system
271	Jet A	2.5% OH		80	35	5.5	0.602	14.3	7.15	5.4	739.6	35.0	0.320		6.16	go	TM-11A trigger system
272	Jet A	2.5% OH		80	35	5.5	0.602	14.3	7.15	5.4	739.9	30.2	0.360		5.11	go	TM-11A trigger system
273	Jet A	2.5% OH		80	35	5.5	0.602	14.3	7.15	5.4	740.0	23.2	0.330			nogo	TM-11A trigger system
274	Jet A	2.5% OH		80	35	5.5	0.602	14.3	7.15	5.4	740.0	25.2	0.370			nogo	TM-11A trigger system
275	Jet A	2.5% OH		80	35	5.5	0.602	14.3	7.15	5.4	739.8	28.0	0.440		4.57	go	TM-11A trigger system
276	Jet A	97.5 wt% Btm		80	35	5.5	0.602	14.3	7.15	5.4	739.8	51.4	0.400			nogo	TM-11A trigger system
277	Jet A	97.5 wt% Btm		80	35	5.5	0.602	14.3	7.15	5.4	740.0	54.9	0.430		4	go	TM-11A trigger system
278	Jet A	85 wt% Btm		80	35	5.5	0.602	14.3	7.15	5.4	740.0	69.8	0.464			nogo	TM-11A trigger system
279	Jet A	86 wt% Btm		80	35	5.51	0.602	14.3	7.15	5.4	739.5	73.5	0.394		3.47	go	TM-11A trigger system, energy with negative spike
280	Jet A	97.5 wt% Btm		80	35	5.5	0.602	14.3	7.15	5.4	740.0	50.9	0.370			nogo	TM-11A trigger system
281	Jet A	97.5 wt% Btm		80	35	5.5	0.602	14.3	7.15	5.4	739.5	51.9	0.430			nogo	TM-11A trigger system
282	Jet A	97.5 wt% Btm		80	35	5.5	0.602	14.3	7.15	5.4	739.6	53.1	0.350			nogo	TM-11A trigger system
283	Jet A	97.5 wt% Btm		80	35	5.5	0.602	14.3	7.15	5.4	740.0	54.0	0.404		3.48	go	TM-11A trigger system
284	Jet A	Base Fuel		80	35	3.4	0.0842	45.1	47.5	5.4	225.0	23.0	0.059			nogo	TM-11A trigger system
285	Jet A	Base Fuel		80	35	3.4	0.0842	45.1	47.5	5.4	225.0	26.1	0.040			nogo	TM-11A trigger system, energy with negative spike
286	Jet A	Base Fuel		80	35	3.41	0.0842	45.1	47.5	5.4	225.0	29.0	0.077		1.77	go	TM-11A trigger system
287	Jet A	Base Fuel		80	35	3.4	0.0842	45.1	47.5	5.4	225.0	26.4	0.085			nogo	TM-11A trigger system
288	Jet A	Base Fuel		80	35	3.4	0.0842	45.1	47.5	5.4	225.0	27.0	0.007			nogo	TM-11A trigger system, energy with negative spike
289	Jet A	Base Fuel		80	35	3.4	0.0842	45.1	47.5	5.4	225.0	27.2	0.025			nogo	TM-11A trigger system
290	Jet A	Base Fuel		80	35	3.4	0.0842	45.1	47.5	5.4	225.0	28.3	0.054		1.7	go	TM-11A trigger system

E Continuous acquisition program

This appendix includes the details of the LabView^{TM} program designed to continuously display the temperature and pressure of the ignition vessel system. The pressure from the Kulite and the MKS gages are displayed as well as the temperature from one of the thermocouples in the ignition vessel set up.

Connector Pane

IggyOnline.vi

Cont(inuous) Acq(uire) & Chart (immediate) demonstrates the software timed, non-buffered technique of data acquisition. Timing functions control the timing of the loop and in each loop AI Single Scan is called to read an immediate scan of the channels listed. Each scan is plotted on the chart after it is read. This example uses the lower level intermediate VIs: AI Config and AI Single Scan.

See Cont Acq&Chart (easy immed) for a functionally identical but simpler version using a single higher level intermediate VI. This example is also similar to the Cont Acq&Chart (hw timed) and (buffered) examples.

A common reason to use untimed, immediate acquisition is that some kind of processing needs to be done for each data point. You will probably want to add more functions to the diagram to customize this VI for your application. The acquisition rate you can achieve depends on how much processing and display the VI must do. This VI calls a subVI named My Single-Scan Processing. Add whatever processing you need to this subVI, or replace it with one of your own. The data processing subVI also demonstrates how to use error clusters in your own subVIs, so they can be included in the error data flow chain.

Before running this VI, set the values of the controls on the front panel. Select Show Help Window from the Help menu to see a description of each control. If the values you select for all the controls are values you will usually use, select Make Current Values Default from the Operate menu and save the VI. Or, you may save individual control's default values by popping up on the control, selecting Data Operations, then selecting Make Current Value Default, and saving the VI.

Front Panel

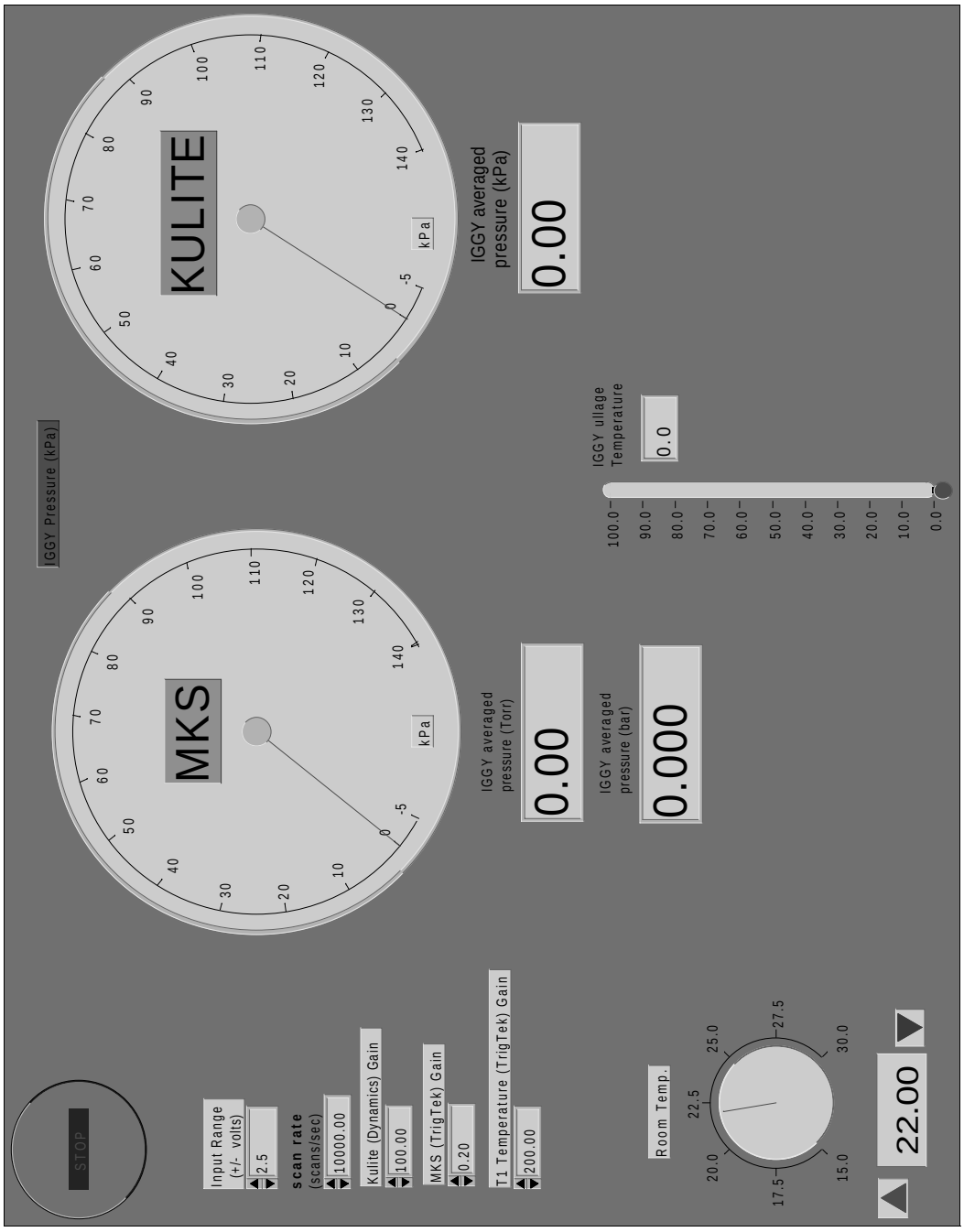
STOP
IGGY Pressure (kPa)
MKS
KULITE
kPa
IGGY averaged pressure (kPa)
0.00
IGGY averaged pressure (Torr)
0.00
IGGY averaged pressure (bar)
0.000
IGGY ullage Temperature
0.0
Input Range (+/- volts)
2.5
scan rate (scans/sec)
10000.00
Kulite (Dynamics) Gain
100.00
MKS (TrigTek) Gain
0.20
T1 Temperature (TrigTek) Gain
200.00
Room Temp.
22.00

Block Diagram

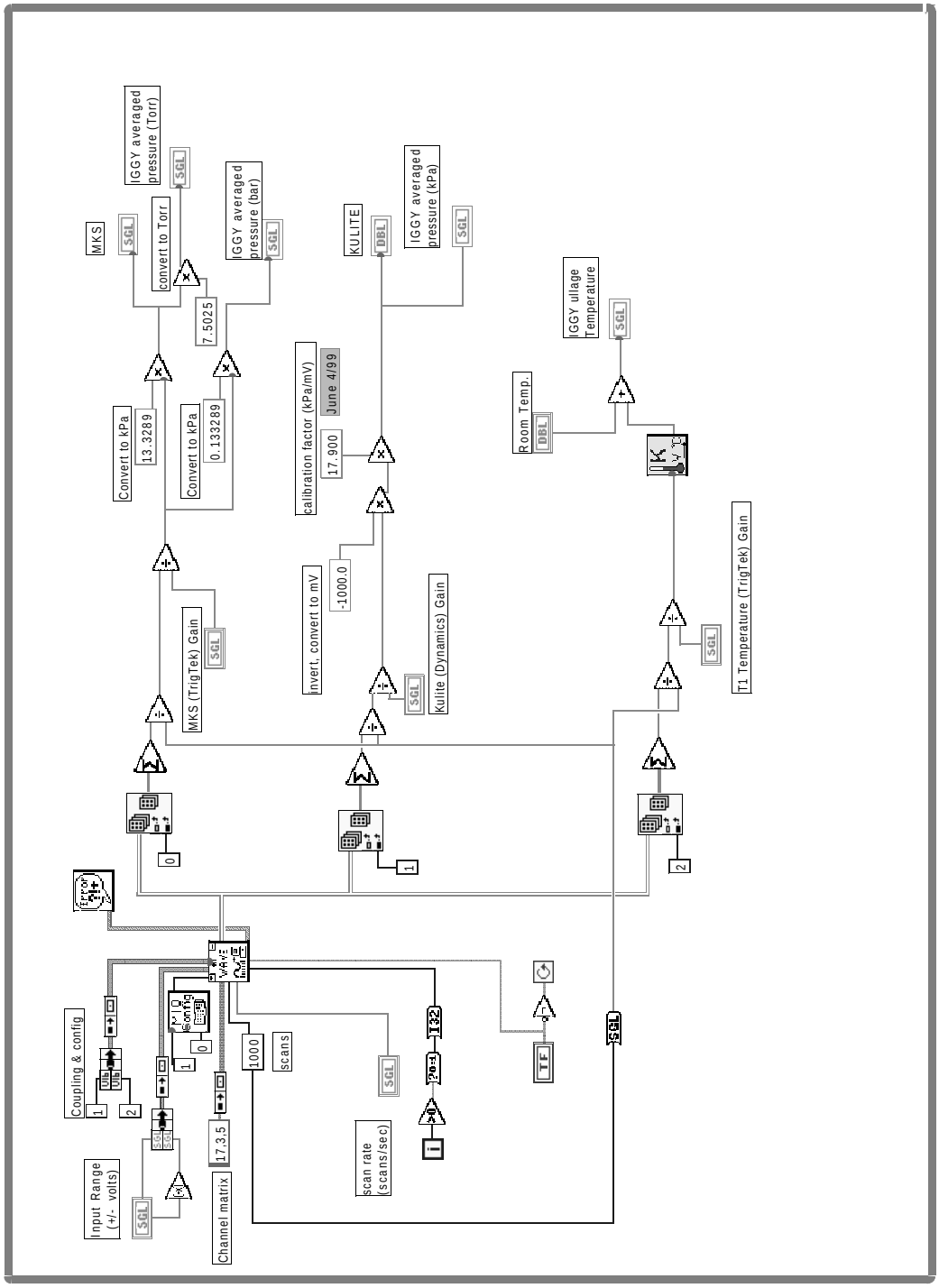

F Offset measurement program

This appendix includes the details of the LabView^{TM} program designed to measure the voltage offsets on the high voltage probe during a calibration test.

Connector Pane

offset_gain3.vi

Reads the voltages(ch1,ch3) and current(ch2) from the Tektronics TDS 640A scope and calculates the spark power and energy using:
V+= voltage on positive electrode (DC offset entered manually)
V-= voltage on negative electrode (DC offset entered manually)
i = current from current transformer
P+ = (V+) * (i)
P- = (V-) * (i)
E+ = integral (P+)
E- = integral (P-)
Ediff = (E+) - (E-)
N.B. P+ and P- are on the same plot, E+ and E- are on the same plot. The data is also saved into a file.

Front Panel

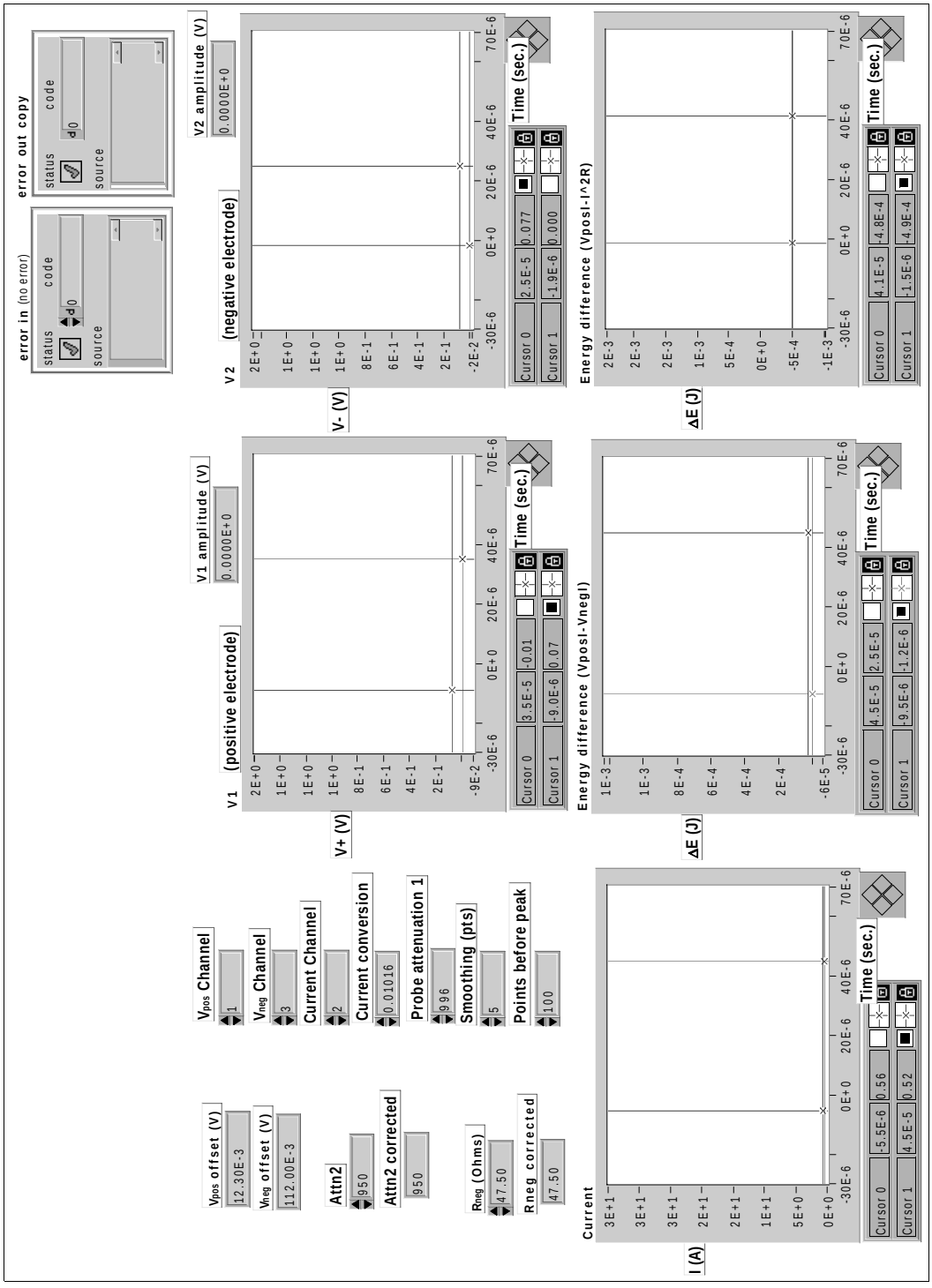
error in (no error)
status
code
source
error out copy
V2 amplitude (V)
V2 (negative electrode)
V- (V)
Time (sec.)
V1 amplitude (V)
V1 (positive electrode)
V+ (V)
Energy difference (Vposl-Vnegl)
ΔE (J)
Energy difference (Vposl-I^2R)
Vpos Channel
Vneg Channel
Current Channel
Current conversion
Probe attenuation 1
Smoothing (pts)
Points before peak
Vpos offset (V)
Vneg offset (V)
Attn2
Attn2 corrected
Rneg (Ohms)
Rneg corrected
Current
I (A)

Block Diagram

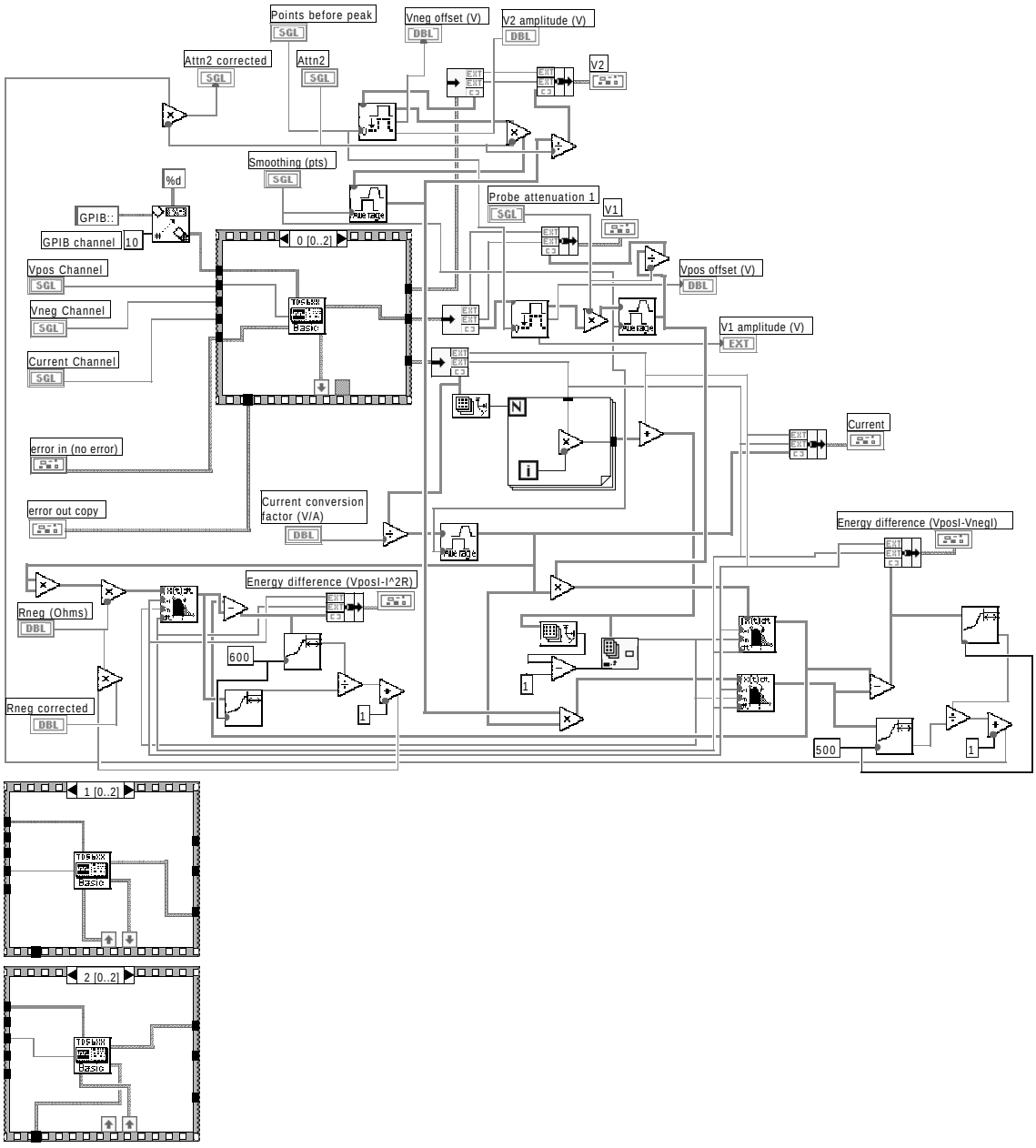

G Pressure and temperature acquisition program

This appendix includes the details of the LabView^{TM} program designed to acquire the pressure and temperature histories from the ignition vessel, store them in files on the resident computer, and display the histories on the screen.

Connector Pane

IggyAcq.vi

Front Panel

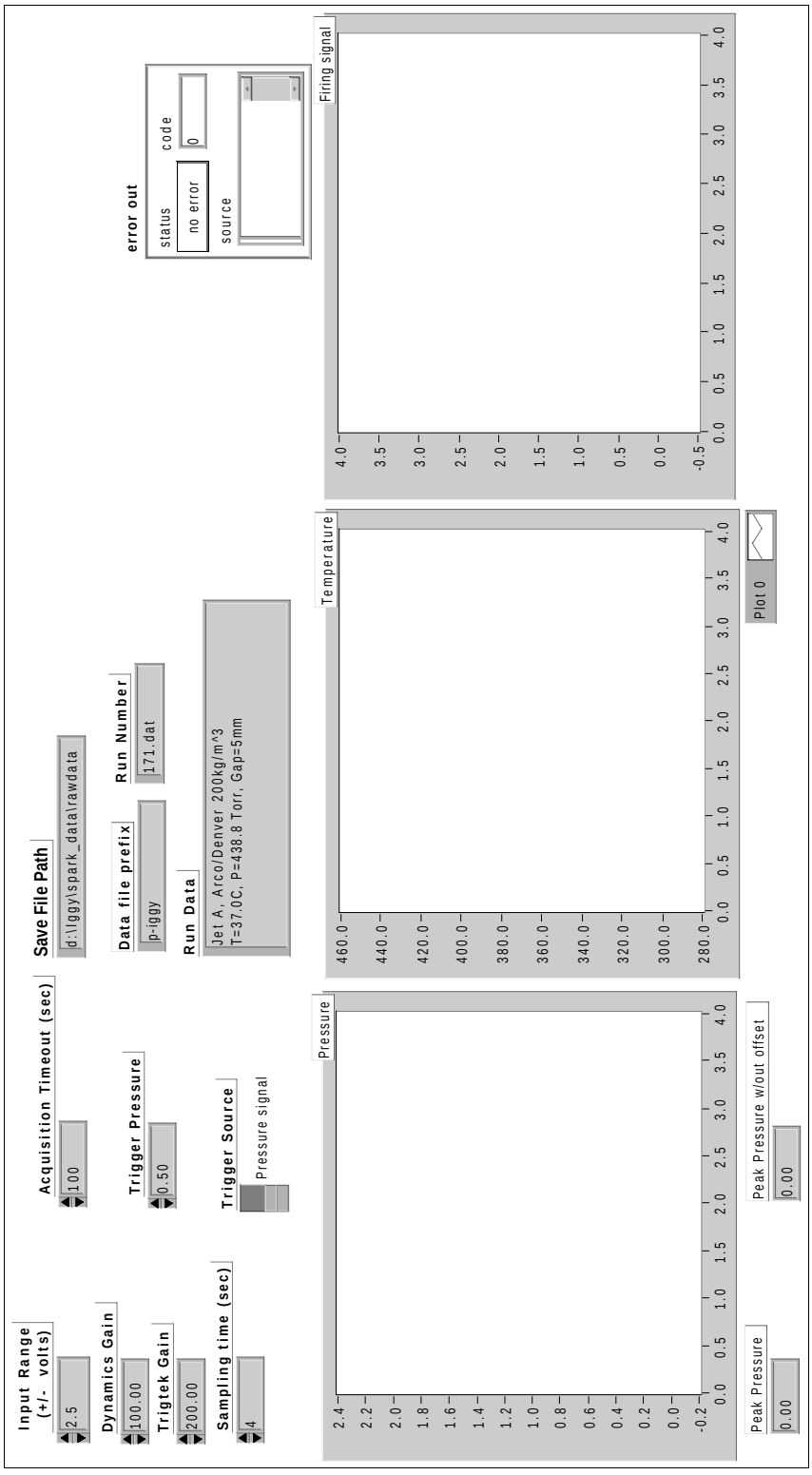
Input Range (+/- volts)
2.5
Dynamics Gain
100.00
Trigtek Gain
200.00
Sampling time (sec)
4
Acquisition Timeout (sec)
100
Trigger Pressure
0.50
Trigger Source
Pressure signal
Save File Path
d:\iggy\spark_data\rawdata
Data file prefix
p-iggy
Run Number
171.dat
Run Data
Jet A, Arco/Denver 200kg/m^3
T=37.0C, P=438.8 Torr, Gap=5mm
error out
status
no error
code
0
source
Pressure
Peak Pressure
0.00
Peak Pressure w/out offset
0.00
Temperature
Plot 0
Firing signal

Block Diagram

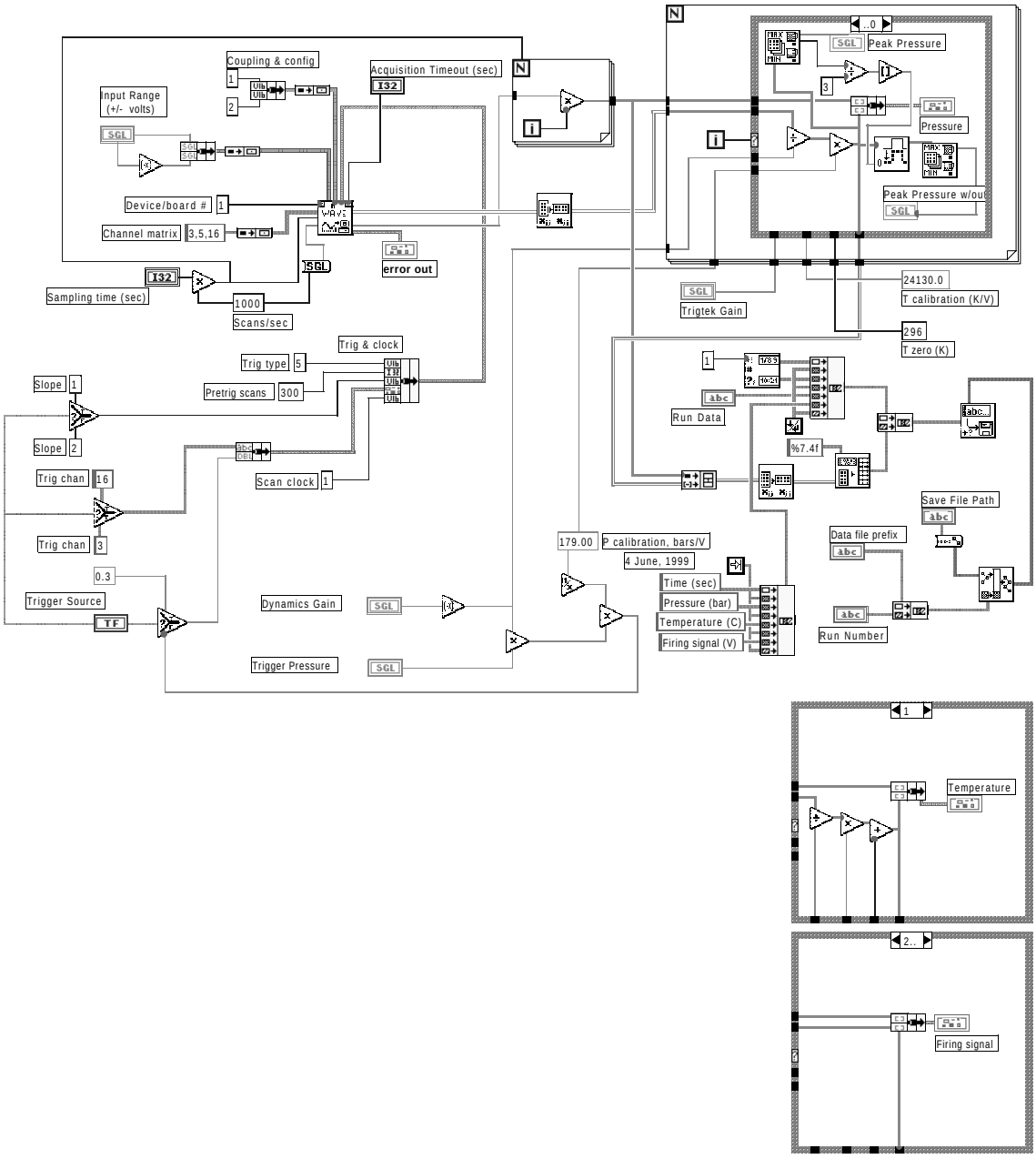

H Spark energy signal processing program

This appendix includes the details of the LabView^{TM} program designed to process the voltage and current histories of the spark and calculate the energy dissipated in the spark.

Connector Pane

SparkRead3.vi

Reads the voltage(ch1) and current(ch2) from the Tektronics TDS 640A scope and calculates the spark power and energy using:
V= voltage on positive electrode
i = current from current transformer
P+ = (V+) * (i)
P- = (i)^2 * R
E+ = integral (P+)
E- = integral (P-)
Ediff = (E+) - (E-)
N.B. P+ and P- are on the same plot, E+ and E- are on the same plot. The data is also saved into a file.

Front Panel

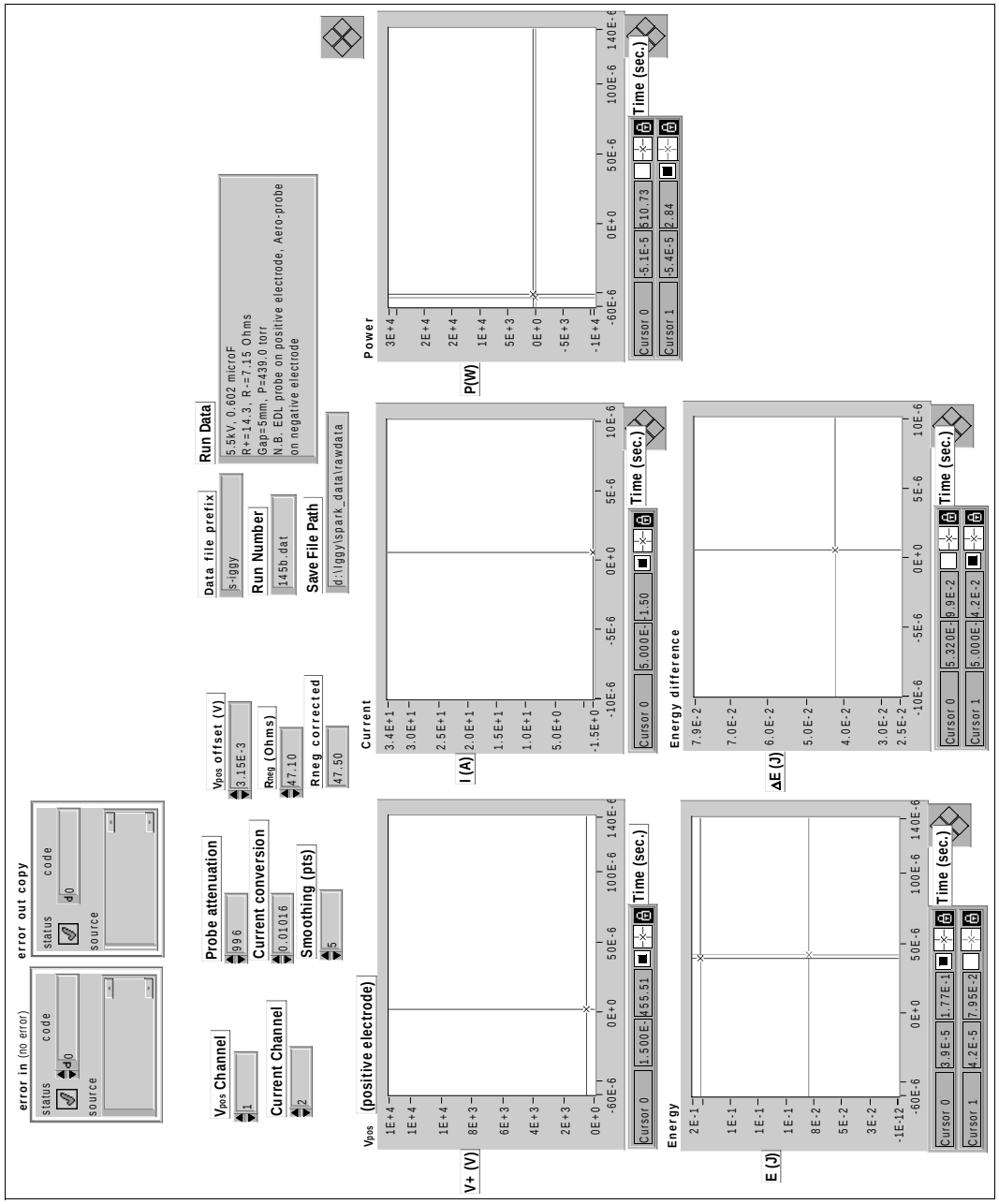
error in (no error)
status
code
source
error out copy
Vpos Channel
Current Channel
Probe attenuation
Current conversion
Smoothing (pts)
Vpos offset (V)
Rneg (Ohms)
Rneg corrected
Data file prefix
Run Number
Save File Path
Run Data
5.5kV, 0.602 microF
R+=14.3, R-=7.15 Ohms
Gap=5mm, P=439.0 torr
N.B. EDL probe on positive electrode, Aero-probe on negative electrode
Vpos (positive electrode)
V+ (V)
Time (sec.)
Current
I (A)
Power
P(W)
Energy difference
ΔE (J)
Energy
E (J)

Block Diagram

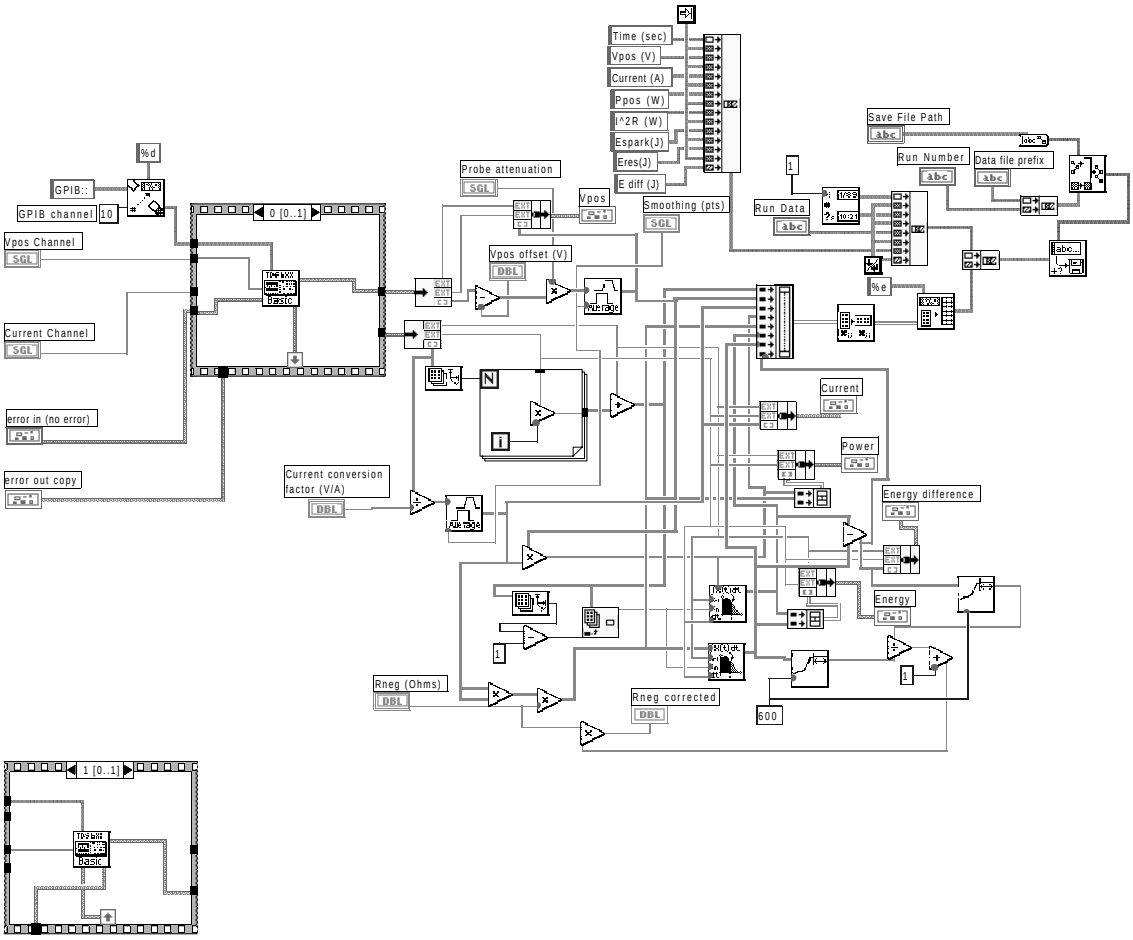

I Corrections to the One-Shot test series

A basic requirement of the One-Shot method is that the test variable for the experiment must follow a normal distribution. In the present experiment, the assumption that the logarithm of the spark energy is normally distributed may be false. Determining the statistical behavior of a test variable requires an extensive exploration of the distribution, which according to Dixon and Massey Jr. (1983), can involve thousands of data points. If the distribution is found to be not normal, another test variable in the experiment that is normally distributed must be identified. It was not feasible to perform such an extensive statistical study in the present study. The data obtained in the present experiment is insufficient to determine the normality of the distribution. However, if the data points are concentrated around the median, it is usually possible to approximate the shape of the distribution in this region as normal, unless there is insufficient data or a bias in the data.

The One-Shot and Bruceton methods are designed to focus the testing levels around the median value of the distribution in order to determine the statistical properties with a relatively small number of data points. Hence, it is important that the testing levels be close to the mean to properly represent the statistical properties of the experiment. In the present ignition energy system, there is an intrinsic scatter in the energy of the spark, even when the circuit conditions are maintained constant. Because the spark energy cannot be accurately set in advance, certain tests were performed at energies which may have been too far from the mean, possibly rendering the data unsuitable for One-Shot analysis.

Efforts were made to correct for phenomena which may cause a systematic bias or error in the spark energies. Three sources of scatter and bias were corrected for: the difference in temperature between tests, weathering caused by tests repeated with the same fuel sample, and an uneven number of “go” and ”no go”points.

There was a 1°C difference in temperature between some of the tests. One series of tests was conducted at 39°C (tests#134-140) while the other was conducted at 38°C (tests# 147-164). After the first series of tests was conducted at 39°C, it was found necessary to reduce the temperature by 1°C in the next series in order to ensure that all the spark energies necessary for the One-Shot test were within a convenient range for the spark system. This discrepancy in the test temperatures was compensated for by assuming that the main statistical properties of the ignition energy, i.e., the shape of the distribution and the standard deviation, was the same at 39°C and 38°C and that only the mean value was shifted.

The correction was done by shifting the spark energies of the 39°C tests up according to the dependence of the ignition energy on temperature. The ignition energy correlation used to shift the spark energies was Eq. 16. It was assumed that performing tests at a higher temperature is equivalent to increasing the spark energy. The logarithm of the spark energies of the tests performed at 39°C were thus corrected to 38°C by shifting them up using the relation:

$$(lnE)_{temp} = lnE + 0.757(T_2 - T_1) \tag{27}$$

where T_1 is the original temperature of the test series, T_2 is the temperature corrected to, $(lnE)_{temp}$ is the logarithm of the ignition energy corrected for temperature. The correction resulted in an increase in the logarithm of the energy of tests# 134-140 of about 20% to 40%.

When several tests were performed on the same batch of fuel, the fuel composition changed slightly each time the vapor space was evacuated. This was the case when ignition occurred and the combustion products had to be evacuated for the next test, effectively weathering the fuel. For the evacuation procedure, the vessel vapor space was evacuated down to about 10 Torr and immediately vented back up to the pressure required for the next test. The evacuation process lasted only 3 to 5 seconds, thus minimizing the removal of fuel components from the liquid. In spite of these precautions, a systematic change in the combustion properties was observed after each evacuation.

First, the flash point was measured to observe any influences of evacuations. The average flash point was measured to be between 46.4°C for fresh fuel and 46.3°C for fuel that was subjected to 5 evacuations. Hence, the change in flash point, if any, was too small to be measured.

The peak combustion over-pressure, however, was found to decrease, as shown in Fig. 37. The peak over-pressure is seen to decrease steadily from 2.96 bar to 2.85 bar after four ignition and evacuation procedures. A fifth evacuation did not change the peak over-pressure, suggesting that pressure decrease is due to the depletion of a small amount of volatile (light) fuel components and that after 4 evacuations, the remaining fuel components were present in sufficient amounts so as to not be significantly affected by subsequent evacuations.

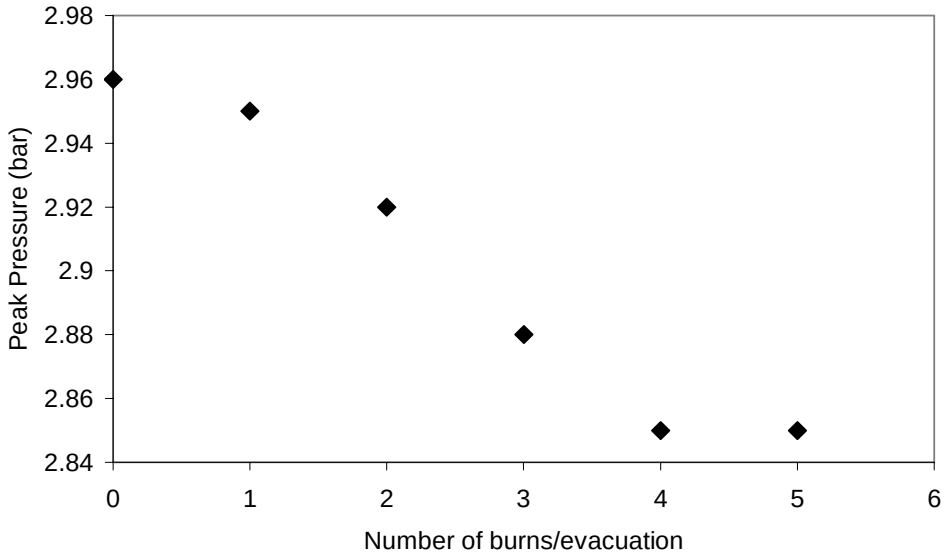

Figure 37: The dependence of peak combustion pressure at 39°C for a quarter-full vessel (200 kg/m^3) on the number of evacuations.

As for the temperature discrepancy, the effect of weathering was compensated for by assuming that weathering causes only a shift in the mean ignition energy and no change in the standard deviation and distribution shape. The One-Shot tests were corrected for weathering by shifting the spark energies down by an increasing amount as the number of tests on the fuel sample increased.

In order to determine the magnitude of this shift, the weathering effect was related to a

change in the temperature of the fuel. The ignition energy for a 50 mJ spark was measured by slowly increasing the temperature at 0.585 bar, 200 kg/m^3, until ignition occurred. For fresh fuel, the vapor space ignited at 38°C. For fuel subjected to 5 evacuations, the vapor space ignited at about 39°C. Hence, the minimum temperature for ignition was found to increase by about 1°C after 5 evacuations. We assume that the entire ignition energy dependence on temperature is shifted towards a higher temperature under the effect of weathering. By further assuming that the ignition energy depends linearly on the number of evacuations, we infer that the ignition energy increases linearly with the number of evacuations. By using the correlation of the ignition energy to the temperature (Eq. 16), an ignition energy curve for weathered fuel was formulated assuming a linear shift of 1°C after 4 evacuations. By assuming that shifting the ignition energy curve towards higher temperatures is equivalent to reducing the spark energy, a correction to the logarithm of the spark energy was done using the following expression:

$$(lnE)_w = \begin{cases} lnE - 0.757(n/4) & \text{for } n \geq 0 \\ lnE - 0.757 & \text{for } n > 4 \end{cases} \tag{28}$$

where n is the number of evacuations and $(lnE)_w$ is the logarithm of the spark energy corrected for weathering. The corrections resulted in a reduction in the spark energies by up to 40%.

The final type of correction used on the One-Shot test series was to make the number of "go" results and "no go" results the same. The One-Shot and Bruceton methods are designed to produce an equal number of each type of result so that at the end of the test series, the number of each should not differ by more than one. Because of the scatter of the results, there were more "no go" results in the test series (Fig. 14). This was corrected by eliminating the "no go" results that were furthest from the median value. Consequently, the results from tests# 149, 151, 153, 156, and 157 (Appendix D) were removed to form a reduced test series with an equal number of "go" and "no go" results.

The spark energies corrected for temperature discrepancies, weathering, and an uneven number of "go" and "no go" results are shown in Fig. 38. The median value is calculated for the corrected test series using the Method of Minimum Contradictoriness and is found to be -3.27. Even with these corrections to the test series data, the One-Shot analysis could not solve for the statistical properties of the ignition energy data.

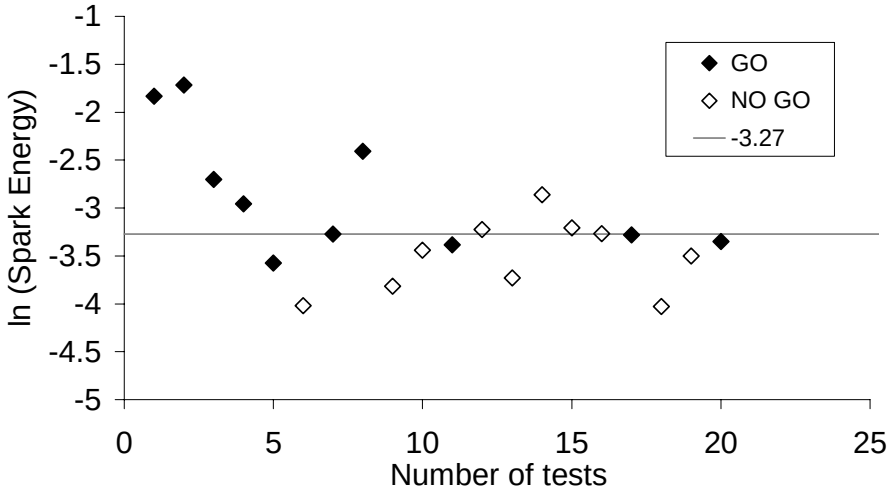

Figure 38: The One-Shot series of ignition energy tests (Fig. 14) at 38°C or 39°C 0.585 bar, for a quarter-full vessel (200 kg/m^3), corrected for temperature discrepancies, weathering, and unequal number of “go” and “no go” results. The median value of -3.27 is also shown.